XA9642557

INDC   INTERNATIONAL NUCLEAR DATA COMMITTEE

EVALUATION OF NEUTRON DATA FOR CURIUM-246

V.M. Maslov, E.Sh. Sukhovitskij, Yu.V. Porodzinskij,
A.B. Klepatskij, G.B. Morogovskij

Radiation Physics & Chemistry Problems Institute,
220109 Minsk-Sosny, Belarus

April 1996

EVALUATION OF NEUTRON DATA FOR CURIUM-246

V.M. Maslov, E.Sh. Sukhovitskij, Yu.V. Porodzinskij,
A.B. Klepatskij, G.B. Morogovskij

Radiation Physics & Chemistry Problems Institute,
220109 Minsk-Sosny, Belarus

Abstract

The evaluation of neutron data for Cm-246 is made in the energy region from 10^{-5}eV up to 20 MeV. The results of the evaluation are compiled in ENDF/B-6 format and compared in graphical plots with available experimental data and with the JENDL-3 evaluation.

Date of Manuscript: February 20, 1996

NEXT PAGE(S)
left BLANK

Contents

1 Introduction

The advanced nuclear fuel cycle studies request the nuclear data of transplutonium isotopes[1]. The neutron data for curium isotopes are especially important in this respect. Recently we have evaluated[2] the data for ^{243}Cm and ^{245}Cm. In this work the evaluation of ^{246}Cm neutron data is performed. The next isotope, which neutron data would be evaluated is ^{241}Am. The curium and americium isotopes data to be evaluated were requested by the General Manager of Japan Nuclear data Center Dr. Y. Kikuchi. The quantities evaluated are resolved and unresolved resonance parameters, total, elastic and inelastic scattering, fission, capture, (n,2n) and (n,3n) reaction cross sections, angular and energy distributions of secondary neutrons, including partial (n,xn) and (n,xnf) reaction spectra, fission spectra and number of neutrons per fission. The incident neutron energy range covered is from 10^{-5} eV up to 20 MeV. The evaluated quantities are compared with JENDL-3 evaluation[3].

2 Resolved resonance region

2.1 Previous evaluations of resolved resonance parameters

The resonance parameter evaluation[4] of ENDF/B-VI is based on total cross section data measured from 0.01 eV up to 30 eV by Berreth et al.[5], from 0.5 eV up to 158 eV by Benjamin et al.[6]and from 20 eV up to 385 eV by Moore et al.[7] Up to 388 eV Breit-Wigner single-level parameters of Moore et al.[7] were adopted.

In JENDL-3 evaluation[3] the resonance parameters of Berreth et al.[5], Benjamin et al.[6], Belanova et al.[9] and Cote et al.[10] up to 84 eV were employed, at higher neutron energies resonance parameters of Moore et al.[7] up to 331 eV were modified, assuming radiation width $\Gamma_\gamma = 31$ meV . Fission data by Stopa et al.[11] were used to get first and second resonance fission widths. However, resonance parameters are made consistent with available thermal fission data[8,12] by increasing the fission width value of first resonance and adding a smooth 1/v-type background fission cross section. Measured fission resonance values[8,12] are well-reproduced. In previous JAERI evaluation[13] the thermal fission cross section and fission resonance integral data were reproduced by increasing the fission width values of first and second resonances, which leads to drastic overestimation of fission cross section[11] in the energy region of the first and second resonances.

The purpose of current resonance parameter evaluation is to extend the resolved resonance region up to 400 eV and to reconcile the available fission data by Maguire et al.[14], revised by Danon et al.[15], with resonance parameters by Moore et al.[7]

2.2 Measured data fitting

2.2.1 Fission cross section

The bomb-shot fission cross section data of Moore et al.[7] are available in the energy region of 25 - 400 eV. Recently the fission data measurements, made with linac at RINS spectrometer were reported by Maguire et al.[14] Subsequently they were corrected by Danon et al.[15] for the impurity of ^{247}Cm in ^{246}Cm sample.

2.2.2 Other data

Thermal capture cross section was measured by Halperin et al.[16], Thomson et al.[17] and Gavrilov et al.[18]. Thermal fission cross section was measured by Benjamin et al.[8] and Zhuravlev et al.[12] The radiation and neutron widths values for the first two resonances are available from the transmission measurements in 0.01 - 30 eV region by Berreth et al.[5] Benjamin et al.[6] provide reduced neutron widths and radiation widths for five resonances below ~158 eV, instead of radiation width Belanova et al.[9] provide total width values. Cote et al.[10] determined reduced neutron width and radiation width for the first resonance.

2.2.3 Energy region below 25 eV

The first resonance occurs at 4.315 eV. The fission cross section below 25 eV is reported by Maguire et al.[14] and revised by Danon et al.[15] The averaged values of Γ_n^o and Γ_γ for the 4.315-eV and 15.33-eV resonances, reported by Berreth et al.[5],Benjamin et al.[6],Belanova et al.[9] and Cote et al.[10] are used as starting values. First, we define the average radiation width for the first and second resonances as the weighted average of the data by Berreth et al.[5], Benjamin et al.[6] and Cote et al.[10], it equals 34.7 meV. Then we assume this value for other resonances and obtain neutron and fission width values, using fission and capture areas due to Moore et al.[7] The radiation width of the first resonance was chosen on the basis of the shape analysis by Benjamin et al.[6] and slightly increased to describe thermal capture cross section and resonance capture integral. To get the fission resonance integral cross section value, compatible with measured data[8,12], the first resonance fission width was almost tripled. Hence, the first resonance parameters disagree with fission data by Maguire et al.[14], revised by Danon et al.[15], below 10 eV (see fig.2.1). That is the price to be paid for getting reasonable

fission resonance integral value. Thermal fission cross section is fitted with smooth $1/v$ background of 0.09 barns at 0.0253 eV. The second resonance parameters fit the data by Maguire et al.[14], revised by Danon et al.[15]

2.2.4 Energy region 25 ÷ 400 eV

The Γ_n^o and Γ_f resonance parameters, reported by Moore et al.[7] were modified for the new value of the radiation width Γ_γ =34.7 meV. Five weak resonances were added at E_r =32.95 eV, E_r=47 eV, E_r=131 eV, E_r=193.5 eV, E_r=232.8 eV, we provide also the parameters of the resonance doublet around 361 eV: E_r=358 eV, E_r=361.5 eV. The figures 2.1, 2.2, 2.4, 2.6, 2.8, 2.10, 2.12 show the comparison of fission cross section, calculated with present resonance parameters with data by Moore et al.[7] The same figures show comparison of calculated fission cross section broadened with resolution function[14] of RINS spectrometer, with data by Maguire et al.[14], revised by Danon et al.[15] The data by Moore et al.[7] appear to be systematically different from the more recent fission data by Maguire et al.[14], revised by Danon et al.[15], although the resonance fission areas around 158.1-eV resonance and combined area of 84.4-eV and 91.8-eV resonances are fairly compatible. Unfortunately, the latter data fully resolve only first and second resonances. To reconcile the data by Moore et al.[7] and by Maguire et al.[14], revised by Danon et al.[15], we compare fission areas above 25 eV up to 400 eV for both data sets. They appear to be systematically shifted, the data by Moore et al.[7] being systematically low, especially in the valleys between resonances. The smooth background is employed which is a linear interpolation between energy points given in Table 2.1, below 1 eV we assume $1/v$-shape background. The figures 2.3, 2.5, 2.7, 2.9, 2.11, 2.13 demonstrate the comparison of calculated capture cross section with Moore et al.[7] data.

Table 2.1

E, eV	σ_f , barns
1	0.014315
24.5	0.18
235	0.142
357	0.282
400	0.216

2.2.5 Resonance parameter analysis

We have got 17 resonance parameters up to 400 eV. The average resonance parameters, thermal cross sections and resonance integrals are presented in Table 2.2. Thermal cross sections and resonance integrals are fairly compatible with respective measured data.

Table 2.2

	ENDF/B-VI	JENDL-3	This evaluation
$\langle \Gamma_n^0 \rangle$, meV	1.907	3.210	2.014
$\langle \Gamma_f \rangle$, meV	0.904	0.467	0.412
$\langle \Gamma_\gamma \rangle$, meV	34.6	30.364	34.538
$\langle D \rangle$, eV	41.865	37.678	23.549
σ_t , barn	11.045	12.510	10.664
σ_γ , barn	1.297	1.291	1.311
σ_f , barn	0.063	0.140	0.144
σ_n , barn	9.685	11.079	9.208
g_γ	1.00918	1.00866	1.00842
g_f	1.00965	1.00332	1.00375
I_γ , barn	103.858	112.943	114.596
I_f , barn	10.420	9.898	10.281

The thermal total σ_t,capture σ_γ,and scattering σ_n cross sections, $g_\gamma-$, and g_f—factors, as well as resonance integrals $I\gamma$ and I_f values are calculated with a code INTER[19]. In case of JENDL-3 and present evaluations the multi-level Breit-Wigner formalism was used, while for ENDF/B-IV evaluation single-level formula was employed.

3 Unresolved resonance region

3.1 Review

Unresolved resonance region of ^{246}Cm is supposed to be from 0.4 keV up to 43.0277 keV. The lower energy is the end-point of resolved resonance region, the upper energy is the threshold energy of the inelastic scattering. We suppose $s-$, $p-$ and $d-$wave neutron-nucleus interactions to be effective.

3.2 The s-wave average resonance parameter evaluation

3.2.1 Estimate of resonance level missing influence on $\langle D_{obs} \rangle$ and $\langle S_0 \rangle$

The preliminary estimates of average partial widths were obtained by averaging the evaluated resolved resonance parameters. Figure 3.1 shows the cumulative sum of resolved resonance levels. Figure 3.2 shows the cumulative sum of experimental reduced neutron widths. The averaged resolved resonance parameters are as follows:

$$\langle \Gamma_n^0 \rangle = 2.014 \times 10^{-4} \ (\mathrm{eV})^{1/2}$$
$$\langle \Gamma_f \rangle = 0.41 \ \mathrm{meV}$$
$$\langle D_{obs} \rangle = 23.5 \ \mathrm{eV}$$
$$\langle \Gamma \gamma \rangle = 34.7 \ \mathrm{meV}$$

Note that due to missing of weak resonances these values overestimate actual reduced neutron width $\langle g\Gamma_n^0 \rangle$ and neutron resonance spacing $\langle D_{obs} \rangle$. To get a physically justified values of $\langle g\Gamma_n^0 \rangle$ and $\langle D_{obs} \rangle$ we employ a method, which is described elsewhere.[20] Both reduced neutron width and neutron resonance spacing distributions are obtained in a unified approach. We take into account the correlation of weak resonance missing and resonance missing due to poor experimental resolution. The resolution function parameters as well as $\langle g\Gamma_n^0 \rangle$ and $\langle D_{obs} \rangle$ values are obtained by maximum likelihood method when comparing experimental distributions of reduced neutron width and resonance spacing with Porter-Thomas and Wigner distributions, modified for the resonance missing. The latter distributions will be called expected distributions.

3.2.2 Evaluation of $\langle D_{obs} \rangle$, $\langle S_0 \rangle$, $\langle \Gamma_\gamma \rangle$ and $\langle \Gamma_f \rangle$ based on the resonance parameters

To evaluate average neutron resonance spacing $\langle D_{obs} \rangle$ and s-wave neutron strength function S_0 we apply our method[20] to the resolved resonance data base. We suppose that data up to 400 eV should be taken into account. The evaluated values are:

$$\langle S_0 \rangle = 0.84 \times 10^{-4} \ (\mathrm{eV})^{-1/2}$$
$$\langle D_{obs} \rangle = 21.43 \ \mathrm{eV}$$

Figure 3.3 shows the comparison of expected and experimental reduced neutron width distributions. Figure 3.4 shows the comparison of distributions for neutron resonance spacing. All the figures are obtained for energy interval 0-400eV. The expected distributions shown on the figures 3.3 and 3.4 demonstrate the effect of resonance missing. The figures 3.3, 3.4 show also that the expected distributions are consistent within statistical errors with the experimental data for energy interval 0-400 eV. That is the reason to consider the $\langle D_{obs} \rangle$ and S_0 estimates reliable. Nevertheless, the $\langle D_{obs} \rangle$ and $\langle S_0 \rangle$ values should be corrected for the impurities of the ^{246}Cm sample, mainly ^{244}Cm, which resonances shadowed some of the ^{246}Cm resonances in bomb-shot measurement by Moore et al.[7] The corrected values are:

$$\langle S_0 \rangle = (0.89 \pm 0.3) \times 10^{-4} \ (\text{eV})^{-1/2}$$
$$\langle D_{obs} \rangle = (17.5 \pm 4.0) \ \text{eV}$$

Average fission and radiation widths are less sensitive to resonance missing, so we adopted values obtained by averaging of resolved resonance parameters up to 400 eV. One must realize that fission widths are governed by the shape of the second well resonances of the double-humped fission barrier of ^{247}Cm. The spacing of the second well resonances is of the order of 1 keV. Hence, the average fission width over the resonance energy region may be appreciably lower than actual average fission width. The heights of the fission barrier humps (see Chapter IV) assume that the second well resonances might be rather narrow.

3.3 The s-, p- and d-wave average resonance parameter evaluation

3.3.1 Neutron width

Average neutron width is calculated as follows

$$\langle \Gamma_n^{lJ} \rangle = S_l \langle D_J \rangle E_n^{1/2} P_l,$$

where P_l is the transmission factor for the lth partial wave, which was calculated within black nucleus model. The p-wave neutron strength function $S_1 = 2.769 \times 10^{-4} \ (\text{eV})^{-1/2}$ was calculated with the optical model, using the deformed optical potential, described below. According to the results of optical model calculations S_0 was assumed to decrease linearly to the value of $S_0 = 0.859 \times 10^{-4} (\text{eV})^{-1/2}$ for neutron energy of 43.0277 keV. The d-wave neutron strength function was taken from optical model calculations: $S_2 = 1.023 \times 10^{-4} \ (\text{eV})^{-1/2}$.

3.3.2 Neutron resonance spacing

Neutron resonance spacing $\langle D_J \rangle$ was calculated with the phenomenological model[21], which takes into account the shell, pairing and collective effects. The main parameter of the model $\tilde{a}$ was normalized to the observed neutron resonance spacing $\langle D_{obs} \rangle = 17.5 \text{eV}$.

3.3.3 Fission width

Fission widths are calculated within a double-humped fission barrier model. Energy and angular momentum dependence of fission width is defined by the transition state spectra at inner and outer barrier humps. We constructed transition spectra by supposing the triaxiality of inner saddle and mass asymmetry at outer saddle. They will be described below. The calculated fission width $\langle \Gamma_f^{1/2+} \rangle$ value at E=400 eV was normalized to $\langle \Gamma_f \rangle =$ 1.33 meV, which allows to describe fission measured data in unresolved resonance region. This value is much higher than average resolved resonance fission width. However, it could be explained by the second well influence on fission width distribution. The predicted[22] magnitude of average fission width $\langle \Gamma_f \rangle$ fluctuations is:

$$\langle \Gamma_{f\,\max} \rangle / \langle \Gamma_f \rangle = \langle \Gamma_f \rangle / \langle \Gamma_{f\,\min} \rangle = 4/(P_A + P_B),$$

were $P_{A,B}$ is the penetrability of the inner(A) and outer(B) fission barrier humps.

3.3.4 Radiative capture width

Energy and angular momentum dependences of radiative capture width are calculated within a two-cascade γ-emission model with allowance for the $(n,\gamma f)$ and $(n,\gamma n)$ reaction competition to the $(n,\gamma\gamma)$ reaction. In this energy region (n,γ) reaction appears to be a radiative capture reaction. The radiative capture width was normalized to the value of $\langle \Gamma_\gamma \rangle =$34.7 meV. (For details see Chapter IV).

3.4 Cross section evaluation in the region 0.4-43.0277 keV

3.4.1 Fitting of fission cross section structure

There are fission data of Moore et al.[7] and data of Maguire et al.[14], revised by Danon et al.[15] covering the unresolved resonance energy region, their shapes are rather different (see fig.3.5). The shape of data by Maguire et al.[14], revised by Danon et al.[15] is reproduced with average resonance parameters. Fission cross section calculations with the average resonance parameters are compatible with data by Maguire et al.[14], revised by Danon et al.[15] within errors, except 0.4-1.0 keV and 2.6 -5.0 keV energy intervals. We fitted the measured data in these intervals adjusting $\langle \Gamma_f^{1/2+} \rangle$ fission width. The calculated fission cross section is compared with measured data on fig.3.5.

3.4.2 Comparison of present and JENDL-3 evaluated data

Evaluated fission cross sections of this work is consistent with JENDL-3 in the unresolved resonance region. Figure 3.6 gives the comparison of fission cross sections σ_f for both evaluations. The discrepancies are noticed when comparing the (n, γ) reaction cross sections (see fig. 3.7) Current evaluated cross section is more than 1.5 times as large as JENDL-3 evaluated capture cross section. This discrepancy is due to different values of radiative strength functions $S_{\gamma 0} = \langle \Gamma_\gamma \rangle / \langle D_{obs} \rangle$ (see below).

4   Fast neutron cross sections

The measured neutron data in fast energy region, i.e. above $\sim$43 keV are available only for fission cross section. The detailed fission cross section data[14,15] are available up to $\sim$80 keV. The bomb-shot data of Moore et al.[7] are rather discrepant with more recent bomb-shot data by Fomushkin et al.[23] in the first plateau region. At higher energies there is only one bomb-shot measurement[24] at 14.1 MeV. So, the available fission data fit would be used as constraint for (n, n') and (n, γ) reaction cross sections calculation. We reproduce also the average resonance fission width within double-humped fission barrier model. To fix fission channel parameters the systematic trends are used.

4.1   Optical potential

The deformed optical potential for n+^{246}Cm interaction is employed. The starting values for the potential parameters were those for n+^{238}U interaction.[25] The isotopic dependences of real and imaginary parts of the potential were calculated using the optical potential parameter systematics.[26] Five levels of the ground state band (0^+, 2^+, 4^+, 6^+, 8^+) are coupled. The deformation parameters β_2 and β_4 are obtained by fitting S_0 value of 0.89×10^{-4} (eV)$^{-1/2}$. We modified the original potential geometry parameters[25] to fit total cross section and differential scattering data for N-odd and even targets above 10 MeV. This procedure of parameter fitting is well tested in case of and ^{233}U, ^{239}Pu, ^{235}U, ^{232}Th and ^{238}U targets. The potential parameters are as follows:

$$V_R = 46.33 - 0.3E, MeV, r_R = 1.26 \ fm, a_R = 0.615 \ fm$$
$$W_D = \begin{cases} 3.68 + 0.4E, MeV, & E \leq 10 MeV, r_D = 1.24 \ fm, a_D = 0.5 \ fm \\ 7.68 \ MeV, & E > 10 \ MeV \end{cases}$$
$$V_{SO} = 6.4 \ MeV, r_{SO} = 1.12 \ fm, a_{SO} = 0.47 \ fm, \beta_2 = 0.203, \beta_4 = 0.009$$

The s-, p-, and d-wave strength functions and potential scattering cross section, calculated with this potential parameters in a coupled channel approach at incident neutron energy of 200 eV are:

$$S_0 = 0.909 \times 10^{-4}(\text{eV})^{-1/2} \quad S_1 = 2.769 \times 10^{-4}(\text{eV})^{-1/2} \quad R' = 9.0323 \text{ fm}$$

and at 43.0277 keV are:

$$S_0 = 0.859 \times 10^{-4}(\text{eV})^{-1/2} \quad S_1 = 2.769 \times 10^{-4}(\text{eV})^{-1/2} \quad S_2 = 1.023 \times 10^{-4}(\text{eV})^{-1/2}$$

The reaction cross sections, calculated with deformed optical potential and spherical optical potential, which is used in JENDL-3 evaluation, are compared on fig.4.1. The significant differences below 1 MeV and above 10 MeV would be manifested in inelastic scattering cross section and $(n, 3n)$ cross section. The total cross sections appear to be rather similar (see fig.4.2), while elastic scattering cross section are rather different above 1 MeV (see fig. 4.3).

4.2 Fission cross section

4.2.1 Status of the experimental data

The data by Maguire et al.[14], revised by Danon et al.[15] are available up to 80 keV. The bomb-shot data of Moore et al.[7] cover the incident neutron energy region from 25 eV up to 2.8 MeV. However, below 100 keV they are rather discrepant with data by Maguire et al.[14], revised by Danon et al.[15], obtained with accelerator-driven neutron source. Below 100 keV both data sets predict different fission cross section shapes, bomb-shot data appear to be systematically higher than data Maguire et al.[14], revised by Danon et al.[15], below 100 keV (see fig.4.4). Another set of bomb-shot data by Fomushkin et al.[23] cover the neutron energy range from 0.3 MeV up to 4.5 MeV. It appears to be rather different from latter data set at incident neutron energies above 1.5 MeV (see fig. 4.5). Below 1.5 MeV both bomb-shot data sets predict similar cross section shapes (see fig. 4.4). At higher energies there is only one bomb-shot measurement by Fomushkin et al.[24] at 14.1 MeV.

4.2.2 Statistical model calculation of fission cross section

We choose to fit data Maguire et al.[14], revised by Danon et al.[15], below 80 keV. At higher neutron energies we will follow the trend of data by Fomushkin et al.[23] Since the systematic error may be present in bomb-shot data, we will give larger weight to data Maguire et al.[14], revised by Danon et al.[15], in describing measured data base. The most peculiar feature of data by Fomushkin et al.[23] is the broad quasi-resonance structure above the fission threshold and steep decreasing trend of data above ~3 MeV incident neutron energies. Both features would be reproduced within the statistical model calculations. To describe the broad quasi-resonance structure above

1 MeV, we assume it to be due to interplay of level densities of even-odd ^{247}Cm fissioning nuclide and even-even ^{246}Cm residual nuclide.

The comparison of calculated fission cross section with measured data is shown in figs. 4.4, 4.5 and 4.6. The statistical theory calculation of fission cross section was accomplished within the double-humped fission barrier model. The approach employed in code STAT is described in more details elsewhere.[27] The procedure of calculating fission transmission coefficients is briefly described below.

4.2.3 Fission transmission coefficient, level density and transition state spectrum

The different behavior of level densities of even-even and even-odd nuclei at low excitation energies should be taken into account. The one-quasiparticle neutron states of even-odd ^{247}Cm fissioning nuclide, lying below the three-quasiparticle states excitation threshoid define the shape of ^{246}Cm(n,f) fission cross section below incident neutron energy of $\sim$1.5 MeV. At higher excitation energies three-quasiparticle states are excited. Each one-quasiparticle state is assumed to have a rotational band built on it with a rotational constant, dependent upon the respective saddle deformation. These levels comprise the discrete transition spectra at both saddles. We construct the discrete transition spectra up to 100 keV, using one-quasiparticle states of Bolsterli et al.[28] (see Table 4.1). At higher excitation energies the continuous level densities are used.

The discrete transition spectra, as well as continuous level contribution to the fission transmission coefficient are dependent upon the order of symmetry for ^{247}Cm fissioning nucleus at inner and outer saddles. Due to the axial asymmetry at the inner saddle[29] we additionally assume $(2J+1)$ rotational levels for each J value. The negative parity bands $K^\pi = 1/2^-, 3/2^-,$ $5/2^-$ ... at outer saddle are assumed to be doubly degenerate due to mass asymmetry[29]. With transition state spectra thus defined (see Table 4.1) the fission barrier parameters are obtained (see table 4.2). The fission width $\Gamma_f^{1/2+} = 1.33$ eV calculated at incident neutron energy of 0.4 keV coincides with average fission width obtained from unresolved resonance region.

The generalized pairing model provides the means of taking into account the discrete character of few-quasiparticle excitations. It was shown to be important in case of even-even fissioning nucleus ^{236}U in the ^{235}U(n,f) reaction[27]. We will model the discrete few-quasiparticle excitation effects in level density in the following approximate way. The level density of axially symmetric fissioning nucleus is calculated in constant temperature approximation, i.e. $\rho(U) = T_f^{-1}\exp((U - U_o)/T_f)$. The respective parameters, nuclear temperature T_f and excitation energy shift U_o are defined at the matching energy $U_c = 2.4$ MeV. At excitation energies above U_c the con-

tinuum part of the transition state spectrum is represented with the phenomenological model[21], which takes into account pairing, shell and collective effects at saddle deformations. The asymptotic value of the main parameter of the level density for fissioning nucleus ^{247}Cm is assumed to be the same, as that of ^{247}Cm compound nuclide. After that the effects of non-axiality and mass asymmetry are included. The detailed procedure of calculating fission transmission coefficient is described elsewhere[27]. The respective parameters: shell correction at saddles δW, pairing correlation function Δ, quadrupole deformation ε,and momentum of inertia at zero temperature $F_0/\hbar^2$ are given in Table 4.3.

The threshold energies for the excitations of few-quasiparticle states are calculated within generalized pairing model[21] using closed-form equations of Fu.[30] The procedure is described in more detail elsewhere.[31] In case of even-odd nuclei the nuclear level density $\rho(U)$ up to the three-quasiparticle excitation threshold is virtually independent on the excitation energy, since the intrinsic state density is constant. In this excitation energy region we will model the level density as $\rho(U) = T_f^{-1}\exp((\Delta_f - U_o)/T_f)$. Above the three-quasiparticle states excitation threshold the constant temperature model is used. For excitation energies below five-quasiparticle states excitation threshold the level density is slightly increased, as compared with constant temperature model approximation: $\rho(U) = T_f^{-1}\exp((U - U_o + \delta)/T_f)$, δ =0.25 MeV. The one- and three-quasiparticle states level density of even-odd fissioning nucleus ^{247}Cm defines the fission cross section shape at incident neutron energies below $\sim$3 MeV (see fig. 4.5). Above $\sim$3 MeV incident neutron energy fission cross section data were fitted (see fig. 4.5) by slight increase of pairing correlation function value. The parameters used for calculation of residual nuclide ^{246}Cm level density for neutron emission competition are described below.

Table 4.1

Transition spectra band-heads of ^{247}Cm

inner saddle		outer saddle	
K^π	E_{K^π}, MeV	K^π	E_{K^π}, MeV
$1/2^+$	0.0	$1/2^+$	0.0
$5/2^+$	0.08	$1/2^-$	0.0
$1/2^-$	0.05	$3/2^+$	0.08
$3/2^-$	0.0	$3/2^-$	0.08
		$5/2^+$	0.0
		$5/2^-$	0.0

Table 4.2

Fission barrier parameters

Nucleus	Barrier	Barrier height, MeV	Curvature, MeV
^{247}Cm	inner	6.17	0.7
^{247}Cm	outer	5.40	0.6
^{246}Cm	inner	6.00	0.9
^{246}Cm	outer	4.80	0.6
^{245}Cm	inner	6.45	0.8
^{245}Cm	outer	5.55	0.6
^{244}Cm	inner	6.43	0.9
^{244}Cm	outer	5.10	0.6
^{243}Cm	inner	6.30	0.8
^{243}Cm	outer	5.60	0.6

Table 4.3

Level density parameters of ^{247}Cm fissioning nucleus and residual nucleus ^{246}Cm

Parameter	inner saddle	outer saddle	neutron channel
δW, MeV	2.5	0.6	-2.439
Δ, MeV	Δ_0 +0.1	Δ_0 +0.1	Δ_0
ε	0.6	0.8	0.24
$F_0/\hbar^2$, MeV^{-1}	100	200	73

Below incident neutron energy of 1.22 MeV the neutron cross sections are calculated within Hauser-Feshbach approach with a width fluctuation correction taken into account. For width fluctuation correction calculation only Porter-Thomas fluctuations are taken into account. Effective number of degrees of freedom for fission channel is defined at the higher (inner) saddle as $\nu_f^{J\pi} = T_f^{J\pi}/T_{f\,\text{max}}^{J\pi}$, where $T_{f\,\text{max}}^{J\pi}$ is the maximum value of the fission transmission coefficient $T_f^{J\pi}$. Above incident neutron energy of 1.22 MeV the Tepel et al.[32] approach is employed.

4.2.4 Fission cross section above emissive fission threshold

The first chance fission cross section of ^{246}Cm(n,f) reaction above the emissive fission threshold is fixed with the level density and fission barrier parameters systematics[27] (see Tables 4.2, 4.3) and secondary neutron spectra

parameterization (see fig. 4.6). A consistent description of a complete set of measured data on (n,f), (n,2n) and (n,3n) for ^{238}U and ^{235}U targets was accomplished with the secondary neutron spectra parameterization[33], which is used here.

The fission barrier parameters of ^{246}Cm are fixed by ^{245}Cm(n,f) reaction data[34,35,36] analysis. The fig.4.7 shows the ^{245}Cm(n,f) measured data description. We modelled the fissioning even-even nuclide ^{246}Cm nuclear level density $\rho(U)$ above the pairing gap up to the four-quasiparticle excitation threshold as $\rho(U) = \rho(\hat{U})/(1 + \exp(U_2 - U + \delta_1)/\delta_2)$. The two-quasiparticle states level density of even-even fissioning nucleus ^{246}Cm defines the fission cross section shape at incident neutron energies $\sim 0.5 \div 2$MeV (see fig. 4.7), the parameters $\hat{U} = 1.7$ MeV, $\delta_1 = \delta_2 = 0.2$ MeV values were extracted. The collective levels, lying within the pairing gap are defined in our previous evaluation[2] of ^{245}Cm(n,f) reaction cross section. Above ~ 2 MeV incident neutron energy fission cross section data were fitted (see fig. 4.7) by slight increase of pairing correlation function.

The fission barrier parameters of ^{245}Cm are fixed by the ^{244}Cm(n,f) reaction data[7,23,37] analysis. The fig.4.8 shows the ^{244}Cm(n,f) data description. One may note that the same, as in case of ^{246}Cm(n,f) reaction above-threshold structure apparent in ^{244}Cm(n,f) fission cross section above 1 MeV incident neutron energy is also reproduced. The other fissioning nuclei ^{244}Cm and ^{243}Cm fission barrier parameters are obtained from ^{243}Cm(n,f) and ^{242}Cm(n,f) data analyses[2] as well as parameter systematics trends (see table 4.2).

The calculated fission cross section is drastically different from JENDL-3 evaluated curve above (n,nf) reaction threshold (see figs. 4.6, 4.9). The calculated fission cross section at 14.1 MeV neutron energy also appears to be lower than the data by Fomushkin et al.[24] This discrepancy is unavoidable, since the measured data by Fomushkin et al.[24] appear to be just as high as reaction cross section at 14.1 MeV, so they are incompatible with the calculated fission cross section.

4.3 Inelastic scattering cross section

The inelastic scattering cross section is calculated with the statistical codes STAT and STAPRE[38]. The discrete level excitation (compound and direct), continuum excitation and pre-equilibrium emission contribute to the inelastic scattering cross section.

4.3.1 Levels of ^{246}Cm

The low-lying levels of scheme of Nuclear Data Sheets[39] appears incomplete at excitation energy above 0.780 MeV (see fig. 4.10). A model treating

low-lying levels of even-even nuclei as a deformable non-axial rotator is published elsewhere[40]. This model predicts energies for all positive parity levels of even-even nucleus up to the excitation energies ~ 2 MeV (assuming five rotational bands). The gap in cumulative number of levels $N(U)$ between 0.5 and 0.8 MeV is due to rather high position of the second $K^\pi=0^+$ band, as compared with other actinides. Recent extension of this model allows the prediction of the negative parity $K^\pi=0^-$ rotational band[41]. We generated the unobserved positive parity levels of ^{246}Cm with high spin values and levels of negative parity rotational band with $K^\pi=0^-$ up to 1.22 MeV. The parameters of the model were adjusted, fitting experimental energies of band-heads $K^\pi=0^+$ ($n_\beta=n_\gamma=n_\zeta=0$), $K^\pi=2^+$ ($n_\beta=n_\gamma=n_\zeta=0$), $K^\pi=0^+$ ($n_\beta=1,n_\gamma=n_\zeta=0$), $K^\pi=0^+$ ($n_\beta=0,n_\gamma=1,n_\zeta=0$), $K^\pi=1^-$ ($n_\beta=n_\gamma=n_\zeta=0$), here n_β,n_γ, and n_ζ are quantum numbers of β,γ -quadrupole, and ζ-octupole vibrations. Rotational levels for bands with $K^\pi=2^-$; 1_1^-; 1_2^- were built as $E_{K^\pi}^J=E_{K^\pi}+ A(J(J+1)-K(K+1))$, the values of rotational constant A were adjusted to describe the measured level energies. We assigned spin and parity $J^\pi=6^-$ for the level E=1340,16 keV, previously unidentified. Adopted level scheme is compared with the experimental (see fig. 4.10). One can see that 3 levels up to 1.22 MeV were added.

In JENDL-3 evaluation there are 29 discrete excited levels up to 1.509 MeV, i.e. the missing of at least 15 collective levels above $\sim$0.78 MeV is ignored (see fig. 4.10). This estimate of level missing is consistent with the adopted constant temperature approximation of cumulative number of levels (see fig. 4.11).

4.3.2 ^{246}Cm level density

The continuum level density below excitation energy $U_c = 3.6$ MeV is calculated with the constant temperature model

$$\rho(U) = T^{-1}\exp((U - U_o)/T),$$

here, energy shift $U_0 = $ -0.0068 MeV, nuclear temperature $T = 0.37326$ MeV are the constant temperature model parameters, . The cumulative number of observed levels is compared with constant temperature approximation on fig.4.11. The anomalous high position of $K^\pi = 0^+$ band explains the gap between 0.5 - 0.8 MeV. At higher excitation energies the phenomenological model[21] is used. The main model parameter $\tilde{a}$ for ^{246}Cm residual nucleus is obtained by fitting the evaluated neutron resonance spacing[2] of ^{245}Cm target nuclide $\langle D_{obs} \rangle = 0.698$ eV.

The generalized pairing model provides the means of taking into account the discrete character of few-quasiparticle excitations just above the pairing

gap. It was shown to be important in case of even-even residual nucleus ^{238}Pu in the ^{239}Pu(n,2n) reaction[31]. We modelled the nuclear level density $\rho(U)$ above the pairing gap U_2 up to the four-quasiparticle excitation threshold U_4 as $\rho(U) = \rho(U_4 - 0.1)/(1 + \exp(U_2 - U + \delta_1)/\delta_2)$. The two-quasiparticle states level density of even-even residual nuclide ^{246}Cm influences the fission cross section shape at incident neutron energies above $\sim$1.4MeV, the parameters, $\delta_1 = \delta_2 = 0.1$ MeV values were extracted. Below the pairing gap the collective levels were employed.

4.3.3 ^{247}Cm level density

The level density of even-odd compound nuclide ^{247}Cm one needs to calculate radiative capture width and (n,γn$'$) reaction contribution to the compound inelastic scattering cross section. The continuum level density below excitation energy $U_c = 2.4$ MeV is calculated with the constant temperature model, the constant temperature model parameters are: energy shift $U_0 = -0.65311$ MeV, nuclear temperature $T = 0.36246$ MeV. The cumulative number of observed levels is compared with constant temperature approximation on fig.4.12. At higher excitation energies the phenomenological model[21] is used. The main model parameter $\tilde{a}$ for ^{247}Cm residual nucleus is obtained by fitting the evaluated neutron resonance spacing of ^{246}Cm target nuclide $\langle D_{obs} \rangle = 17.5$ eV.

4.3.4 Compound inelastic scattering

The residual nucleus ^{246}Cm level density modelling, adopted in present work changes the inelastic scattering cross section below 5 MeV as compared with JENDL-3 evaluation (see fig. 4.13). Above $\sim$1.5 MeV incident neutron energy the discrepancy is due to direct excitation of the ground state band levels. Above 1 MeV incident neutron energy inelastic scattering to the continuum gives a major contribution to the total inelastic scattering cross section. Above 5 MeV incident neutron energy pre-equilibrium emission and direct inelastic scattering are the two reaction mechanisms which define inelastic scattering cross section (see fig. 4.13). The pre-equilibrium model parameters were tested by the statistical model description of ^{238}U+n interaction secondary neutron spectra and consistent description of fission and (n,xn) reaction data for major actinides[33]. Steep decrease of inelastic scattering cross section of JENDL-3 above 5 MeV (see fig. 4.13) is due to missing of pre-equilibrium emission of neutrons.

4.3.5 Direct inelastic scattering

The direct inelastic scattering changes the shape of ground state band levels excitation cross sections above 1 MeV incident neutron energy (see figs. 4.14

- 4.17). This mechanism defines partly the hard-energy tail in total inelastic scattering cross section (see fig. 4.13). The calculations were accomplished with the code COUPLE[26].

Table 4.4

Level scheme of ^{246}Cm

$E^J_{K\pi}$, MeV	J	π	K	band	
0.000	0	+	0	A	
0.042852	2	+	0	A	
0.14201	4	+	0	A	
0.2949	6	+	0	A	
0.5004	8	+	0	A	
0.78207	10	+	0	A	*
0.84167	2	-	2	B	
0.87643	3	-	2	B	
0.92331	4	-	2	B	
0.980	5	-	2	B	
1.0517	6	-	2	B	
1.07885	1	-	1	C	
1.10485	2	-	1	C	
1.1055	12	+	0	A	*
1.12427	2	+	2	D	
1.12802	3	-	1	C	
1.1294	7	-	2	B	
1.16549	3	+	2	D	
1.17474	0	+	0	E	
1.17920	8	-	2	B	
1.1959	4	-	1	C	*
1.21053	2	+	0	E	

*) added

4.4 Radiative capture cross section

The radiative capture cross section is calculated within a statistical approach up to 5 MeV. Radiative capture strength function equals $S_{\gamma0} = 19.828$. At higher incident neutron energies we assume radiative capture cross section to be 1 mbarn. The radiative capture width was calculated with (n,γf) and (n,γn') reactions competition against "true" capture reaction (n,γγ). Due to high fission threshold for ^{247}Cm compound nuclide the competition of (n,γn') reaction is stronger than that of (n,γf) reaction. The influence of (n,γn') and

$(n, \gamma f)$ reaction competition on radiative capture cross section is illustrated on fig.4.18 by sharp decrease of capture cross section above 1 MeV incident neutron energy, as compared with $(n, \gamma x)$ reaction cross section. The capture cross section of JENDL-3 is systematically lower than present evaluation due to lower value of $S_{\gamma 0} = 9.779$.

4.5 Cross sections of (n,2n) and (n,3n) reactions

The current and JENDL-3 evaluated (n,2n) and (n,3n) cross sections are drastically different. The magnitude of (n,2n) cross section below the (n,2nf) reaction threshold is defined by (n,nf) and (n,2n) reaction competition. The present and JENDL-3 evaluated fission cross sections are rather different, as well as reaction cross sections above 10 MeV incident neutron energy (see fig. 4.1). To calculate the (n,2n) reaction cross section we use an approach, developed for description of the ^{238}U(n,2n) reaction cross section.[33] The present and JENDL-3 evaluations are compared in fig. 4.19. There is no hard-energy tail in (n,2n) reaction cross sections of JENDL-3 evaluation. In case of (n,3n) reaction the difference in reaction cross section above 11 MeV (see fig. 4.1) contributes essentially to the discrepancy, shown on fig. 4.20.

5 Energy distributions of secondary neutrons

There is no measured data on secondary neutron spectra. To calculate neutron energy distributions of $(n, xn\gamma)$ and (n, xnf), x=1, 2, 3 reactions we use a simple Weisscopf-Ewing evaporation model[42] taking into account fission and gamma competition to neutron emission. The pre-equilibrium emission of first neutron is included.

5.1 Model calculations of (n,nx) reaction spectra

The first neutron spectra for the (n,nx) reaction is the sum of evaporated and pre-equilibrium emitted neutron contributions. The pre-equilibrium emission contribution is calculated with a parameter systematics tested in case of n+^{238}U and n+^{235}U interactions[27,33]. We have calculated the 1st, 2nd and 3d neutron spectra for the $(n, n\gamma)$, (n,2n) and (n,3n), where applicable. According to the ENDF/B-VI format we included the secondary neutron spectra in the following way. The calculated spectra were summed up and tabular spectra for the $(n, n\gamma)$, (n,2n) and (n,3n) reactions were obtained. To clarify the competition of neutron, γ-emission emission and fission in case of (n,nx) and (n,2nx) reactions we have chosen the following presentation of spectra. Figure 5.1 shows the spectrum of 1st neutron of the reaction (n,nx) and its partial contributions for $(n, n\gamma)$, (n,2n), (n,nf) (n,2nf) and (n,3n) reactions. Figure 5.2 shows the spectrum of 2nd neutron of the reaction

(n,2nx) and its partial contributions for (n,2n), (n,3n) and (n,2nf) reactions. The spectra of 1st and 2nd neutrons are normalized to unity. The partial neutron spectra shown on figs. 5.1, 5.2 are normalized to the contributions of appropriate cross sections to the (n,nx) and (n,2nx) reaction cross sections, respectively.

Table 5.1 Average energies of secondary neutron spectra

E_n, MeV	1st neutron average energy, MeV									
	(n, n')		(n, 2n)		(n, n'f)		(n, 3n)		(n, 2n'f)	
	pres.	J - 3	pres.	J - 3	pres.	J-3	pres.	J - 3	pres.	J-3
2.0	0.42	0.83								
8.0	3.04	1.07	0.80	1.07	1.08					
14.0	9.46	1.45	2.79	1.45	2.53		0.73	1.45	0.56	
20.0	15.5	1.74	9.08	1.74	3.88		2.96	1.74	2.48	

E_n, MeV	2nd neutron average energy, MeV						3d neutron	
	(n, 2n)		(n, 3n)		(n, 2n'f)			
	pres.	J - 3	pres.	J - 3	pres.	J-3	pres.	J - 3
8.0	0.27	0.83						
14.0	1.07	0.95	0.62	0.98	0.47		0.18	0.83
20.0	1.13	1.34	1.44	1.34	1.40		0.78	0.79

The inclusion of pre-equilibrium emission changes significantly the average energies of emitted neutron spectra. That is shown in Table 5.1, where the average secondary neutron energies for current and JENDL-3 evaluations are compared. The most significant is the change of neutron spectra of (n,nγ) reaction. Figures 5.3-5.7 demonstrate the discrepancies of secondary neutron spectra in current and JENDL-3 evaluations.

The 1st neutron spectra of (n,nf) reaction also becomes harder and that influences prompt fission neutron spectra. On the other hand, the spectra of 2nd and 3d neutrons become softer.

5.2 Prompt fission neutron spectra

Prompt fission neutron spectra were calculated within the framework of Madland-Nix model[43].

5.2.1 Model calculations of prompt fission neutron spectra

The model parameters, which should be defined are the following.

5.2.1.1 Fragment masses. The fragment masses are defined as $A_L = 106$ and $A_H = 141$, in accordance with the data of Unik et al.[44] for nearest fissioning nuclei ^{246}Cm and ^{248}Cm. Fragment charges are defined as even values, closest to the ratios of

$$\langle A_{L,H} \rangle / (Z_{L,H} \mp 0.5) = A_F / Z_F.$$

The average fragments adopted are ^{106}Mo and ^{141}Xe.

5.2.1.2 Energy parameters. Average total fission energies $\langle E_R \rangle$ and average fission-fragment separation energies are calculated as in Madland-Nix model using mass tables of Wapstra et al.[45] Total fragment kinetic energy $\langle TKE \rangle$ for ^{247}Cm fissioning nucleus had been defined in evaluation of ν_p for thermal energy and is described below, for other fissioning nuclei $\langle TKE \rangle$ values are taken from our previous evaluation for ^{245}Cm.

5.2.2 Other parameters.

The level density parameter of the fermi-gas model is calculated as $a = A_{L,H}/10.2$, MeV^{-1}. Becchetti-Greenlees[46] spherical optical potential parameters are employed to calculate compound cross section.

5.2.3 Prompt fission neutron spectra evaluation

Below emissive fission threshold prompt fission neutron spectra are calculated with the parameters given in Table 5.2. Figure 5.8 shows the comparison of calculated thermal prompt fission neutron spectrum with maxwellian spectrum ($T = 1.485$ MeV) of JENDL-3. Average energy of fission spectrum is 2.19 MeV, it is compatible with evaluated value 2.22 MeV of JENDL-3, however the spectra shapes are significantly different. Figure 5.9 demonstrates the discrepancy of our calculation and JENDL-3 evaluation. The discrepancy is due to incident neutron energy independent maxwellian fission spectrum presentation in JENDL-3 as well as emissive fission contribution in present evaluation.

Above emissive fission threshold the fission neutron spectra $N(E)$ is the superposition of emissive fission spectra, i.e.

$$N(E) = (\tfrac{\sigma_{nf}}{\sigma_{nF}} \nu_1 N_1(E) + \tfrac{\sigma_{nn'f}}{\sigma_{nF}} [\Phi_{nn'f}(E) + \nu_2 N_2(E)]$$

$$+ \tfrac{\sigma_{n2nf}}{\sigma_{nF}} \left[\Phi^1_{n2nf}(E) + \Phi^2_{n2nf}(E) + \nu_3 N_3(E) \right]) /$$

$$\left[\frac{\sigma_{nf}}{\sigma_{nF}}\nu_1 + \frac{\sigma_{nn'f}}{\sigma_{nF}}(1+\nu_2) + \frac{\sigma_{n2nf}}{\sigma_{nF}}(2+\nu_3)\right],$$

where σ_{nF}, σ_{nf}, $\sigma_{nn'f}$, σ_{n2nf} are the total and i-th chance fission cross sections (i = 1,2,3); $\Phi_{nn'f}$, Φ^1_{n2nf}, and Φ^2_{n2nf} are emitted neutron spectra: for (n,nf) reaction, 1st and 2nd neutrons of (n,2nf) reaction, respectively; ν_i and N_i are multiplicity and prompt neutron spectra for the i-th fissioning nucleus. The pre-equilibrium emission of the first neutron is included, the $\Phi^i_{n,xnf}$ spectra for the emissive fission are calculated with Weisscopf-Ewing evaporation model.[42]

Table 5.2

Parameters of the Madland-Nix model

Fissioning nucleus	A_L fragm.	A_H fragm.	$\langle E_R \rangle$, MeV	$\langle TKE \rangle$, MeV	B_n, MeV
^{247}Cm	^{106}Mo	^{141}Xe	209.144	183.200	5.157
^{246}Cm	^{105}Mo	^{141}Xe	208.340	183.700	6.455
^{245}Cm	^{104}Mo	^{141}Xe	208.564	185.000	5.522

The influence of pre-equilibrium pre-fission neutrons on prompt fission neutron multiplicity ν_i and prompt neutron spectra N_i predictions as well as $N(E)$ and $\nu(E)$, is illustrated in Table 5.3 and Fig. 5.10. In Table 5.3 $\langle E_i \rangle$ denotes average prompt fission neutron energy of i-th fissioning nucleus, $\langle E \rangle$ is the average fission neutron energy, $\langle E_{n'f} \rangle$, $\langle E_{2nf} \rangle^1$ and $\langle E_{2nf} \rangle^2$ are the average energies of neutrons, emitted in (n,nf) and 1st and 2nd neutrons emitted in (n,2nf) reactions, respectively. The Figs. 5.11-5.13 show the partial contributions of i-th chance fission to the total fission neutron spectrum at incident neutron energies of 8, 14 and 20 MeV.

6 Number of neutrons per fission

There are no experimental data on number of prompt fission neutrons ν_p for ^{246}Cm. The systematics of Howerton[47], used in JENDL-3 and ENDF/B-6 evaluations does not reproduce the mass dependence of existing experimental data on ν_p for Cm isotopes (Fig. 6.1). The present evaluation of ν_p is based on calculation within Madland-Nix model. The only free parameter of the model is the average total fragment kinetic energy $\langle TKE \rangle$. The experimental data and systematics predict the linear mass dependence for $\langle TKE \rangle$ (Fig. 6.2). Therefore it is reasonable to define the $\langle TKE \rangle$ for fissioning nucleus ^{247}Cm as linear interpolation between the $\langle TKE \rangle$ values for

neighboring fissioning nuclei ^{246}Cm and ^{248}Cm. The value of $\langle TKE \rangle$=182.7 MeV for ^{248}Cm

Table 5.3 Comparison of Madland-Nix and present approach

Quantity	$E_n = 8$ MeV		$E_n = 14$ MeV		$E_n = 20$ MeV	
	M-N model[43]	Present	M-N model[43]	Present	M-N model[43]	Present
$\langle E_1 \rangle$	2.361	2.361	2.482	2.482	2.592	2.592
ν_1	4.680	4.680	5.224	5.224	6.222	6.222
$\langle E_{n'f} \rangle$	1.153	1.079	1.513	2.531	1.800	3.879
$\langle E_2 \rangle$	2.209	2.211	2.333	2.311	2.449	2.407
ν_2	3.601	3.611	4.351	4.217	5.090	4.823
$\langle E_{2nf} \rangle^1$	-	-	1.513	0.555	1.800	2.481
$\langle E_{2nf} \rangle^2$	-	-	1.007	0.468	1.394	1.400
$\langle E_3 \rangle$	-	-	2.154	2.190	2.277	2.262
ν_3	-	-	3.171	3.373	3.881	3.791
$\langle E \rangle$	2.222	2.217	2.328	2.408	2.385	2.574
ν	4.651	4.655	5.403	5.341	6.105	5.944

was defined by fitting the experimental data of Zhuravlev et al.[48] on thermal ν_p=3.79±0.15 for ^{247}Cm. The obtained value of $\langle TKE \rangle$=183.2 MeV gives calculated thermal ν_p=3.605 for ^{246}Cm (Fig. 6.1), it is compatible with systematics of $\nu_p^{th}=\nu_p^{sp}$+0.1B$_n$ and saw-toothed dependence observed for neutron multiplicity for odd and even nuclei. The comparison of $\nu_p(E)$, calculated with fixed parameters, with JENDL-3 evaluation is shown in fig. 6.3. The calculated slope of $d\nu_p/dE = 0.135$ is considerably lower than that of Howerton systematics[47] prediction, adopted in JENDL-3. However, it is consistent with $d\nu_p/dE$ for neighboring nuclei. The Madland-Nix model calculations predict non-linear shape of $\nu_p(E)$ above emissive fission threshold.

The influence of pre-equilibrium pre-fission neutrons manifests in additional appreciable decrease of $d\nu_p/dE$ above 12 MeV.

The delayed number of neutrons per fission ν_d is taken from systematics of Tuttle[49]. Specifically, $\nu_d = 0.00916$ for incident neutron energies up to 6 MeV and $\nu_d = 0.0064$ for $E_n \geq 8$MeV. The decay constants for six groups of delayed neutrons are taken from Brady et al.[50]

7   Angular distributions of secondary neutrons

The angular distributions of elastically scattered neutrons and those for neutrons, scattered on four levels of ground state band are calculated with the coupled channel method. The isotropic compound scattering contribution is taken into account by renormalizing l-th Legendre polynomial coefficients A_l^{cc}, calculated with coupled channels:

$$A_l = A_l^{cc} \sigma_{dir} / (\sigma_{dir} + \sigma_{comp}),$$

where σ_{dir} and σ_{comp} are the scattering cross section direct and compound contributions, respectively. For the other contributing reactions angular distributions of secondary neutrons are assumed isotropic.

8   Conclusions

The evaluated neutron data file for ^{246}Cm is compiled in ENDF/B-VI format and sent to the International Science and Technology Center (Moscow) and Japan Nuclear Data Center at Japan Atomic Energy Research Institute.

The scarcity of experimental data coupled with possibility of some new data becoming available (for example, ^{246}Cm(n,f) data of Fursov et al. (PPEI, Obninsk, Russia)) may urge some revision of data file. Present version of ^{246}Cm data file may be revised before March of 1998, the expiration date of Project CIS-03-95.

9 References

1. Nakagawa T., Kikuchi Y., Proc. of the Int. Conf. on Nuclear Data and Technology, Gatlinburg, Tenn., USA, 9-13 May, 1994, Dickens J.K. (Editor), 709, ANS Inc., 1994.

2. Maslov V.M., Porodzinskij Yu.V., Sukhovitskij E.Sh., Klepatskij A.B., Morogovskij G.B. INDC(BLR)-2, 1995.
Maslov V.M., Porodzinskij Yu.V., Sukhovitskij E.Sh., Klepatskij A.B., Morogovskij G.B. INDC(BLR)-3, 1996.

3. Japanese Evaluated Data Library, Version 3, JAERI 1319, 1990.

4. C.L. Dunford, Nuclear Data for Science and Technology, Proc. Int. Conf. Julich, 1991,788.Springer-Verlag,1992, Berlin

5. Berreth J.R., Simpson F.B., Rusche B.C. Nucl. Sci. Engng. 49, 145 (1972).

6. Benjamin R.W., Ahlfeld C.E., Harvey J.A. Nucl. Sci. Engng. 55, 440 (1974)

7. Moore M.S., Keyworth G.A. Phys. Rev. C, 3, 1656 (1971)

8. Benjamin R.W., Macmurdo K.W., Spences J.D. Nucl. Sci. Eng. 47, 203 (1972)

9. Belanova T.S., Kolesov A.G., Poruchikov V.A. et al., Neutron Physics, v.2, 260 (1977)

10. Cote R.E., Barnes R.F., Diamond H. Phys. Rev., 134, B1281 (1964)

11. Stopa C.R.S., Maguire H.T., Jr., Harris D.R., Block R.C., Slovacek R.E., Dabbs J.W.T., Dougan R.J., Hoff R.W., Lougheed R.W., 1982 Kiamesha, p. 1090 (1982)

12. Zhuravlev K.D., Kroshkin N.I., Chetverikov Atomnaya Energiya, 39, 907 (1976)

13. Kikuchi Y. JAERI-M, 83-236, 1984.

14. Maguire Jr. H.T., Stopa C.R.S., Block R.C. et al. Nucl. Sci. Eng. 89, 293 (1985)

15. Danon Y., Slovacek R.E., Block R.C., Lougheed R.W., Hoff R.W., Moore M.S. Nucl. Sci. Eng. 109, 341 (1991)

16. Halperin J., Druschel R.E., Eby R.E. ORNL-4437, 20 (1969)

17. Thomson M.C., Hyder M.L., Reuland R.J. J. Inorg. Nucl. Chem. 33, 1533 (1971)

18. Gavrilov V.D. Goncharov V.A., Ivanenko V.V. Atomnaya Energiya 41, 808 (1977)

19. Dunford C.L.: "ENDF Utility Codes Release 6.9", IAEA-NDS-29 (1993)

20. Porodzinskij Yu.V., Sukhovitskij E.Sh., Nuclear Constants, 4, p.27, 1987 (in Russian)

21. Ignatjuk A.V., Istekov K.K., Smirenkin G.N. Sov. J. Nucl. Phys. 29, 450 (1979).

22. Gai E.V.,Ignatjuk A.V., Rabotnov N.S. Sov.J. Nucl. Phys.10,p.542, 1969 (in Russian)

23. Fomushkin E.F., Novoselov G.F., Vinogradov Yu.I., Gavrilov G.F., Zherebtsov Sov. J. Nucl. Phys. 36, 338 (1980).

24. Fomushkin E.F., Novoselov G.F., Gavrilov G.F. et al.,in: Nuclear Data for Science and Technology (Springer-Verlag,1992), p.439.

25. Haouat, Lachkar J., Lagrange Ch., et al., Nucl.Sci. Engng. 81, 491 (1982)

26. Klepatskij A.B., Sukhovitskij E.Sh., private communication.

27. Ignatjuk A.V., Maslov V.M., Proc. Int. Symp. Nuclear Data Evaluation Methodology, Brookhaven,USA, October 12-16, 1992, p.440, World Scientific, 1993.

28. Bolsterli M., Fiset E.O., Nix J.R., Norton J.L. Phys.Rev., C 5, 1050 (1972).

29. Howard W.M., Moller P. Atomic Data and Nuclear Data Tables,25, 219 (1980)

30. Fu C. Nucl. Sci. Engng. 86, 344 (1984).

31. Maslov V.M. Zeit. Phys. A, Hadrons & Nuclei, 347, 211 (1994).

32. Tepel J.W., Hoffman H.M., Weidenmuller H.A. Phys. Lett. 49, 1 (1974).

33. Ignatjuk A.V., Maslov V.M., Pashchenko A.B. Sov. J. Nucl. Phys. 47, 224 (1988).

34. Fursov B.I., Samylin B.F., Smirenkin G.N., et al. Nuclear Data for Science and Technology, Proc. Int.Conf., Gatlinburg, 1994, 269, ANS.

35. Fomushkin E.F., G.F. Novoselov, Y.I. Vinogradov et al., Atomnaya Energiya, 69, 258 (1990).

36. White R.M., Browne J.C. , in: Nuclear Data for Science and Technology (North-Holland, 1983),p.281.

37. Vorotnikov P.E. et al. Sov. J. At. Energy 57, 504 (1985).

38. Uhl M. and Strohmaier B., Report IRK - 76/10 (Vienna,1976).

39. ENSDF, 1995

40. Porodzinskij Yu.V., Sukhovitskij E.Sh . Sov. J. Nucl. Phys. 53, 64 (1991).

41. Porodzinskij Yu.V., Sukhovitskij E.Sh . Sov. J. Nucl. Phys. 59, 1, (1996).

42. Maslov V.M., Porodzinskij Yu.V.,Sukhovitskij E.Sh., Proc. Int. Conf. on Neutron Physics, 14-18 Sept., Kiev, USSR, V.1, p.413, 1988.

43. Madland D.G., Nix J.R., Nucl. Sci. Engng. 81, 213 (1982).

44. Unik J.P. et al.,Physics and Chemistry of Fission, Proc. of a Symp.,Rochester, NW, USA, 13-17 August, 1973, v.II, p. 19, IAEA, Vienna, 1974.

45. Wapstra A.H. et al. At. Data & Nucl. Data Tables, 39, 281 (1988).

46. Becchetti F.D., Greenlees G.W., Phys. Rev. 182, 1190 (1969).

47. Howerton R.J., Nucl. Sci. Engng. 62, 438 (1977).

48. Zhuravlev K.D. et al., Proc. 2nd Nat. Conf. on Neutron Physics, 28May-1June 1973., Kiev, USSR, V.4, p.57, 1974.

49. Tuttle R.J. Proc. Consultants Meeting on Delayed Neutron Properties, 1979, Vienna, INDC(NDS)-107/G, p.29.

50. Brady M.C., Wright R.Q., England T.R., Report ORNL/CSD/TM-226(1991), IAEA-NDS-102, 1992.

33

10. Figures

Table of contents

^{246}Cm FISSION CROSS SECTION

FIG.2.1

FIG.2.2

^{246}Cm CAPTURE CROSS SECTION

FIG.2.3

^{246}Cm FISSION CROSS SECTION
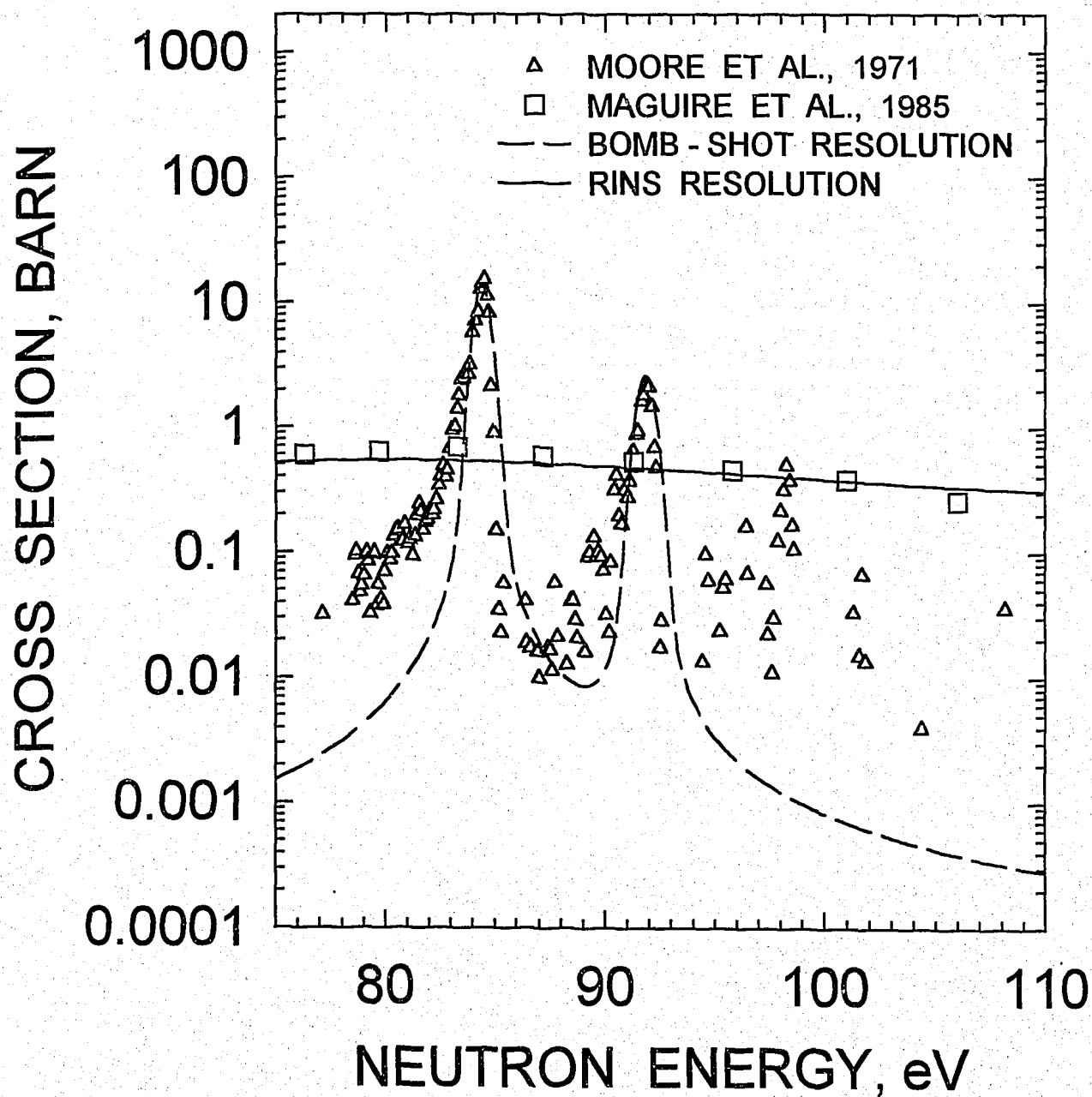
FIG.2.4

^{246}Cm CAPTURE CROSS SECTION
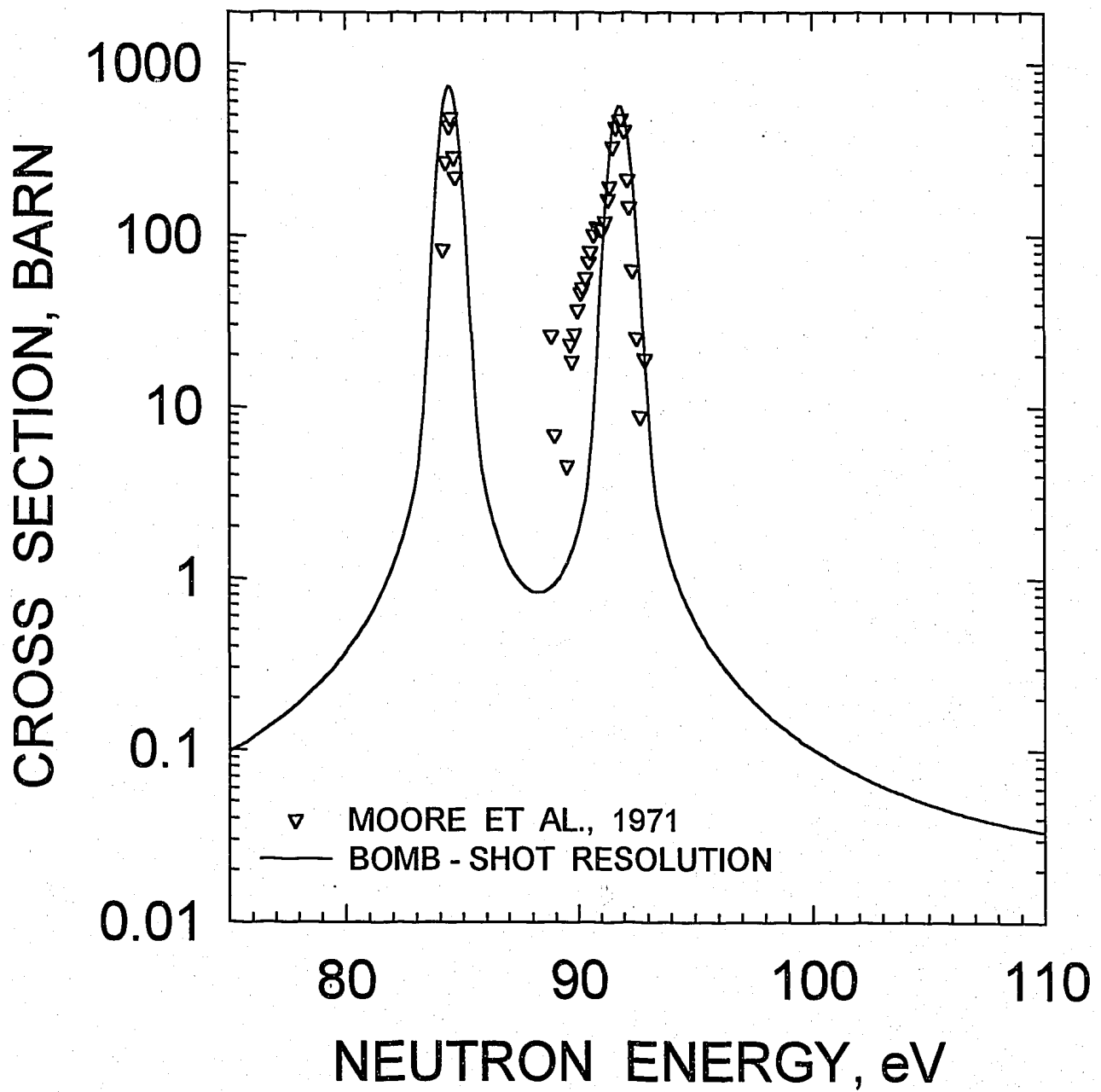
FIG.2.5

^{246}Cm FISSION CROSS SECTION
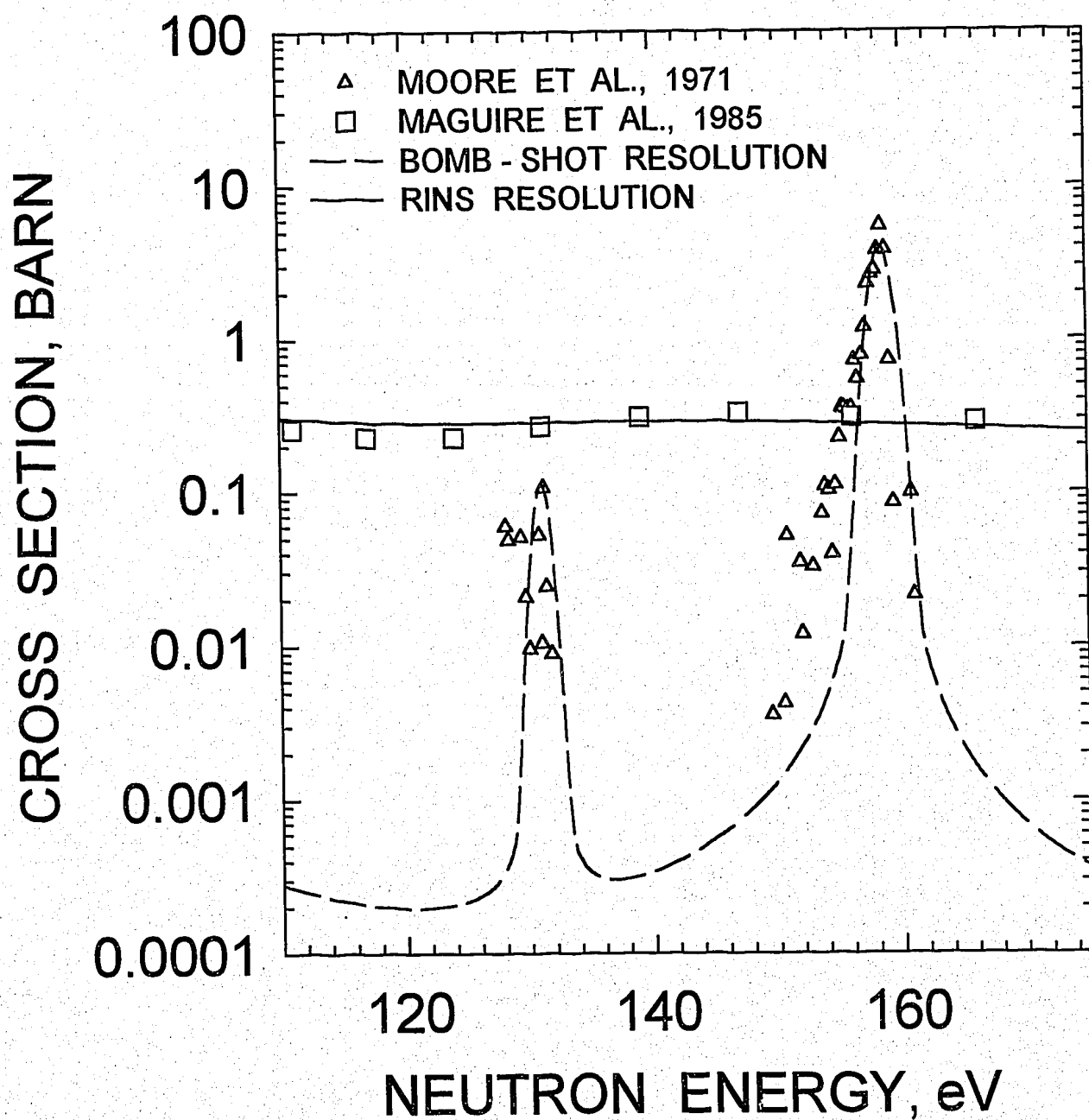
FIG.2.6

^{246}Cm CAPTURE CROSS SECTION
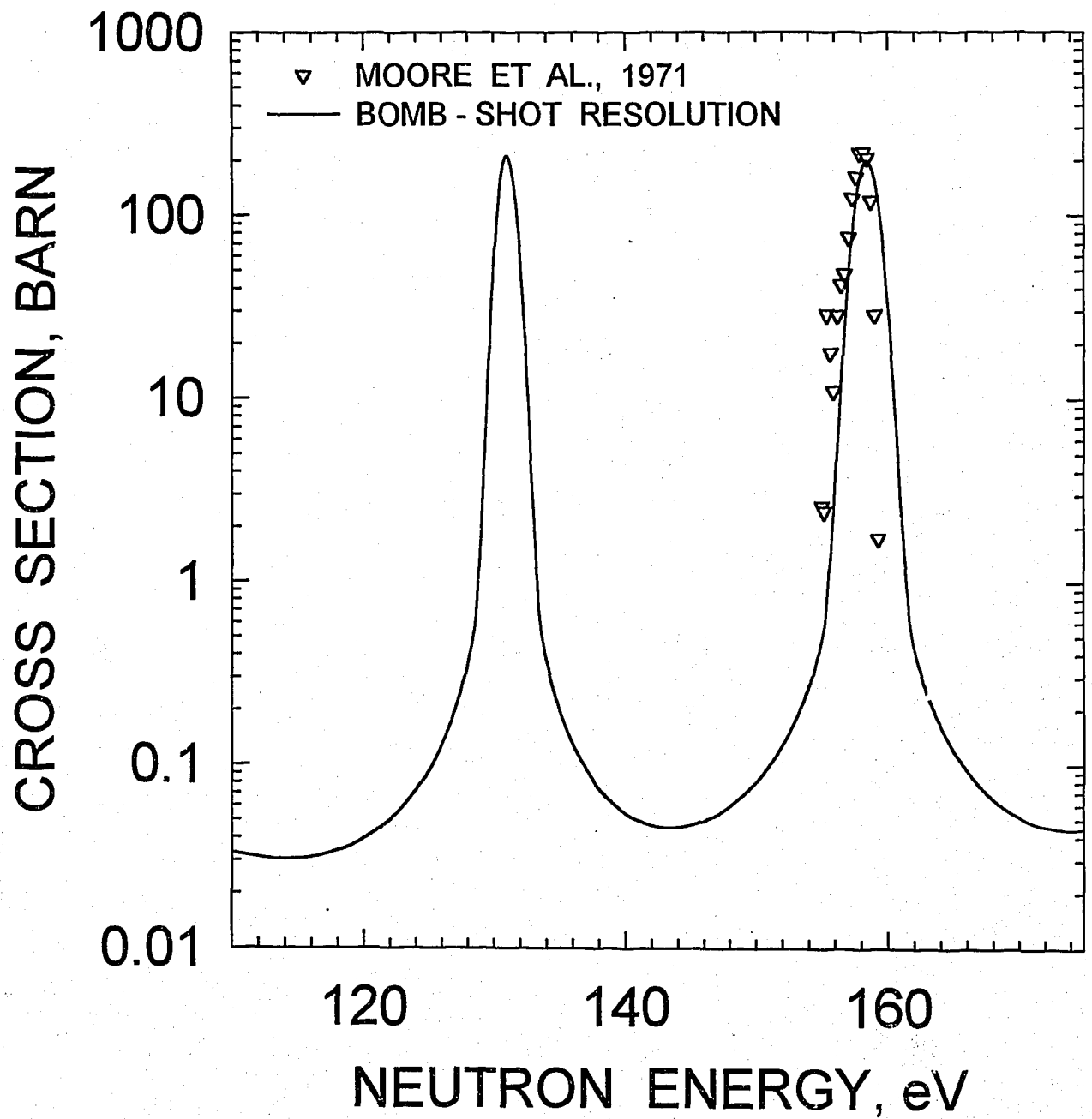
FIG.2.7

^{246}Cm FISSION CROSS SECTION
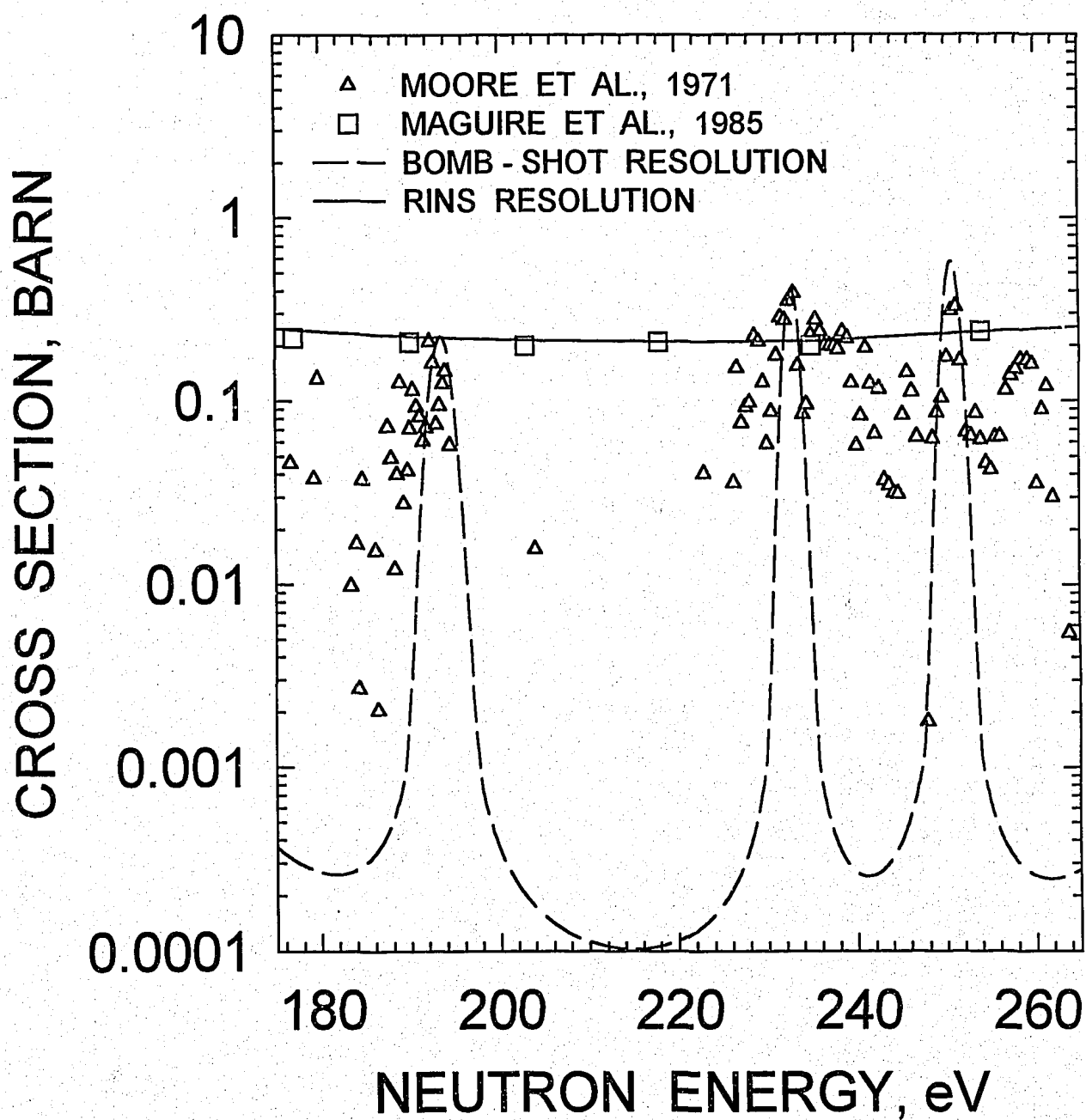
FIG.2.8

^{246}Cm CAPTURE CROSS SECTION
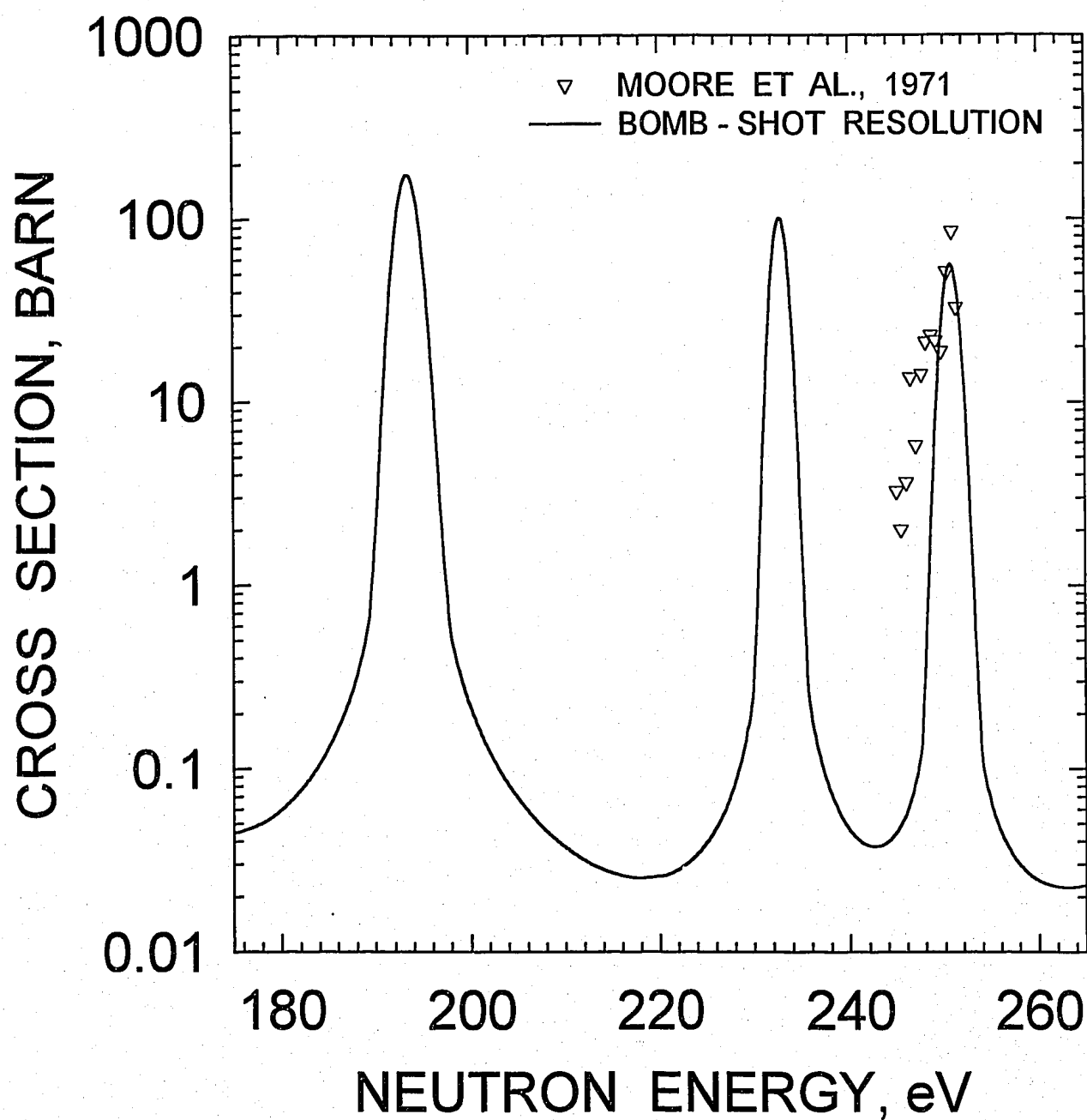
FIG.2.9

^{246}Cm FISSION CROSS SECTION
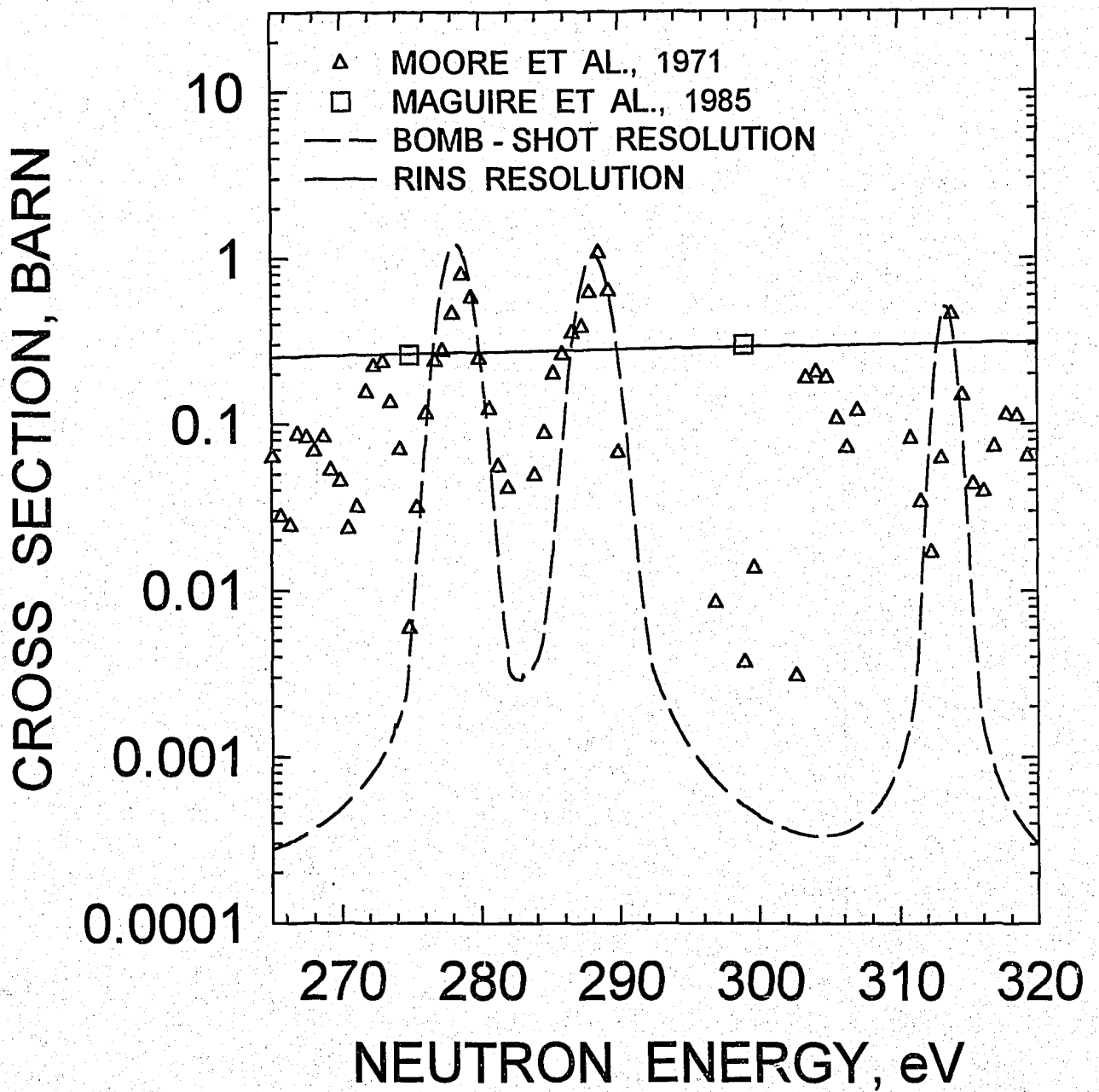
FIG.2.10

^{246}Cm CAPTURE CROSS SECTION
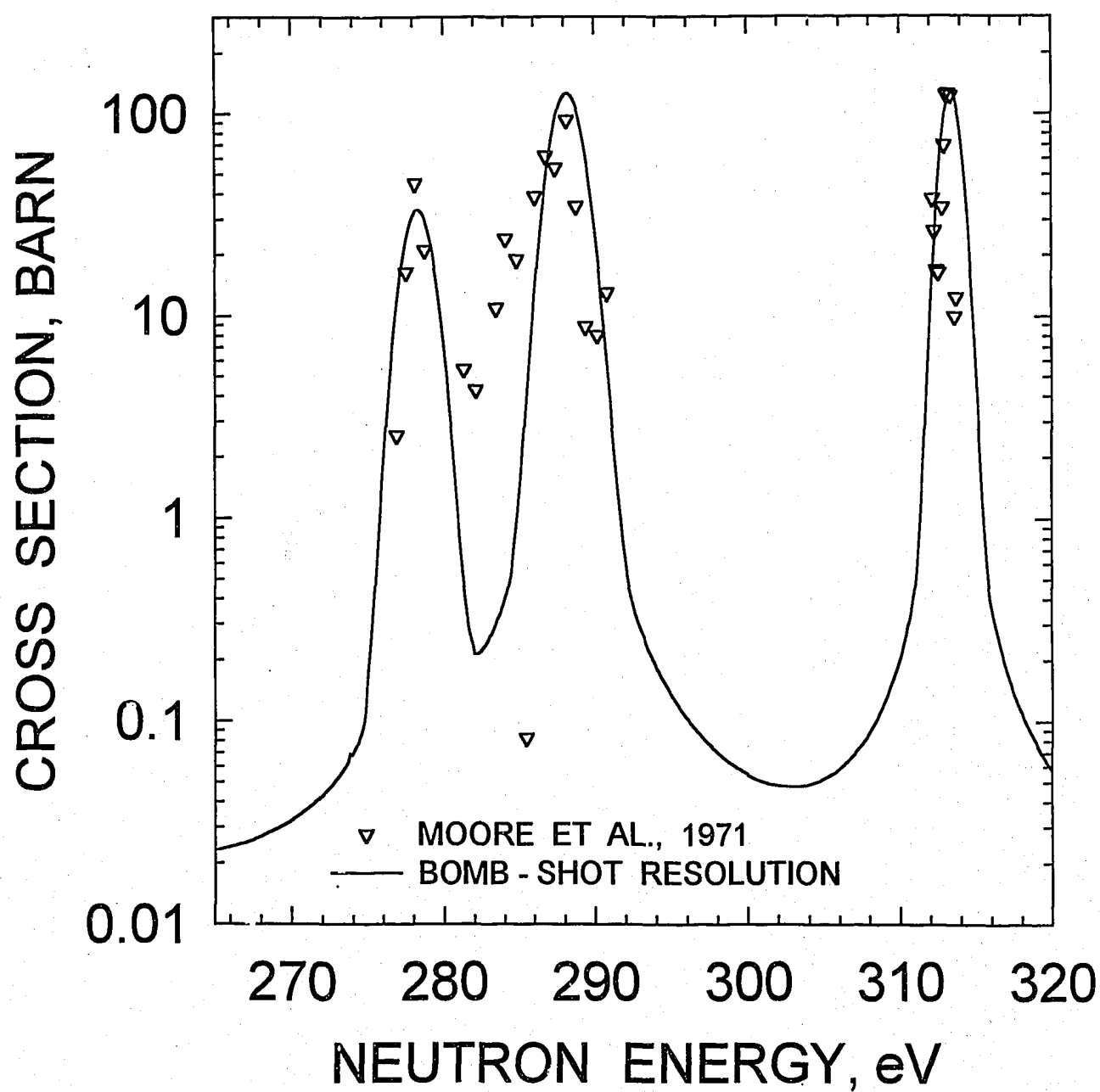
FIG.2.11

^{246}Cm FISSION CROSS SECTION
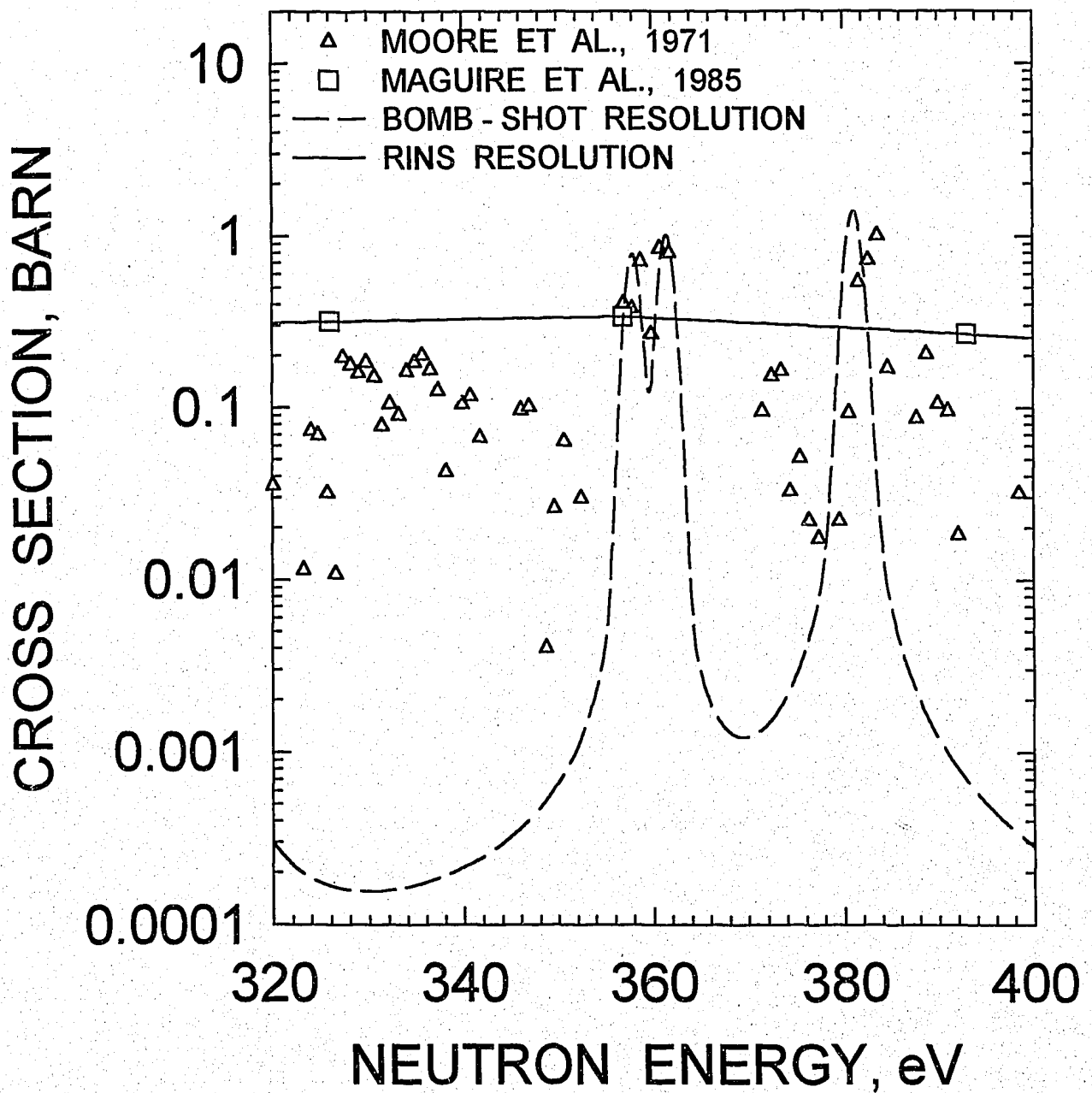
FIG.2.12

^{246}Cm CAPTURE CROSS SECTION
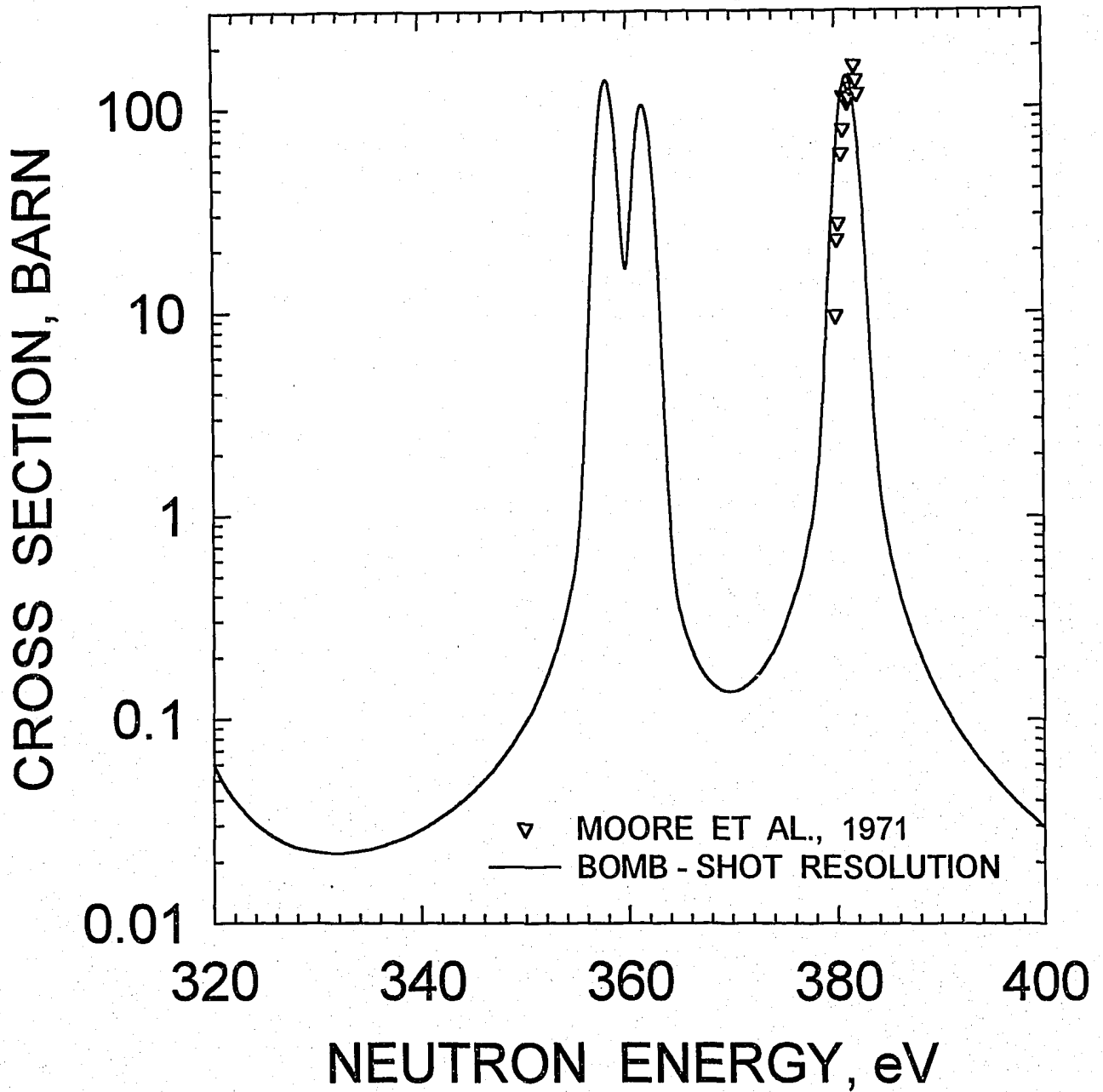
FIG.2.13

FIG.3.1

^{246}Cm CUMULATIVE SUM OF REDUCED NEUTRON WIDTHS
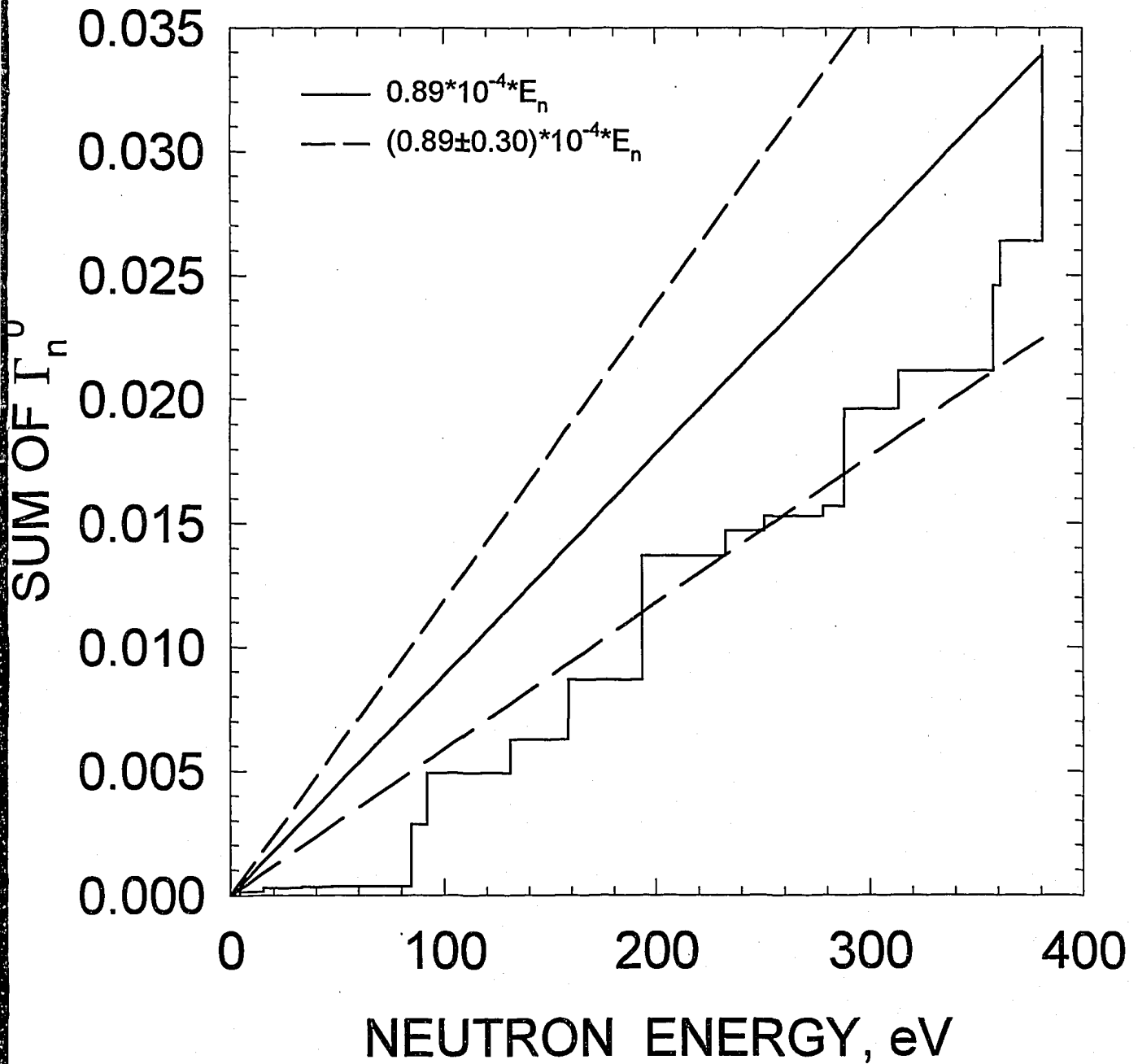
FIG.3.2

^{246}Cm REDUCED NEUTRON WIDTH DISTRIBUTION
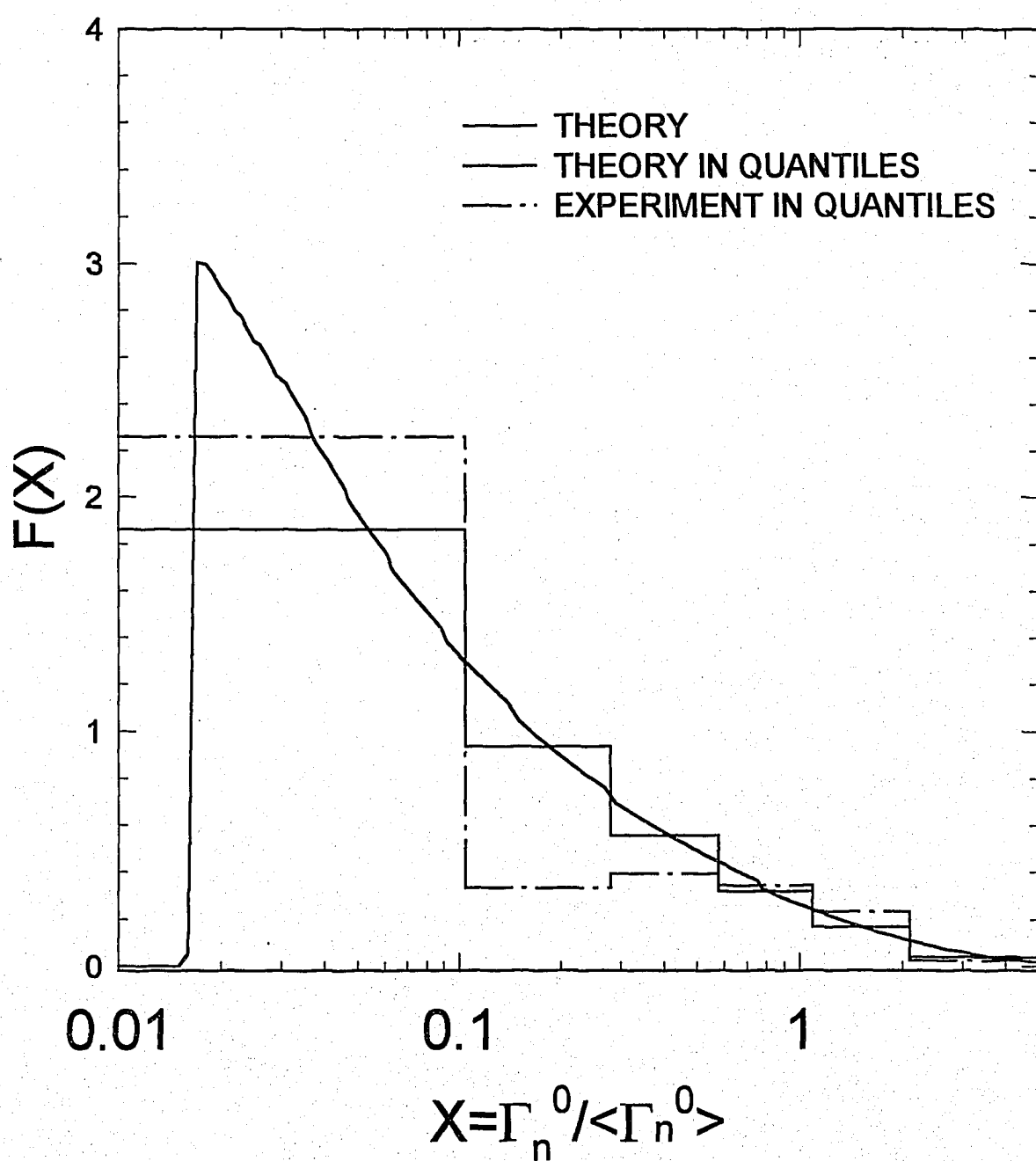
FIG.3.3
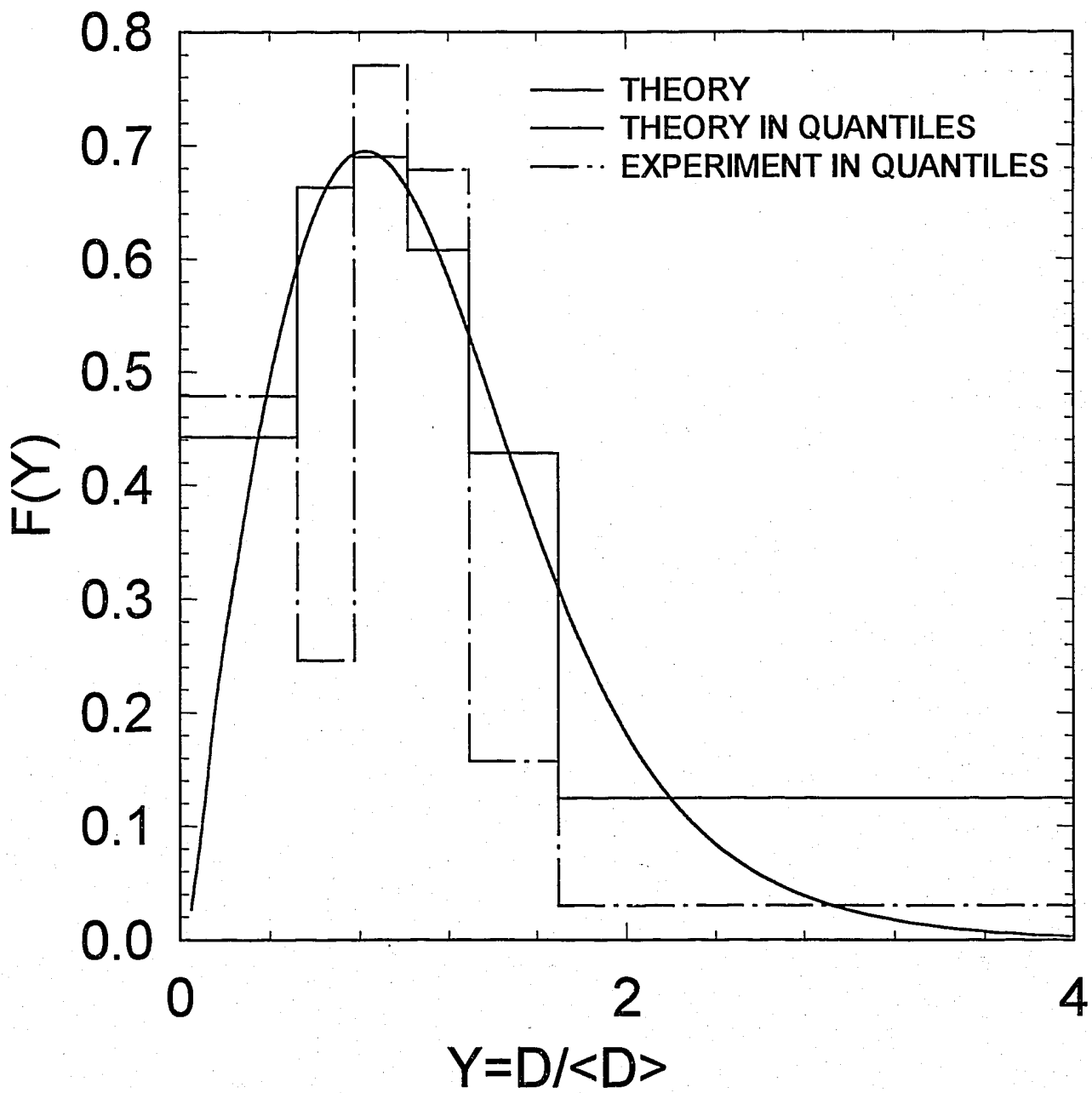
FIG.3.4

^{246}Cm FISSION CROSS SECTION
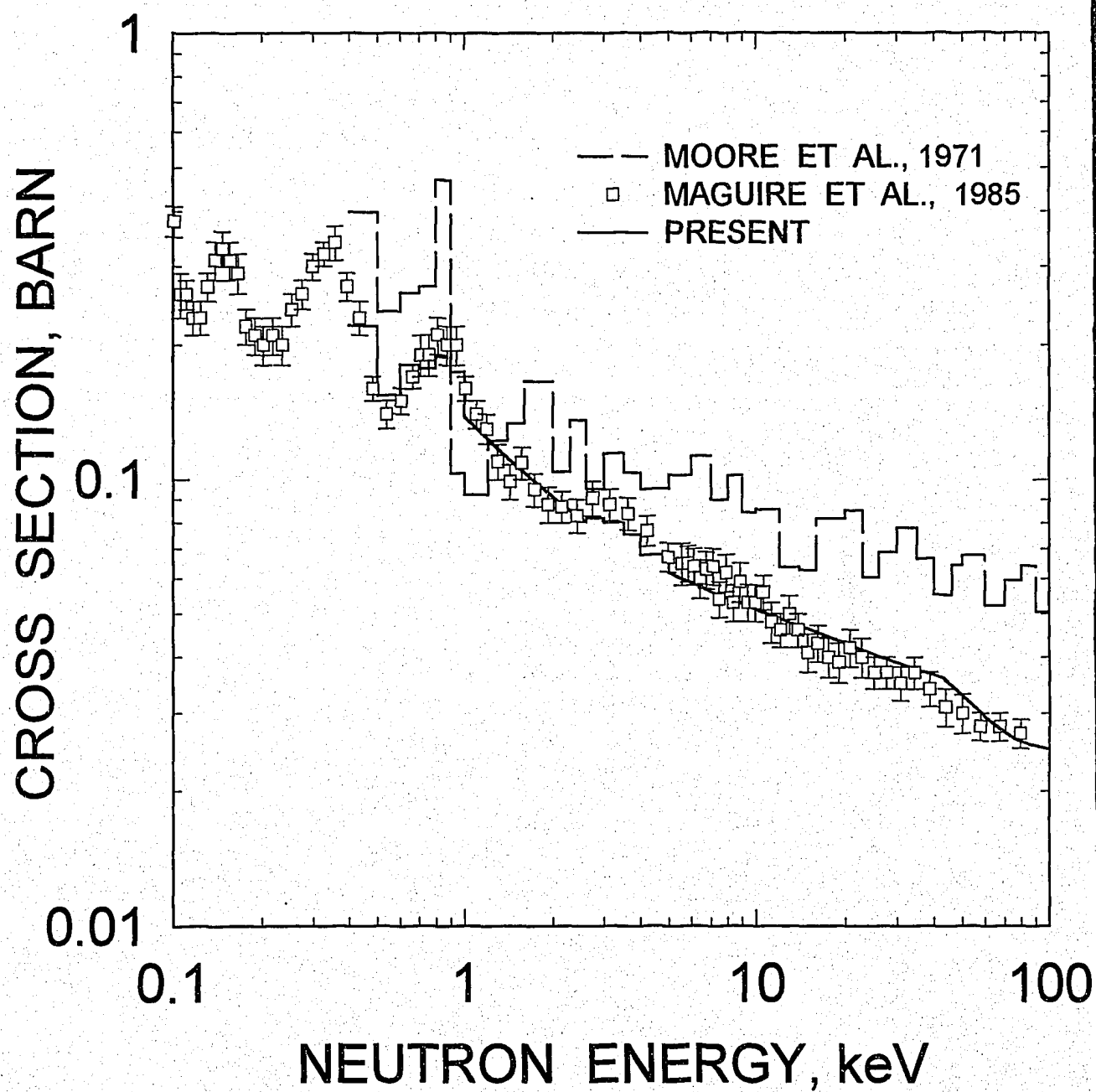
FIG.3.5

^{246}Cm FISSION CROSS SECTION
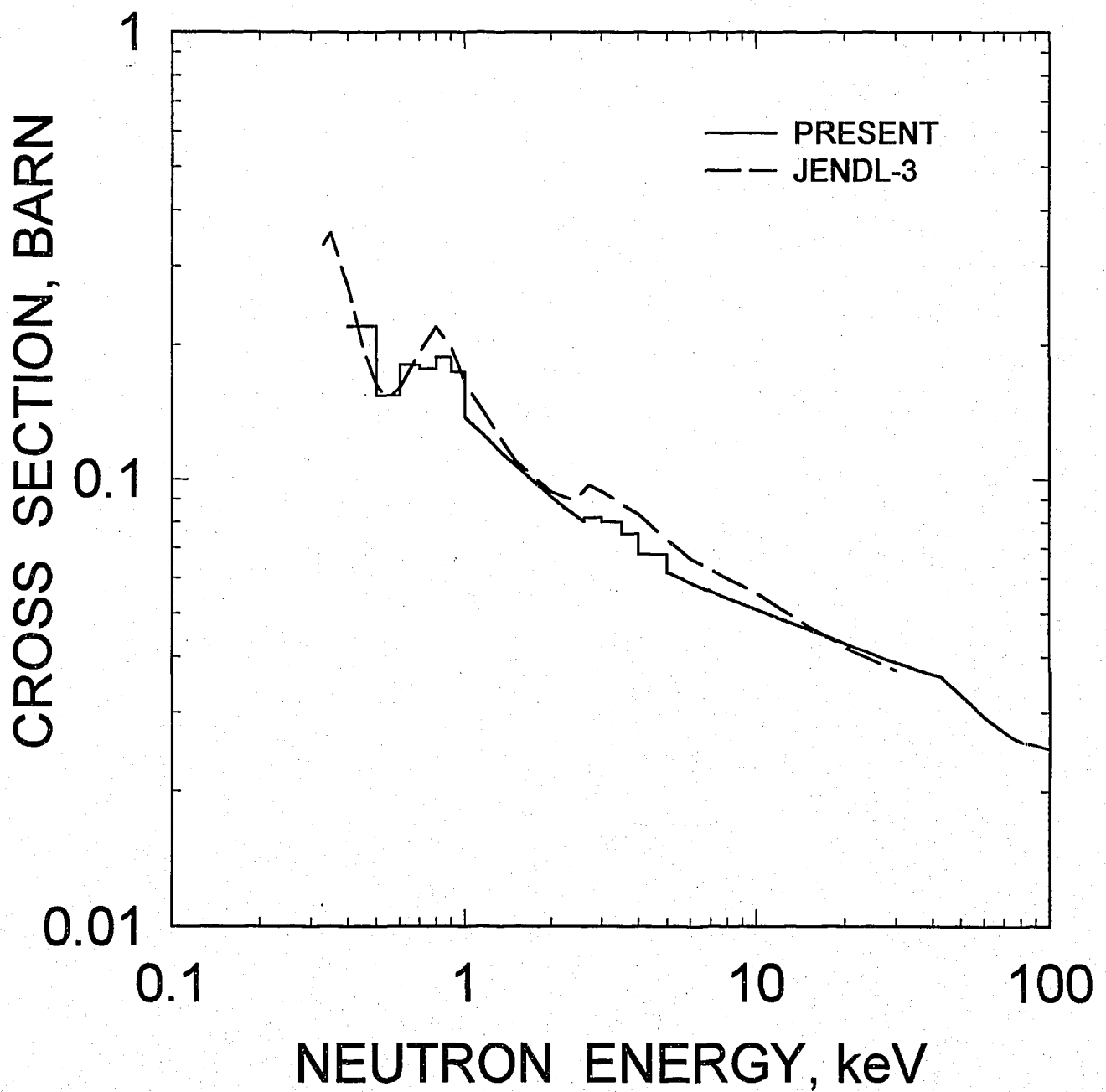
FIG.3.6

^{246}Cm CAPTURE CROSS SECTION
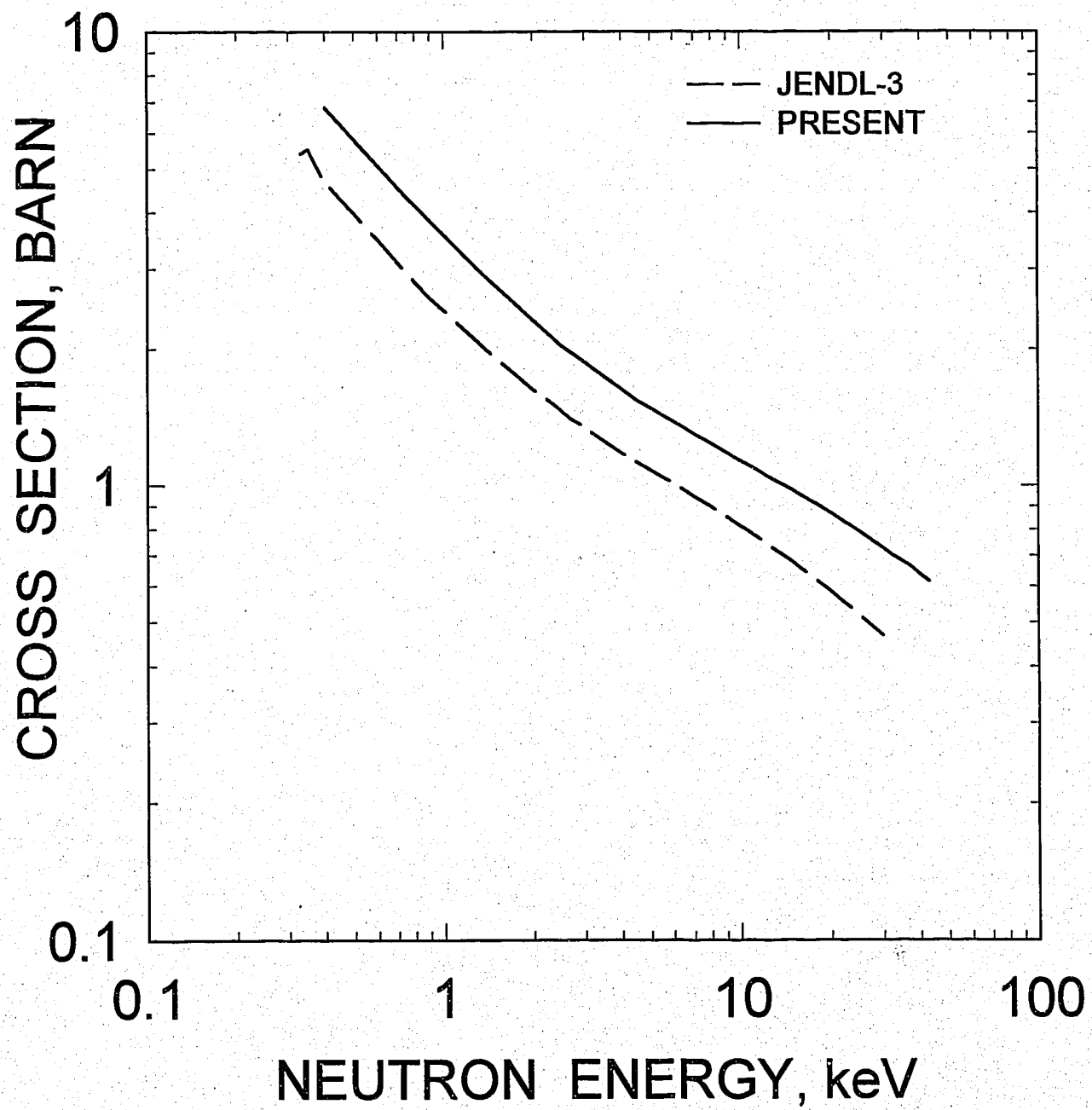
FIG.3.7

^{246}Cm REACTION CROSS SECTION
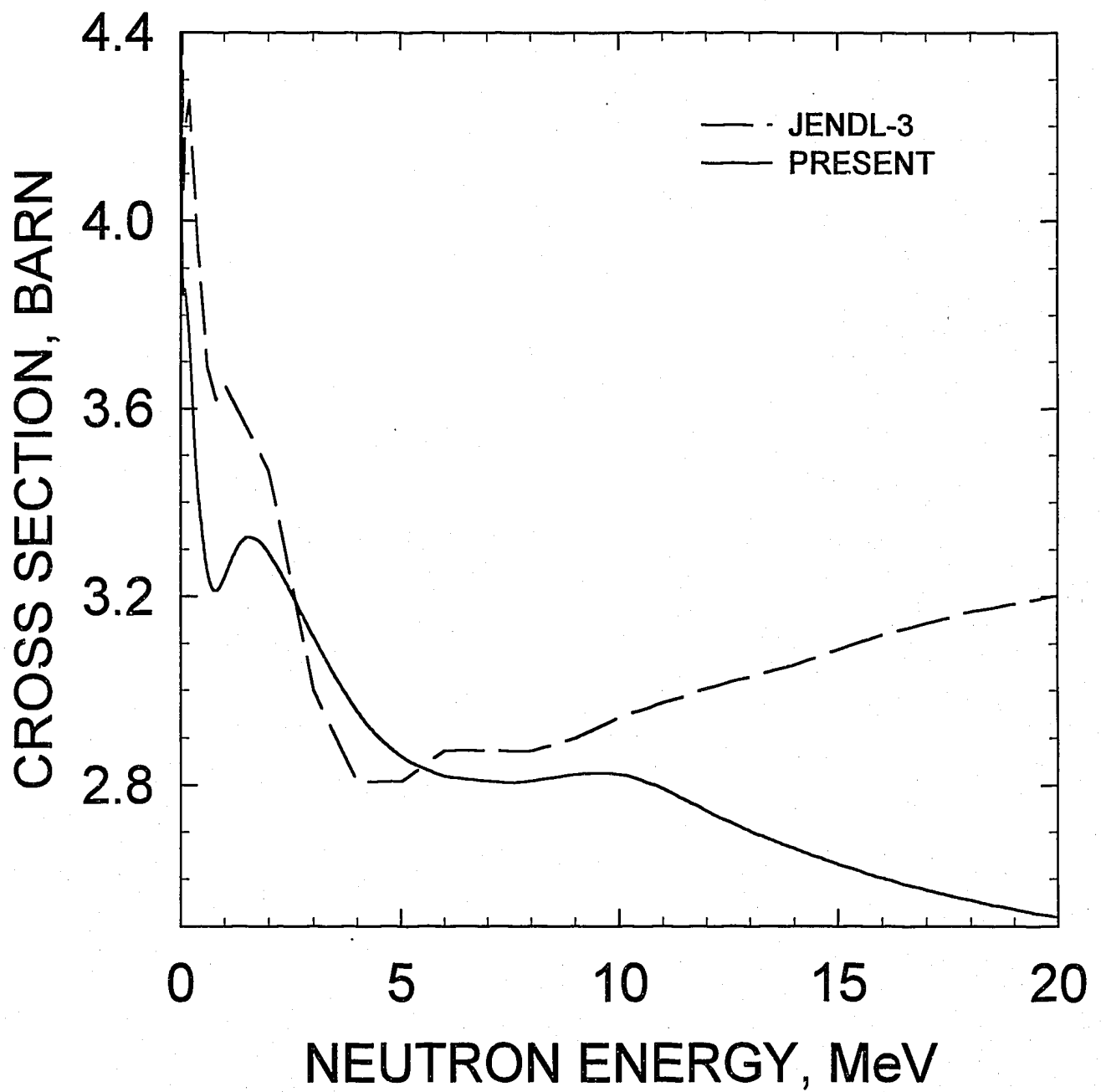
FIG.4.1

^{246}Cm TOTAL CROSS SECTION
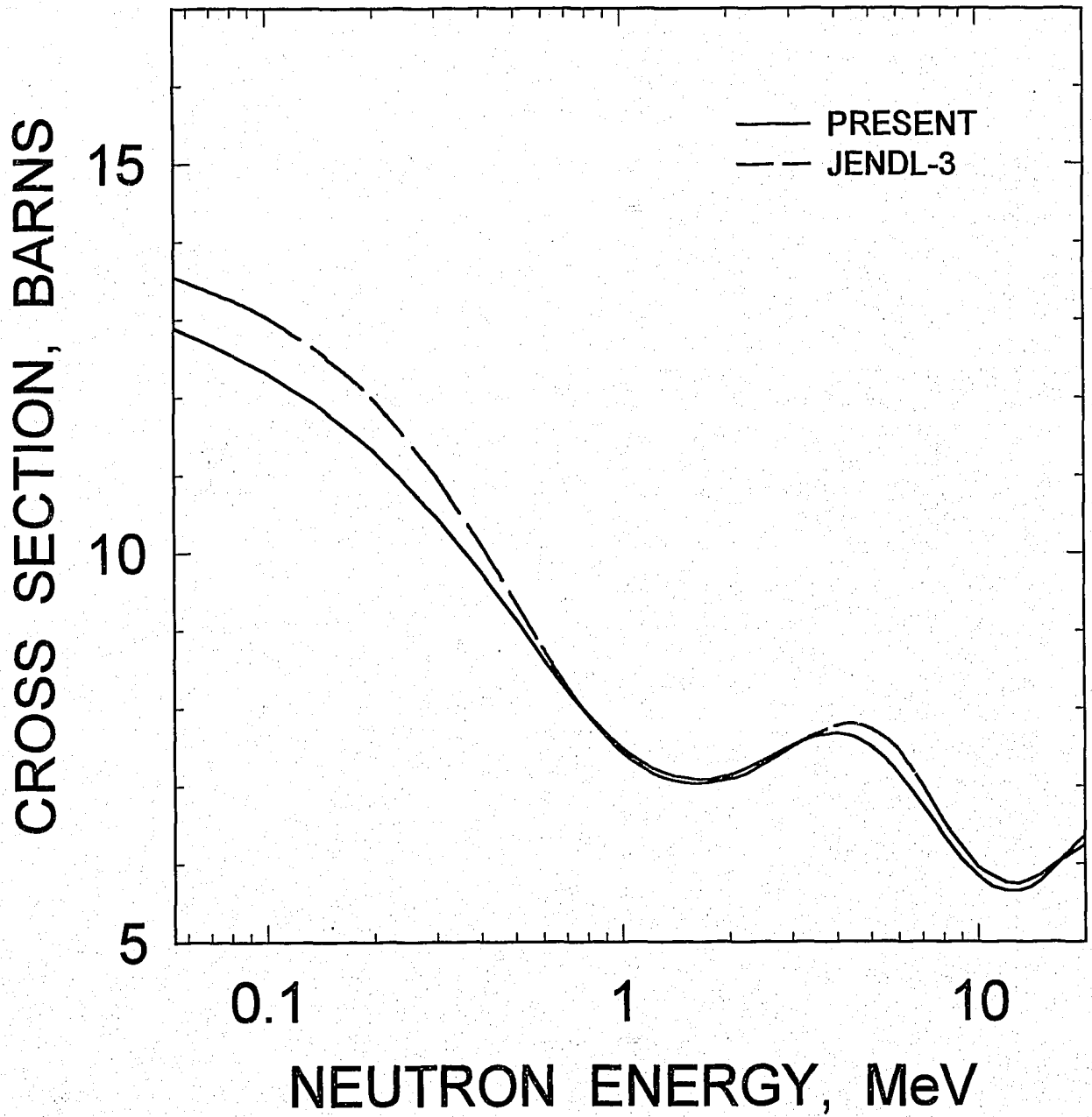
FIG. 4.2

²⁴⁶Cm ELASTIC SCATTERING CROSS SECTION
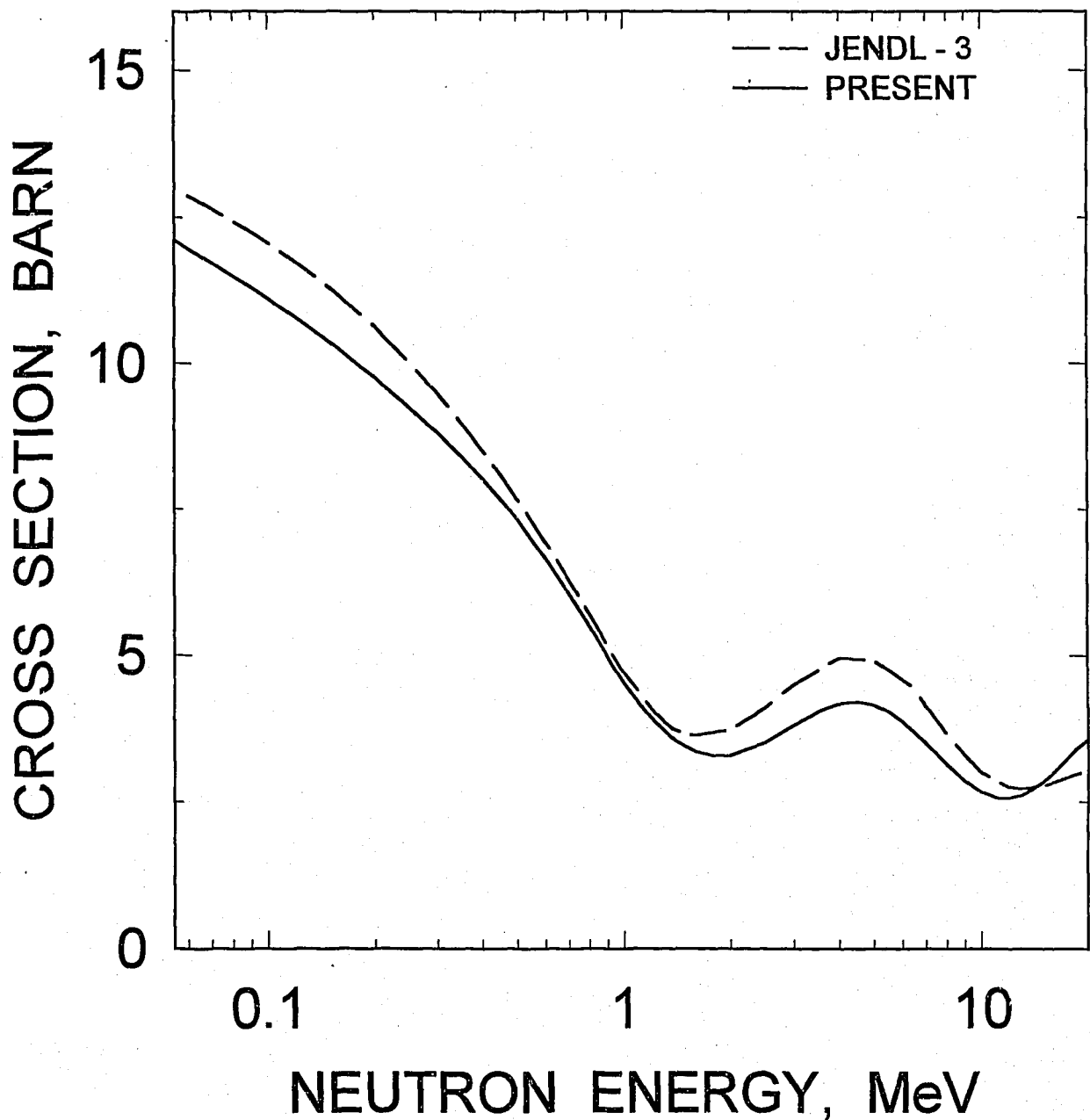
FIG. 4.3

^{246}Cm FISSION CROSS SECTION
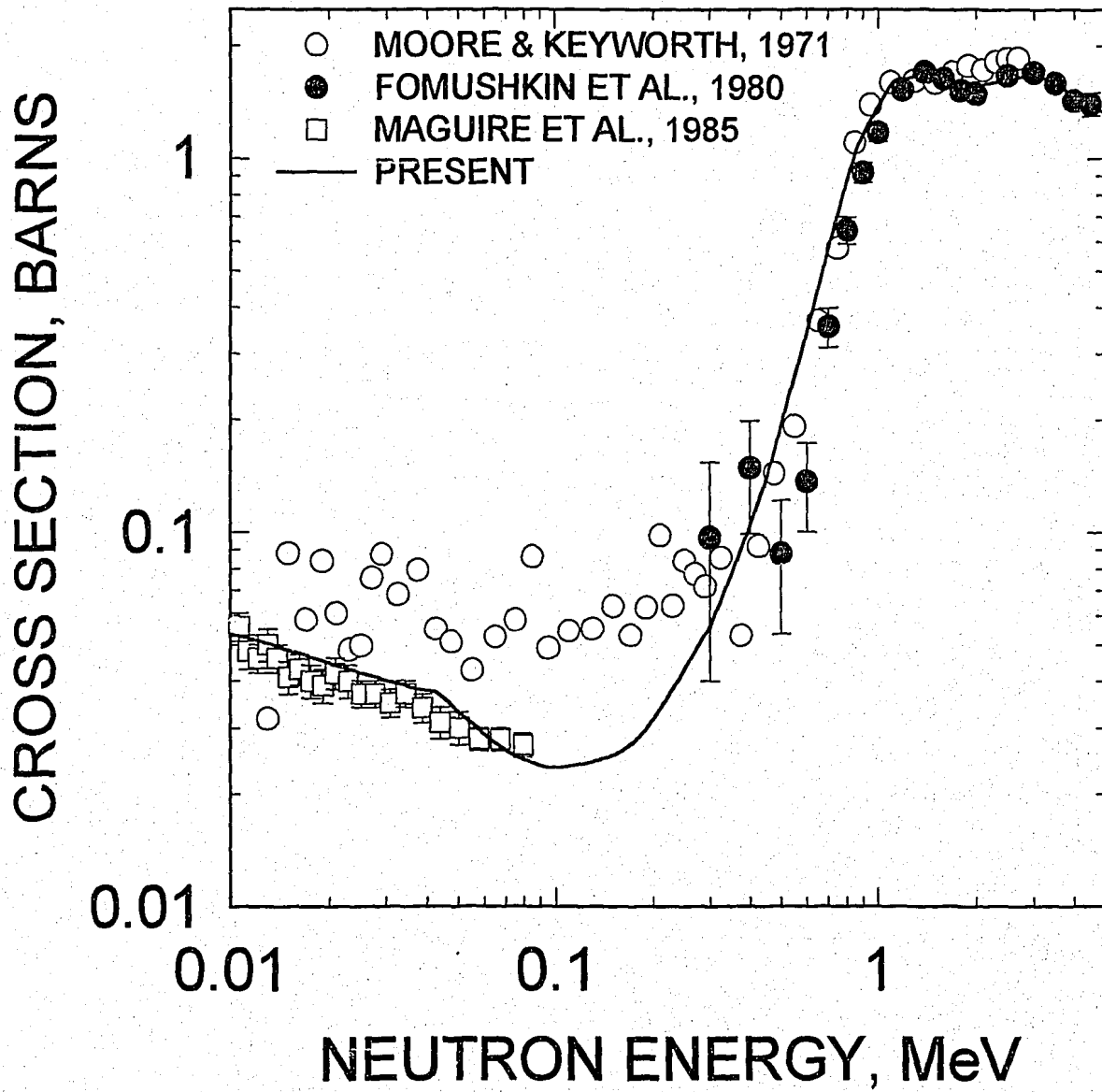
FIG. 4.4

^{246}Cm FISSION CROSS SECTION
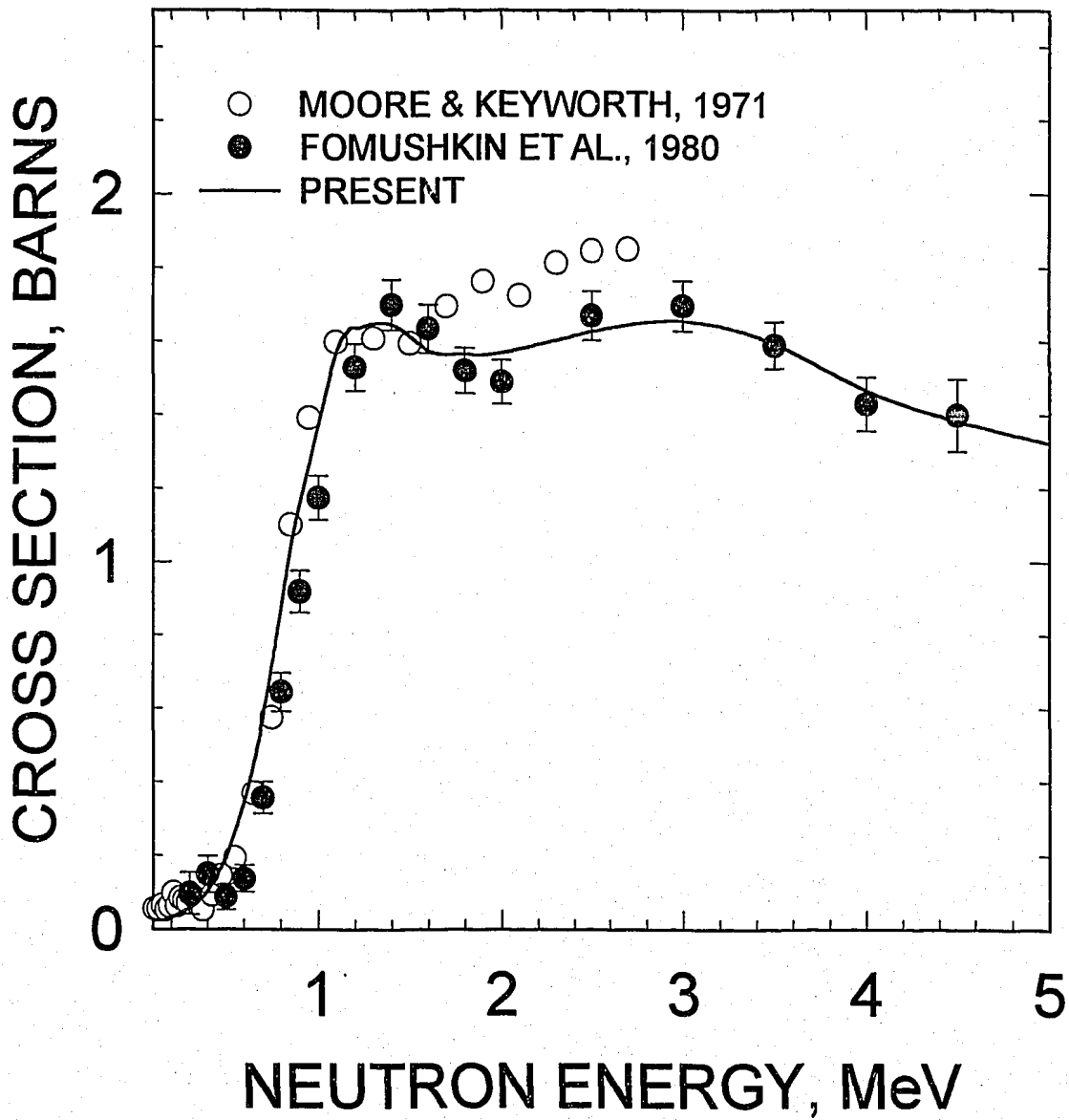
FIG. 4.5

^{246}Cm FISSION CROSS SECTION
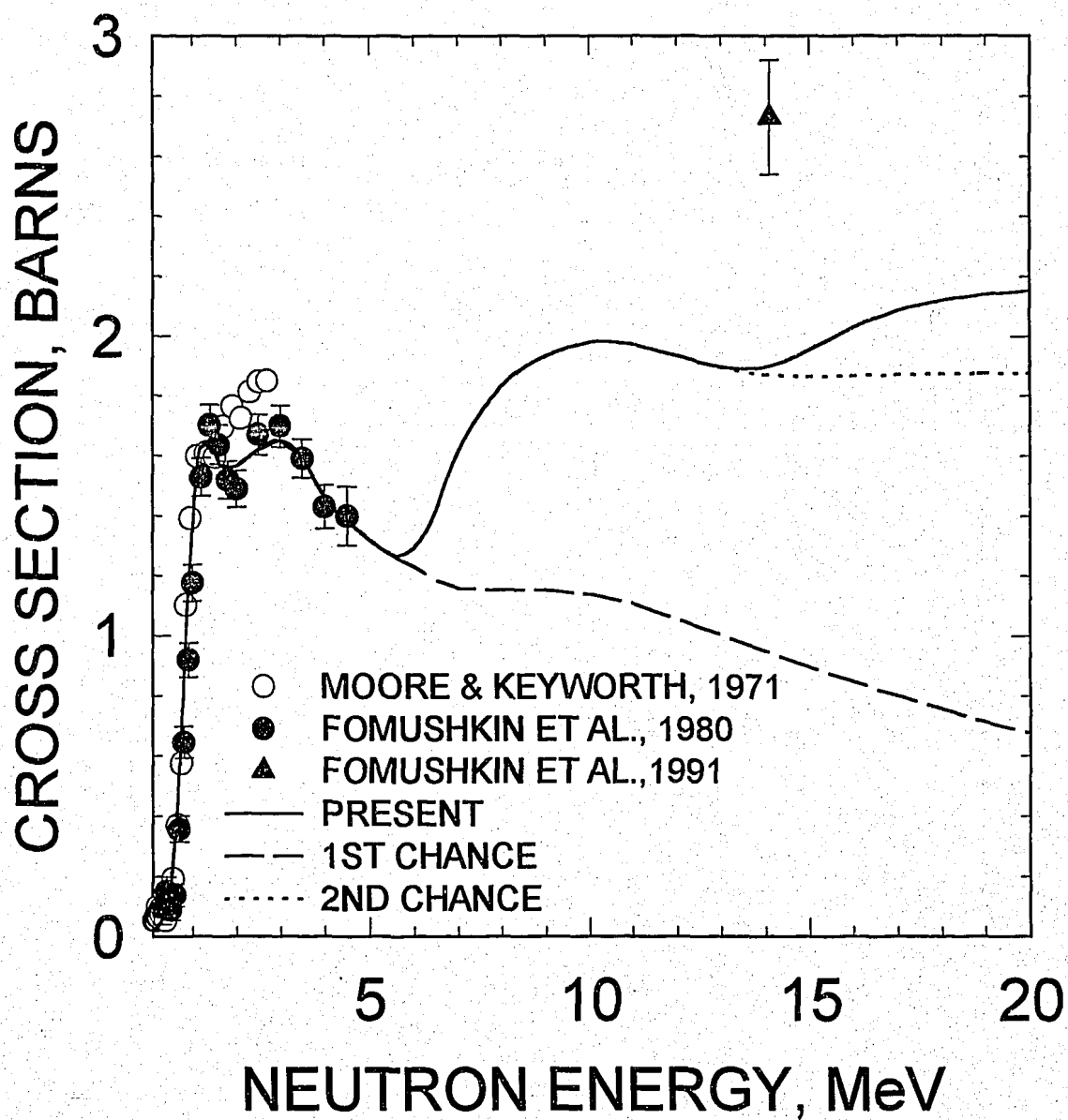
FIG. 4.6

^{245}Cm FISSION CROSS SECTION
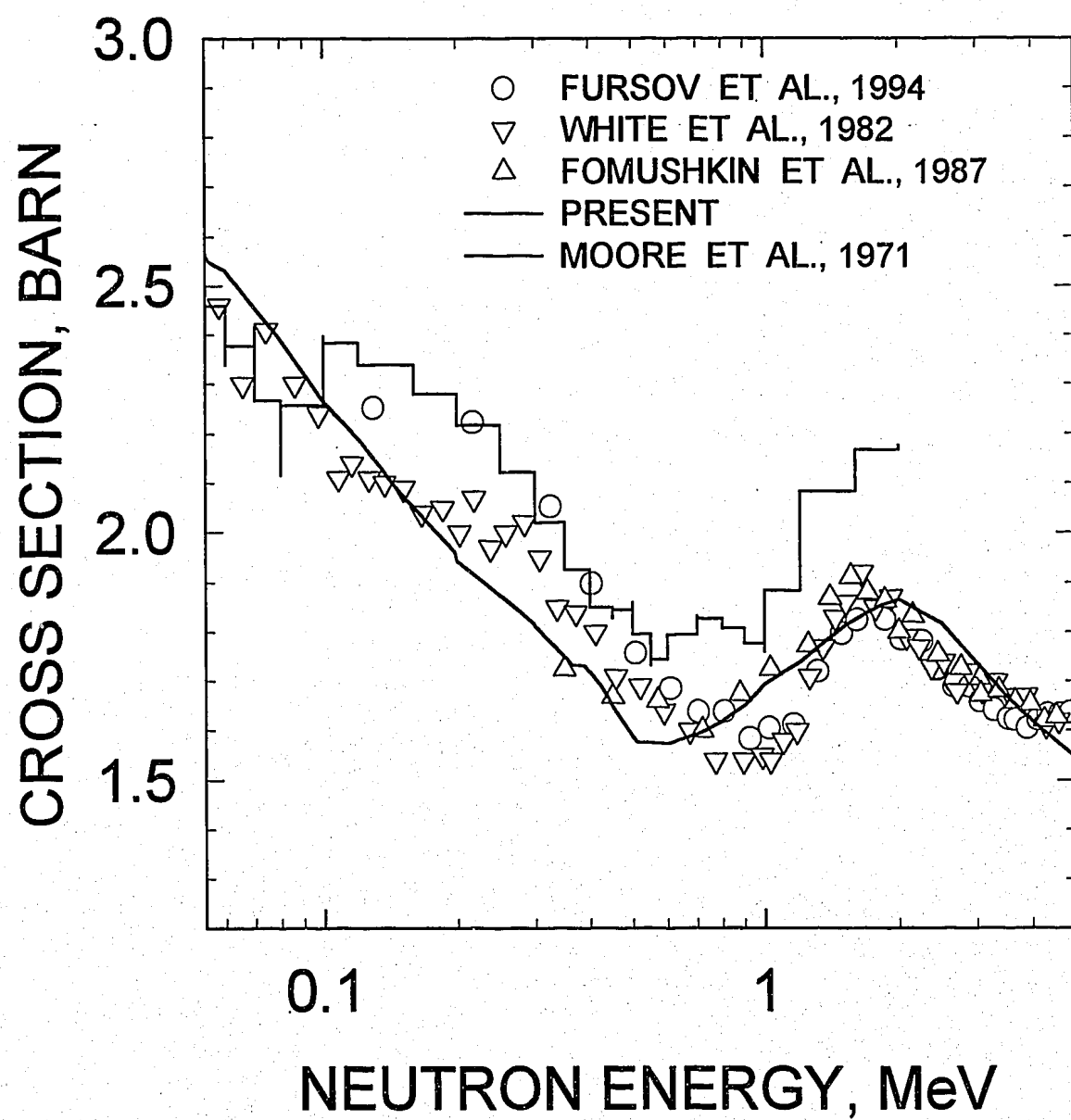
FIG 4.7

^{244}Cm FISSION CROSS SECTION

NEUTRON ENERGY, MeV
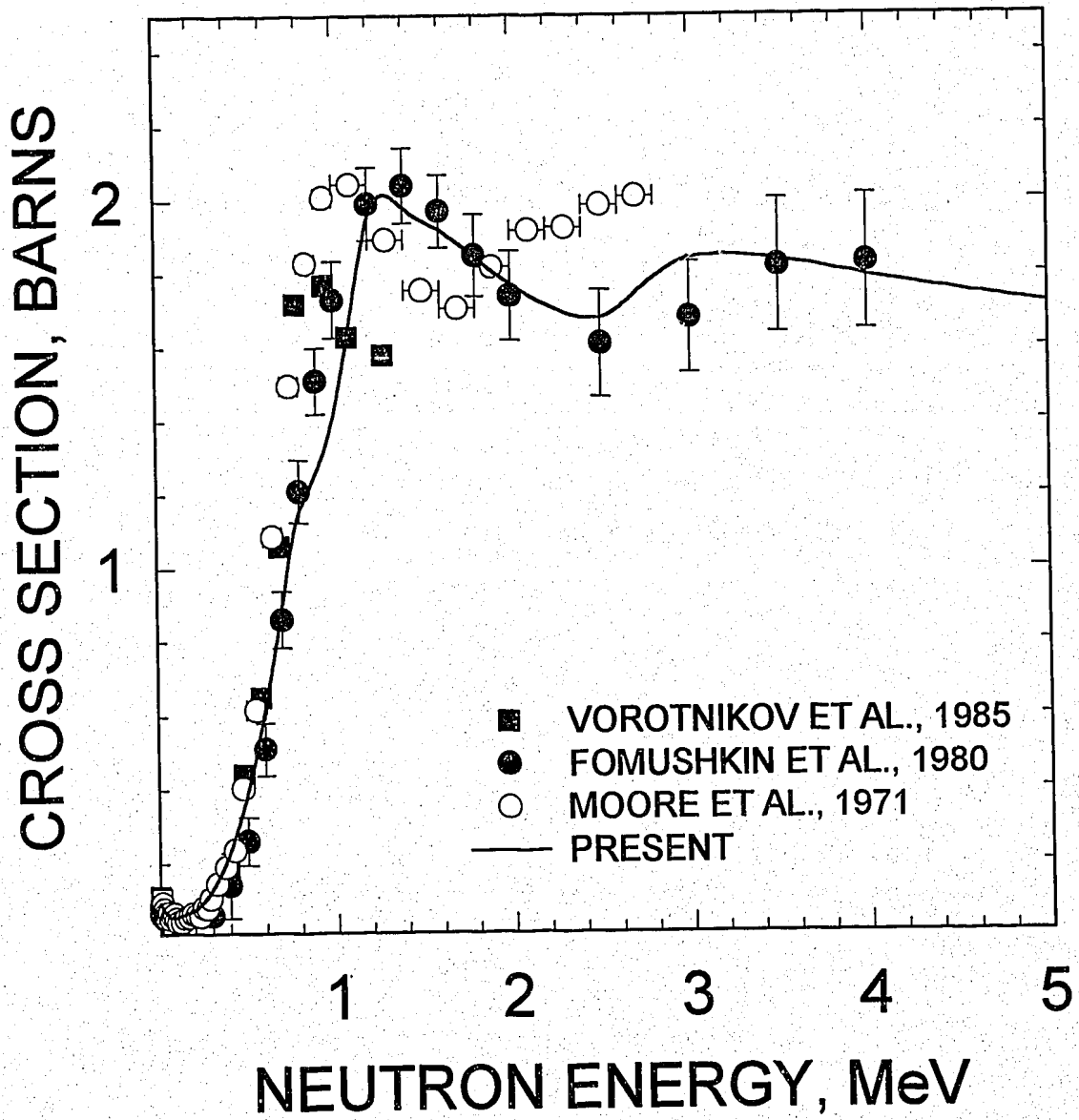
FIG. 4.8

^{246}Cm FISSION CROSS SECTION

FIG. 4.9

FIG.4.10

FIG. 4.11

²⁴⁷Cm

FIG. 4.12

^{246}Cm INELASTIC CROSS SECTION
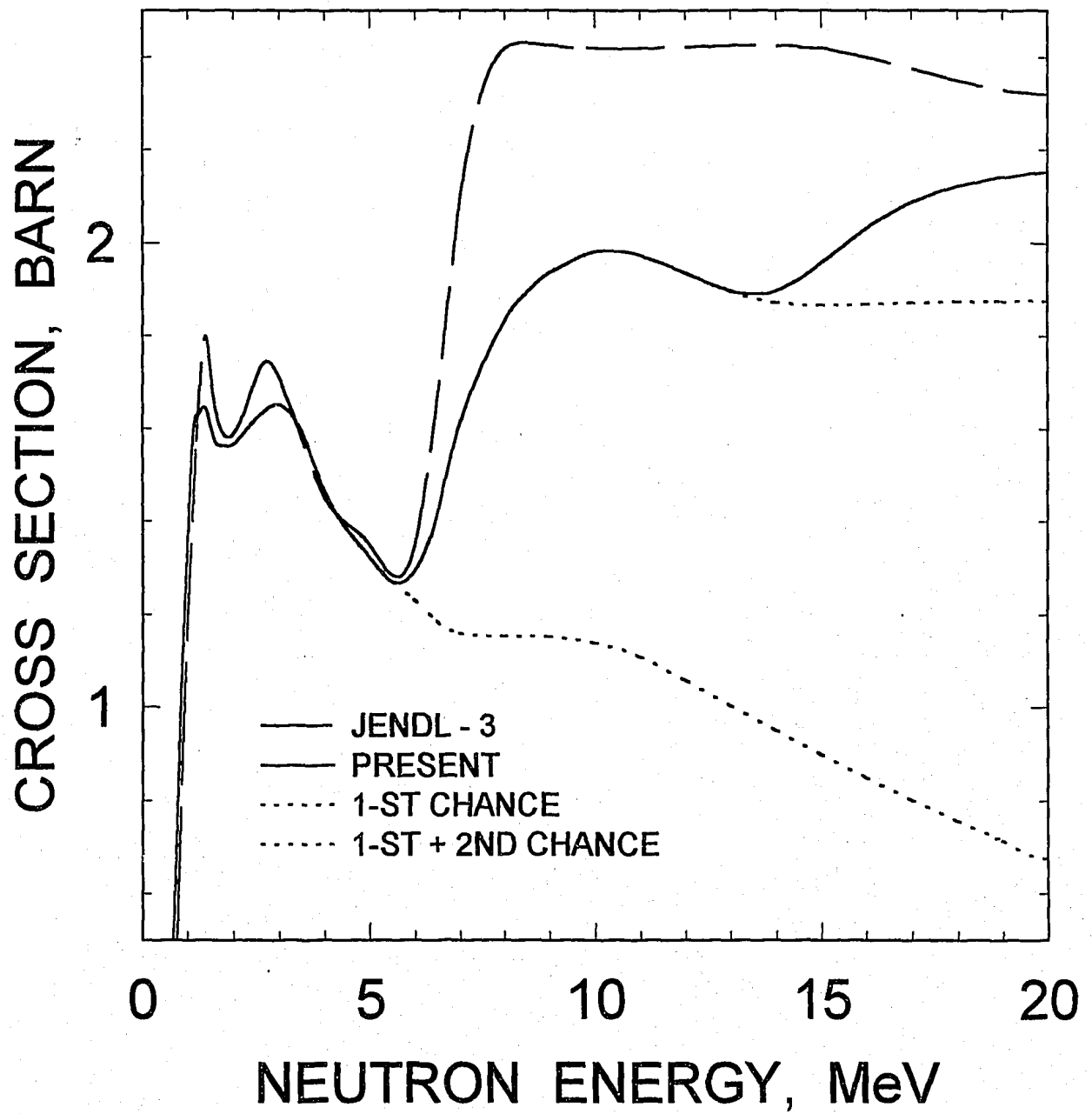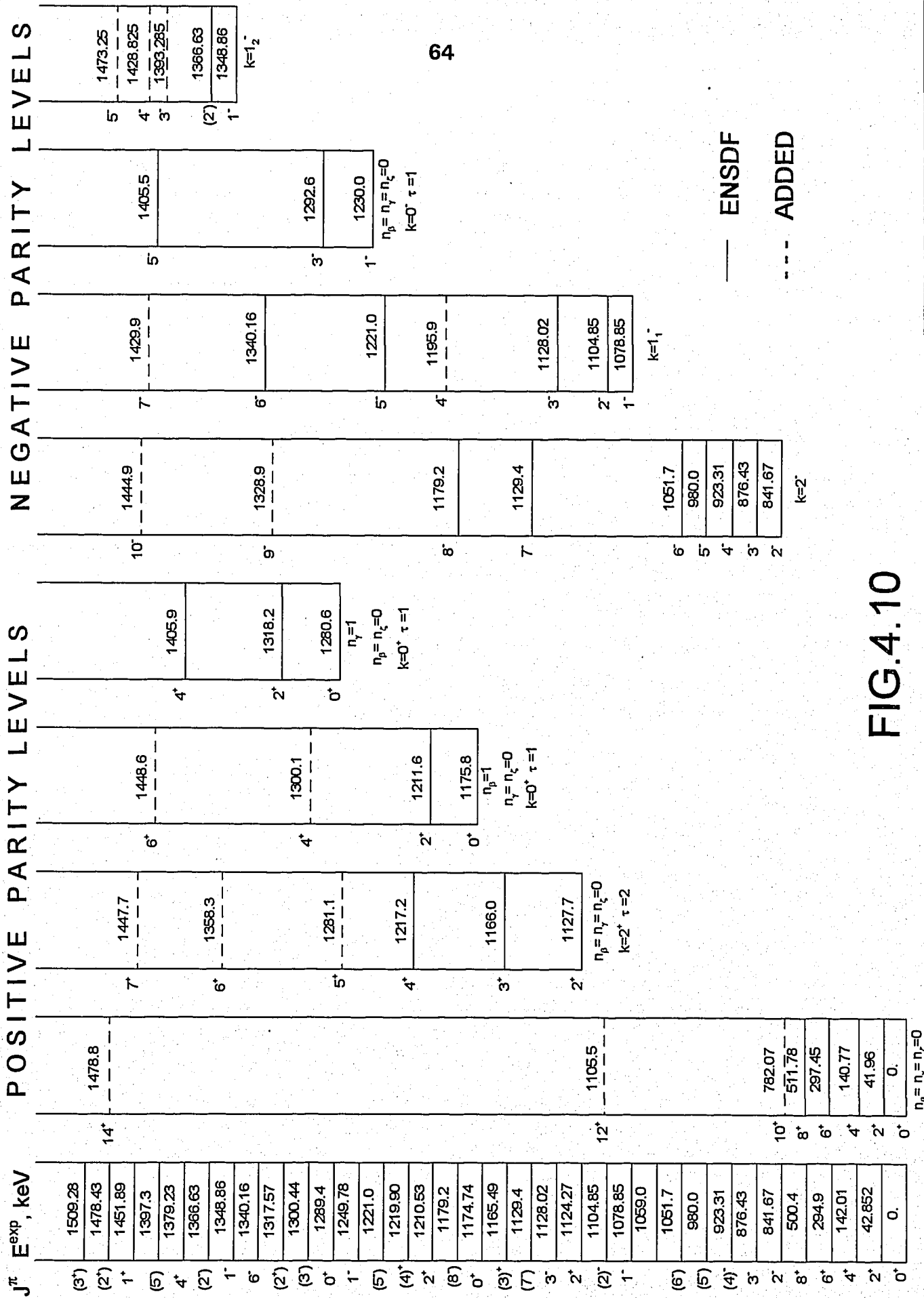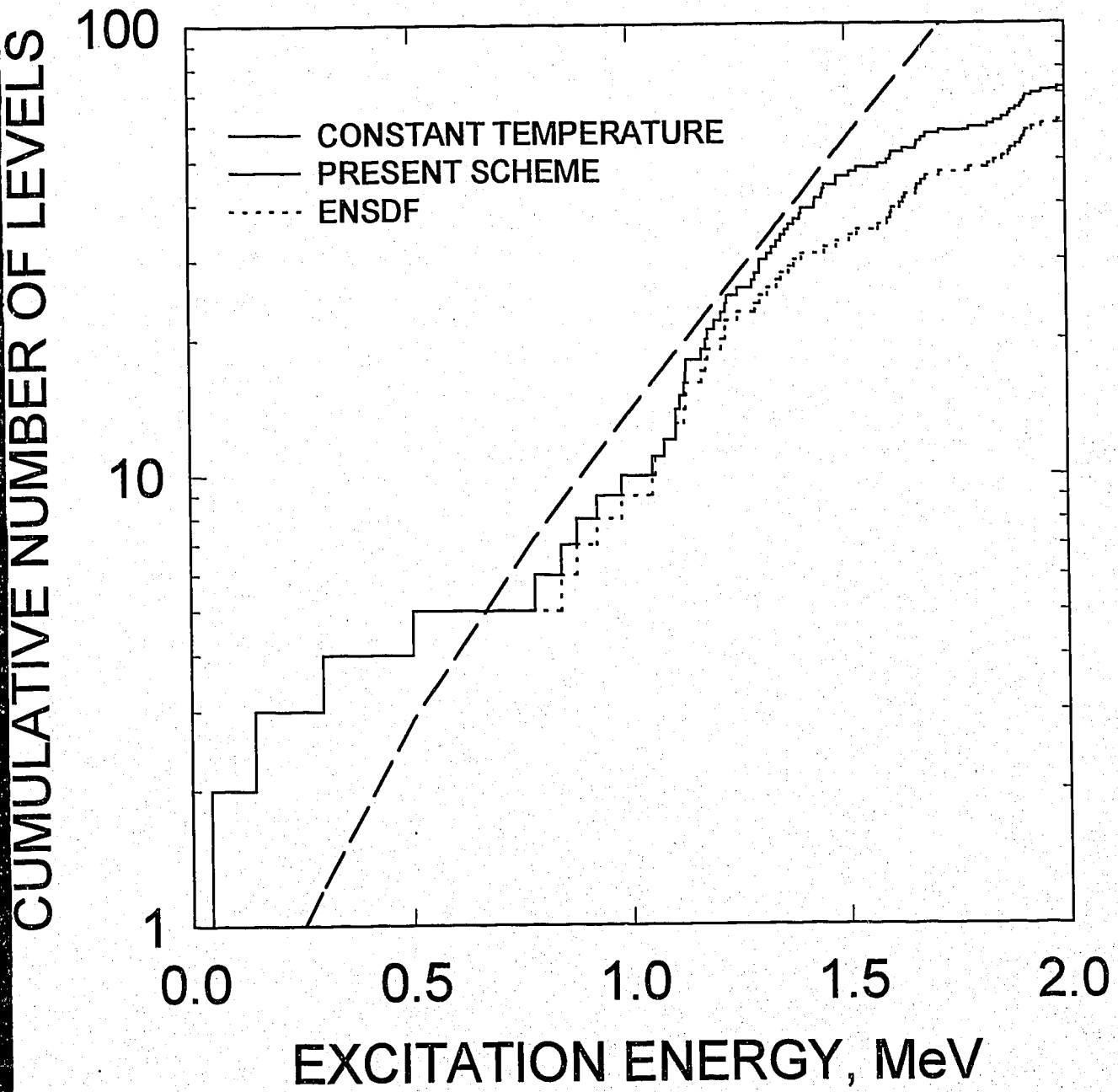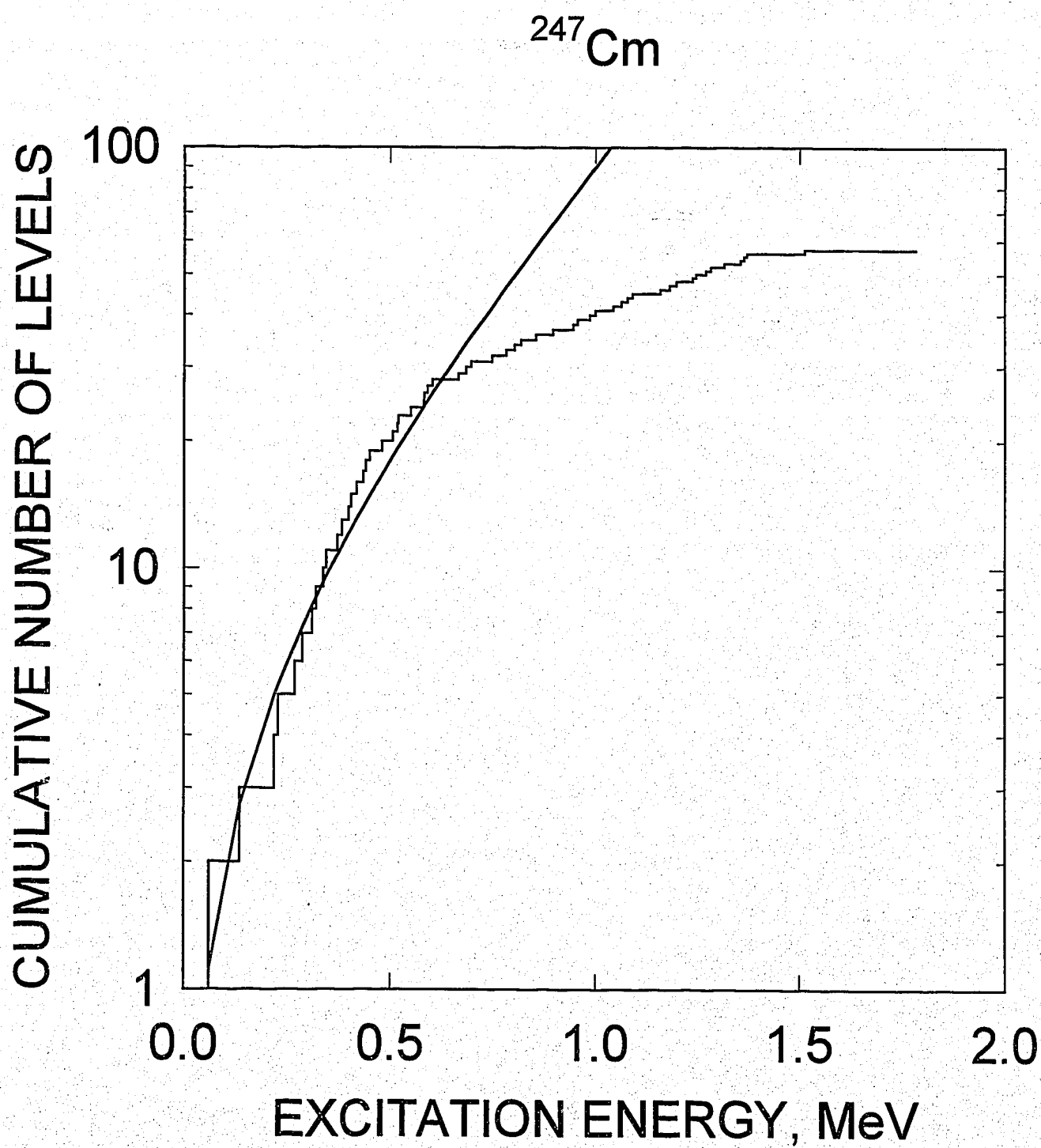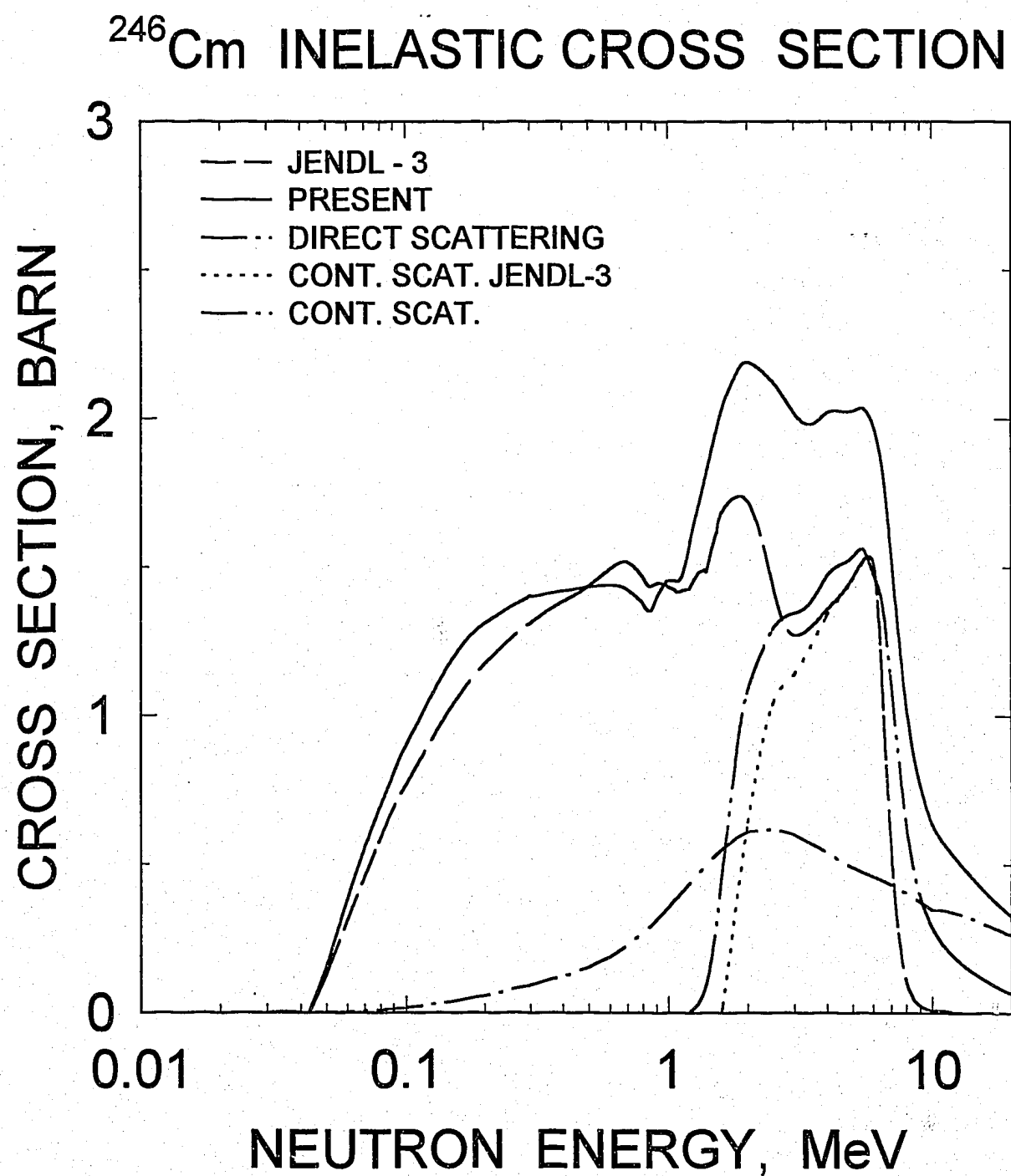
FIG. 4.13

^{246}Cm: 0.04285 MeV, 2$^+$ LEVEL EXCITATION
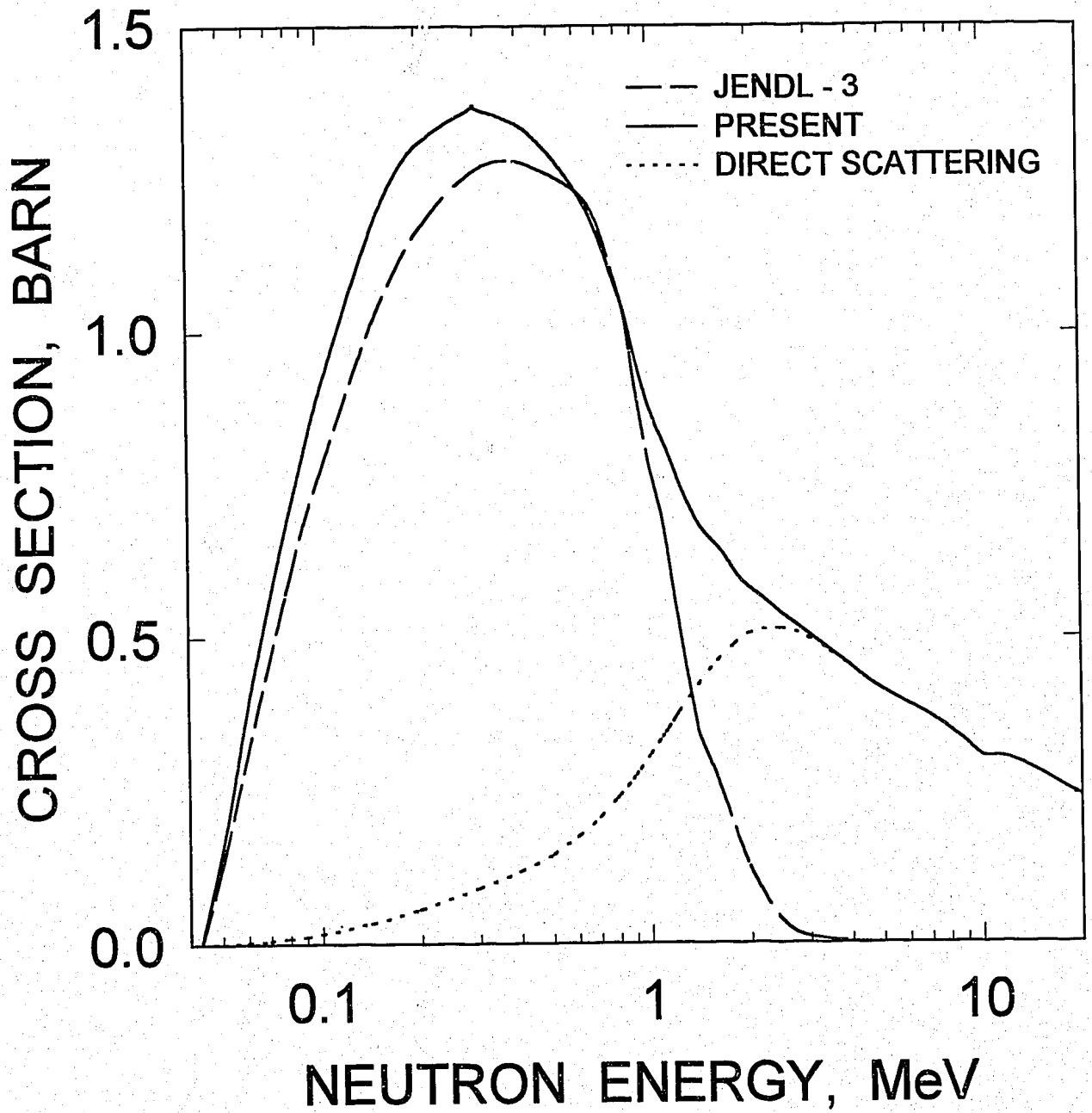
FIG. 4.14

^{246}Cm: 0.142 MeV, 4$^+$ LEVEL EXCITATION
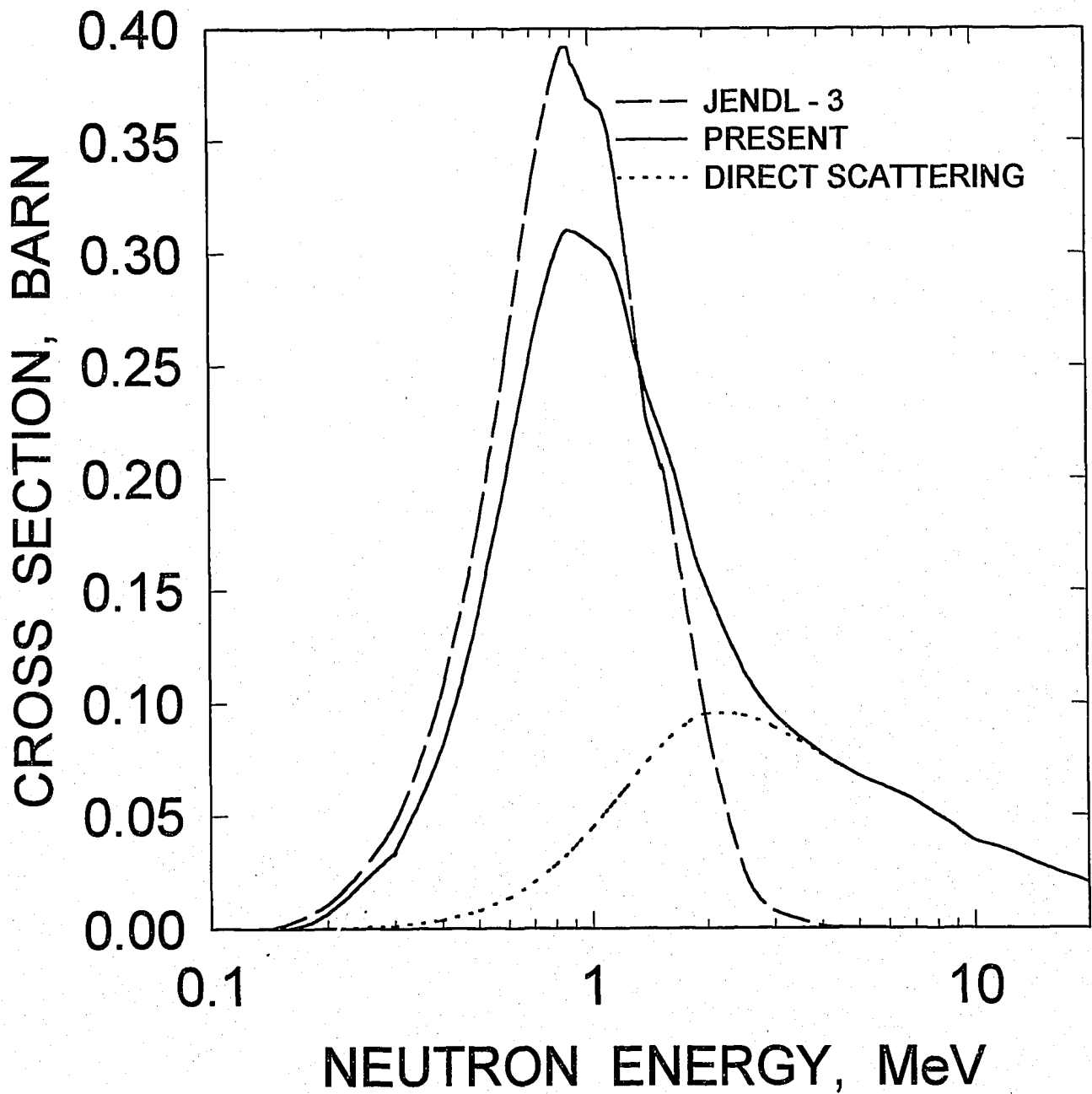
FIG. 4.15

^{246}Cm: 0.2949 MeV, 6^+ LEVEL EXCITATION
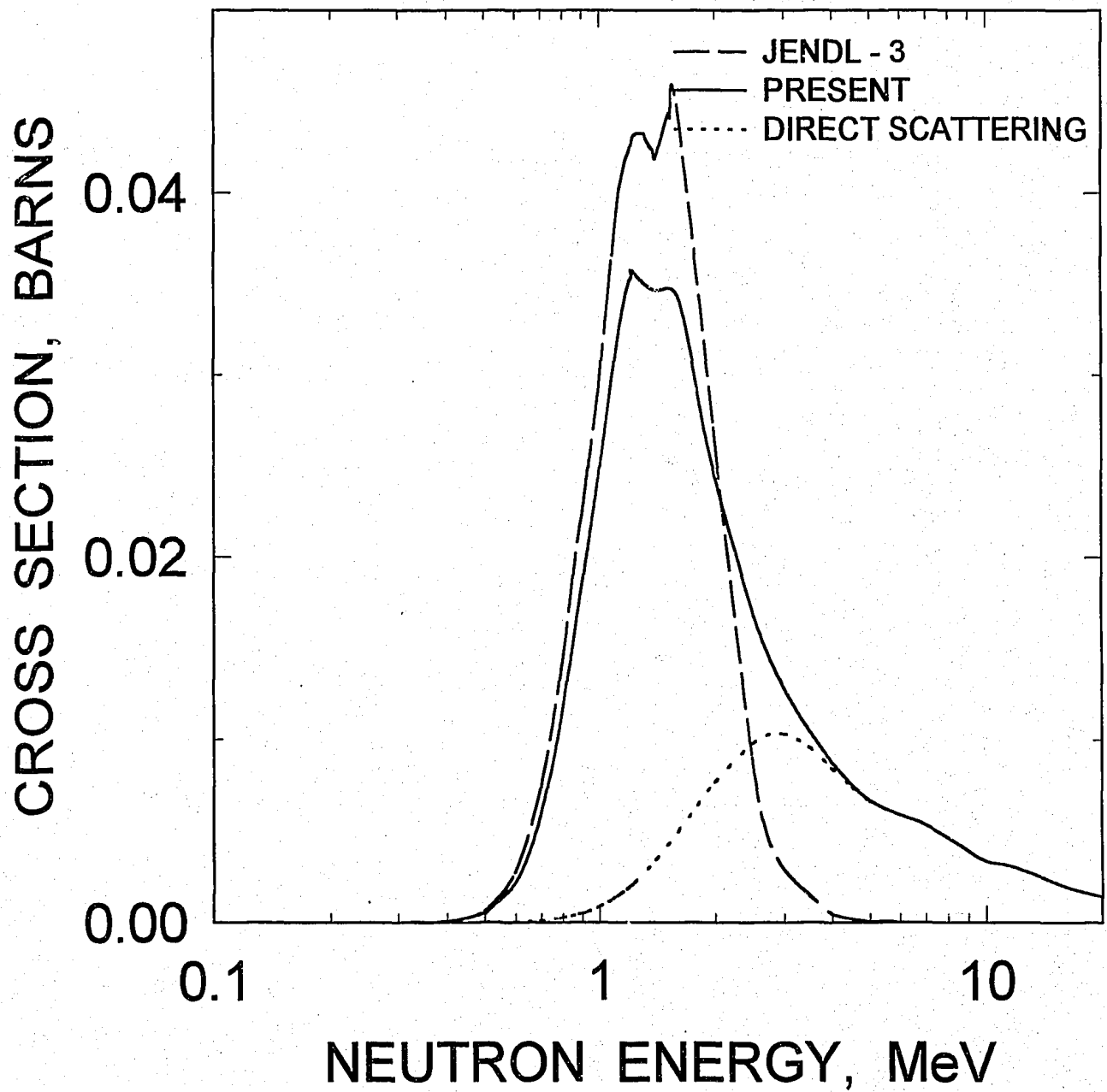
FIG. 4.16

^{246}Cm: 0.5004 MeV, 8$^+$ LEVEL EXCITATION
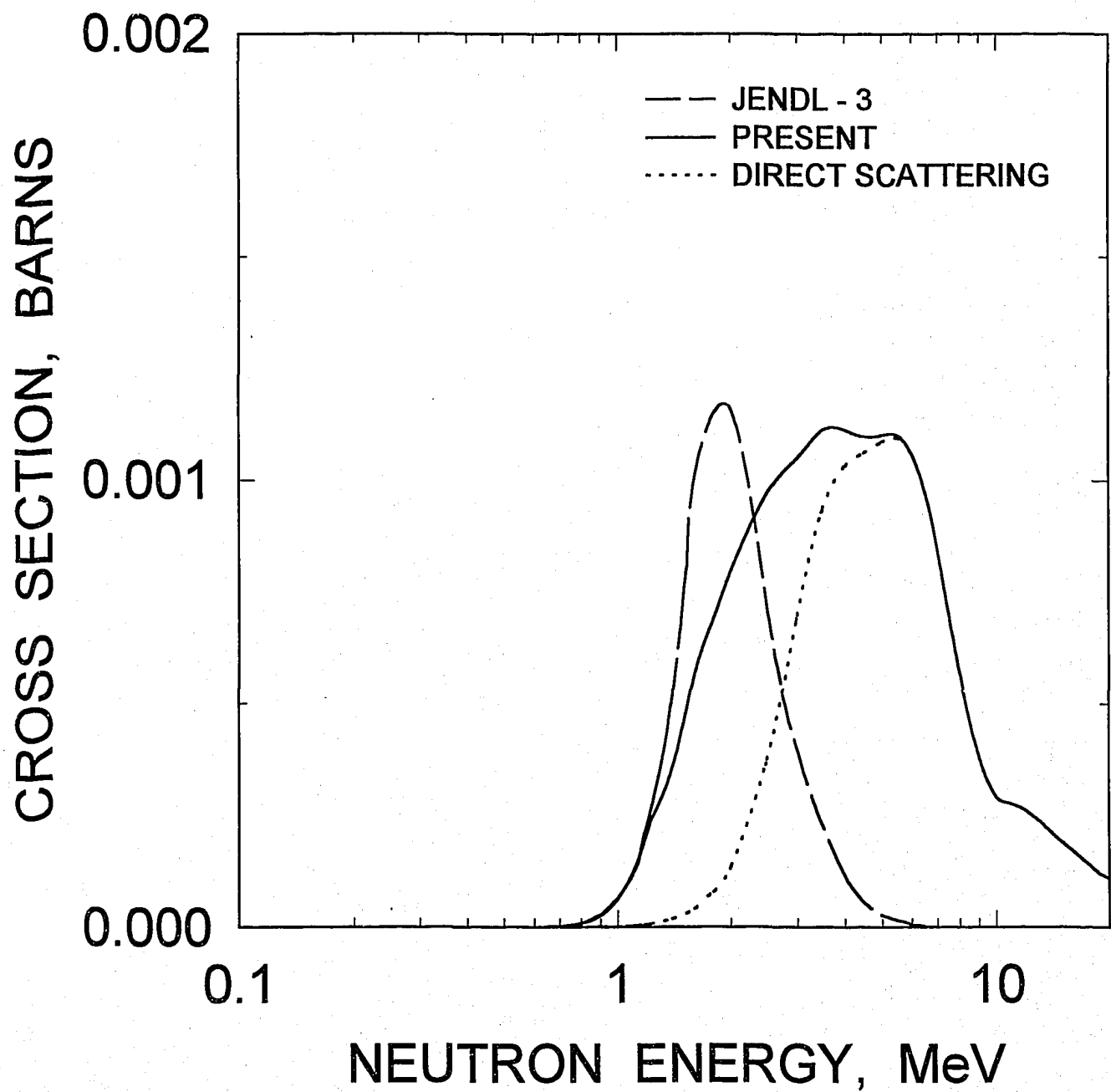
FIG. 4.17
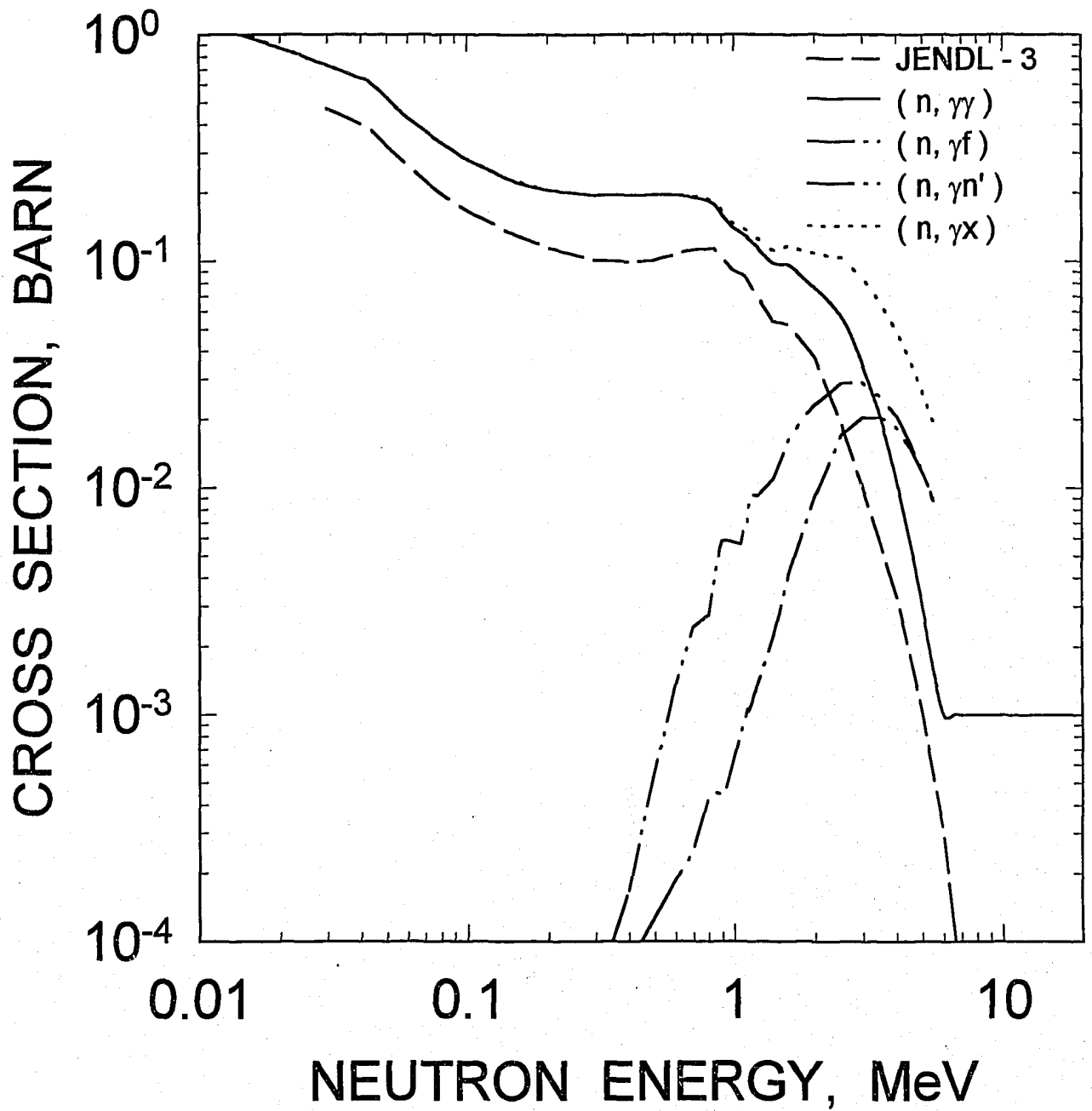
FIG. 4.18

^{246}Cm(n,2n) CROSS SECTION
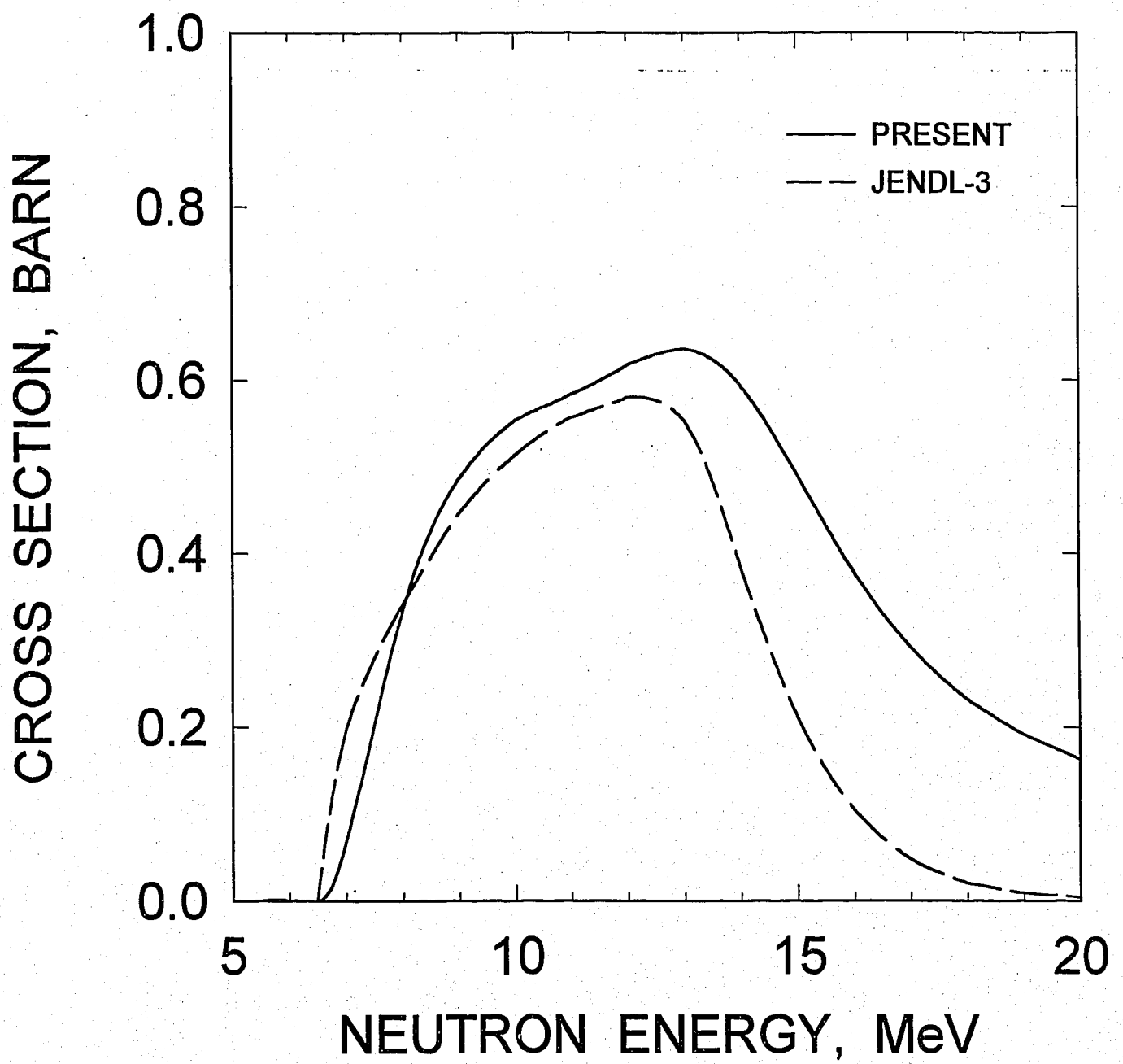
FIG. 4.19

^{246}Cm(n,3n) CROSS SECTION
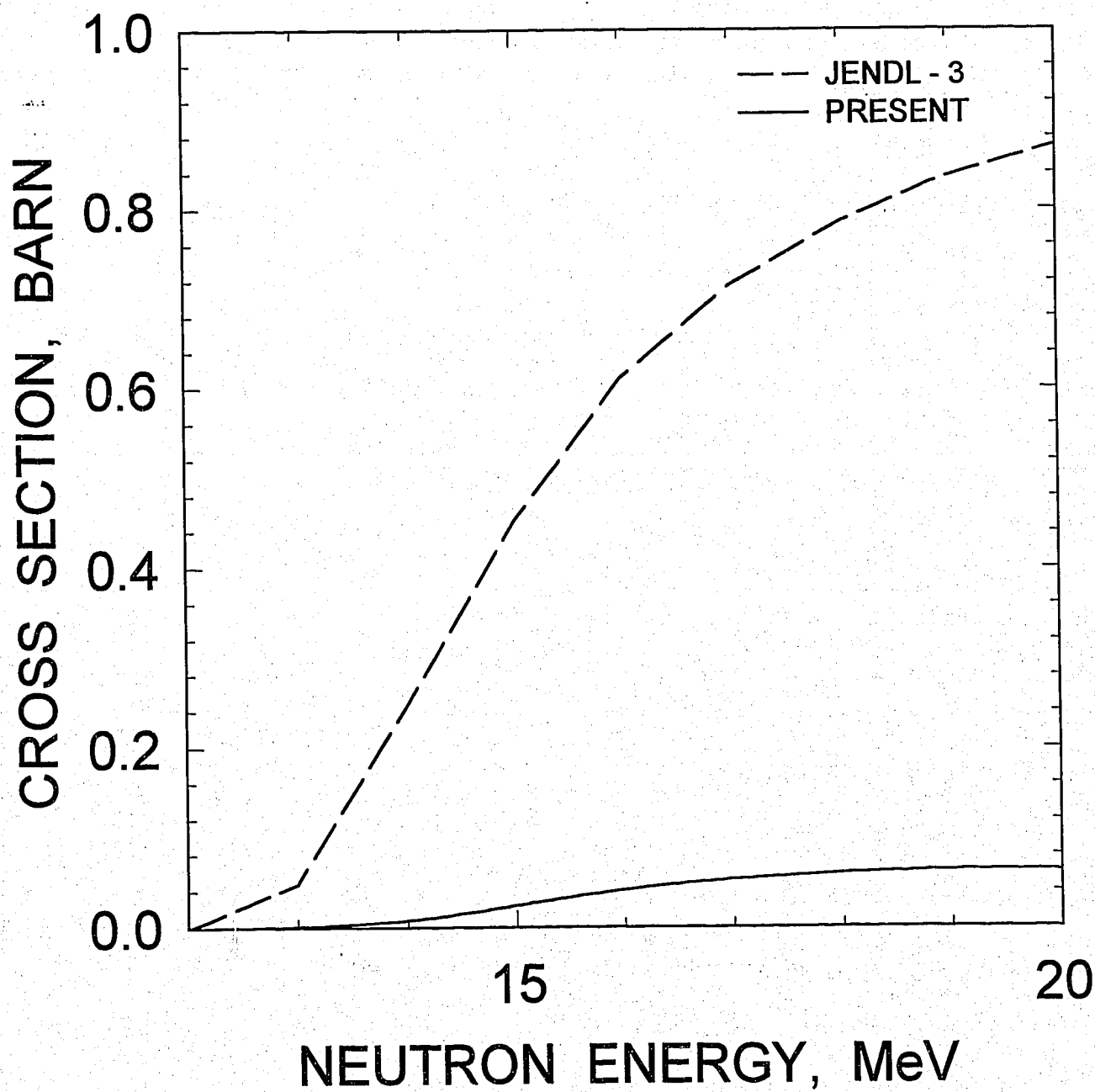
FIG. 4.20

^{246}Cm E_n=14 MeV
COMPONENTS OF FIRST NEUTRON SPECTRUM
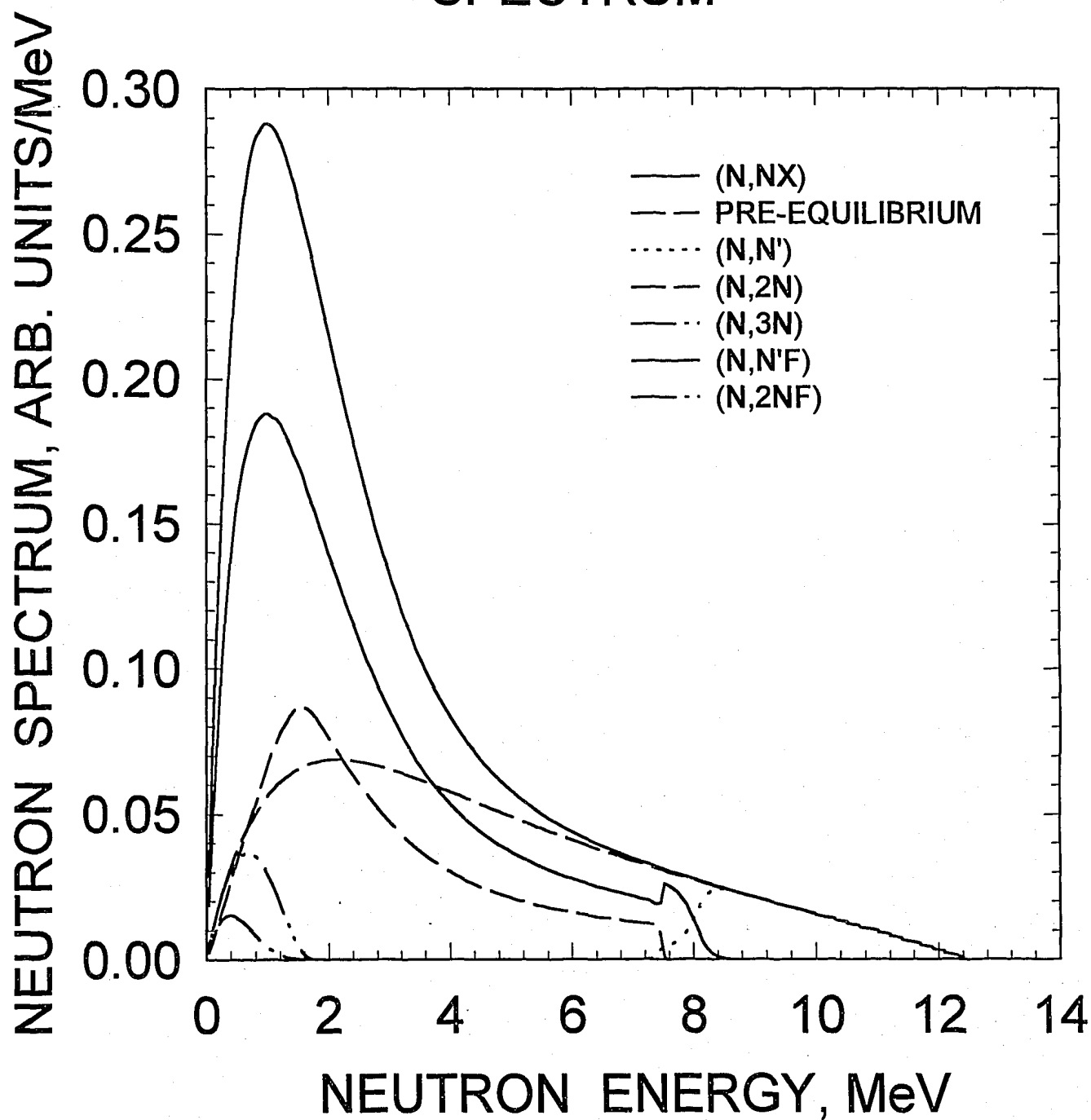
FIG.5.1

^{246}Cm E_n=14 MeV

COMPONENTS OF SECOND NEUTRON
SPECTRUM
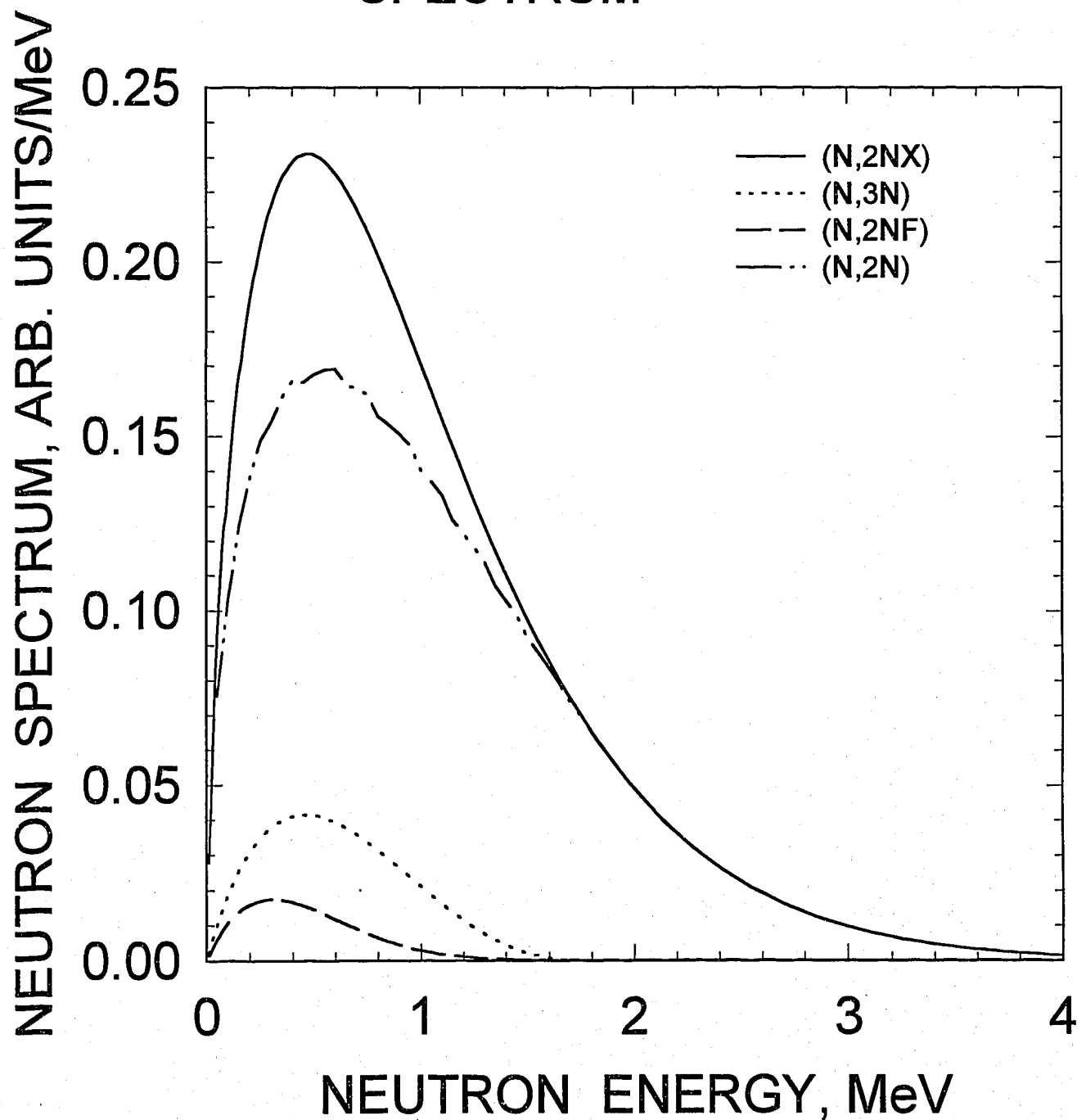
FIG.5.2

^{246}Cm E_n=8 MeV
COMPARISON WITH JENDL-3
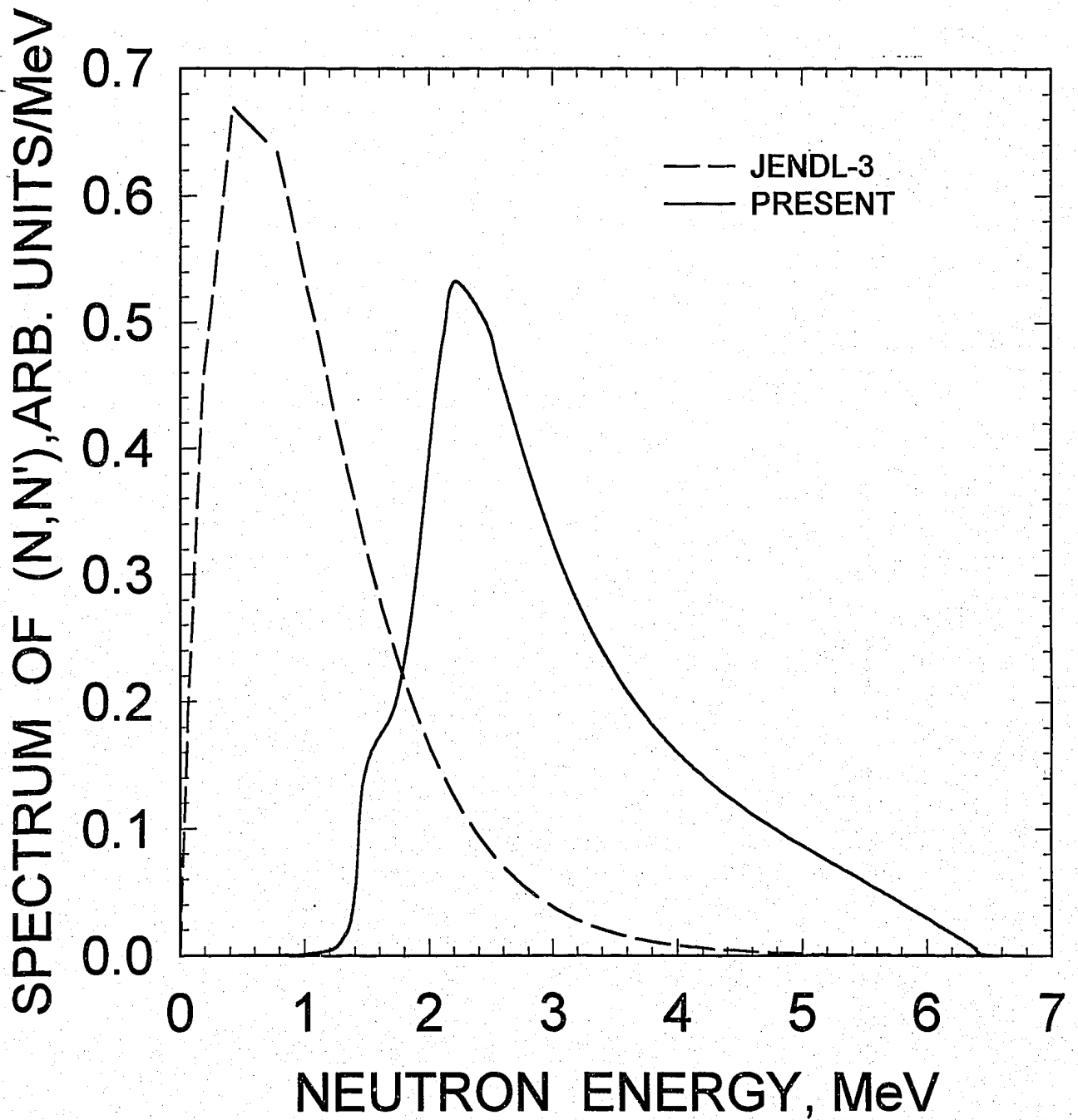
FIG.5.3

^{246}Cm   E$_n$=8 MeV
COMPARISON WITH JENDL-3
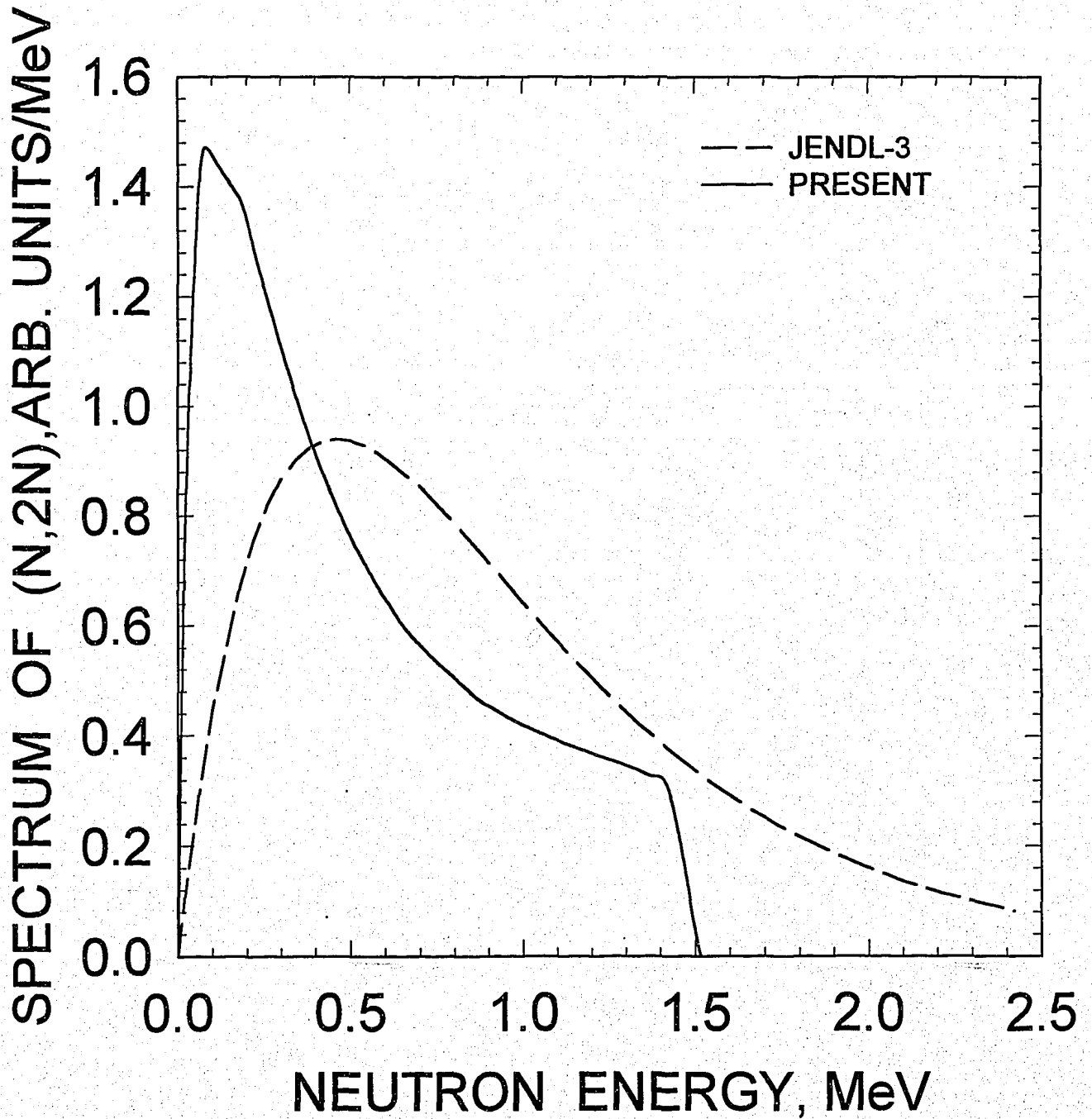
FIG.5.4

^{246}Cm   E$_n$=14 MeV
COMPARISON WITH JENDL-3
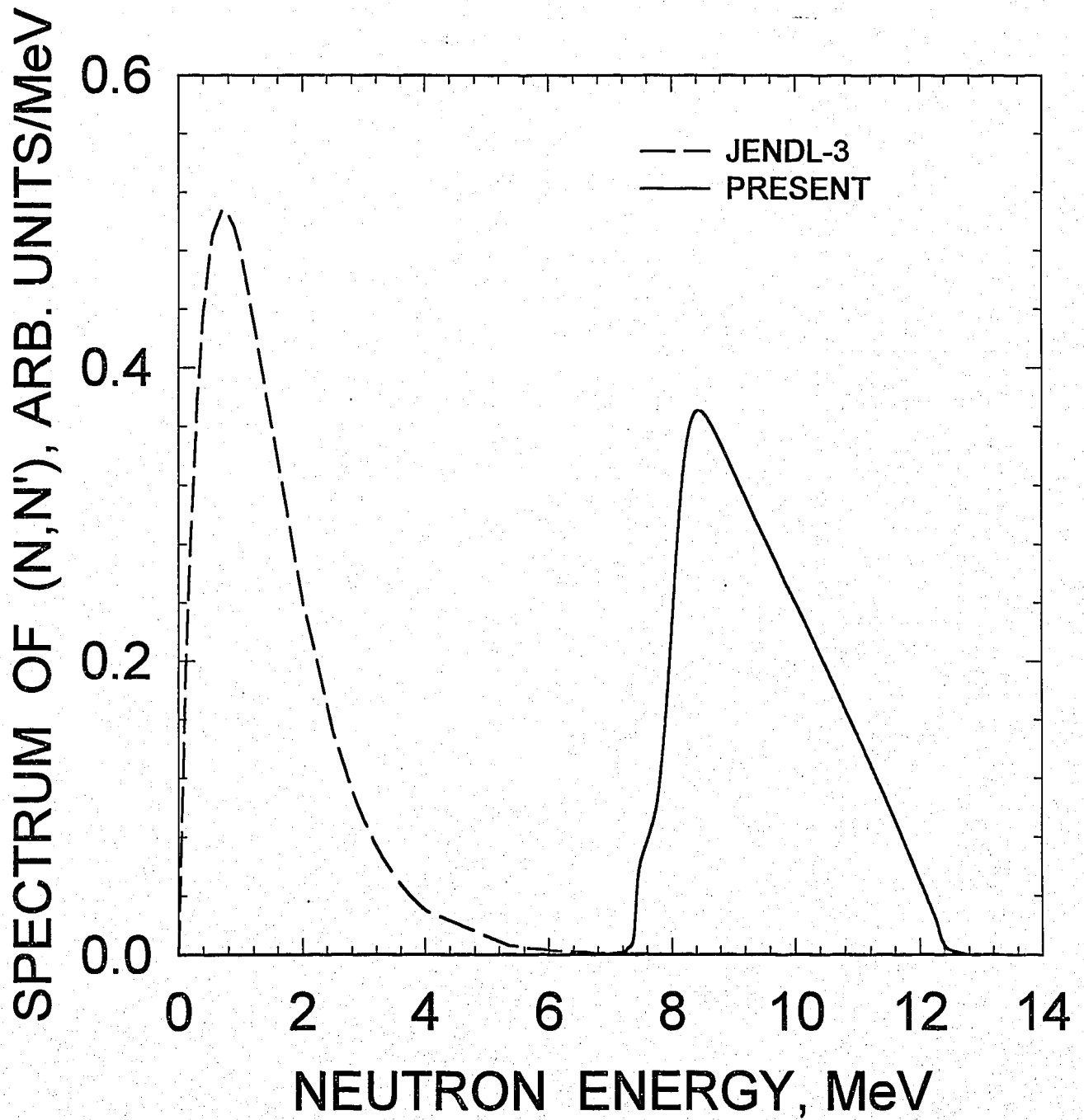
FIG.5.5

^{246}Cm E_n=14 MeV
COMPARISON WITH JENDL-3
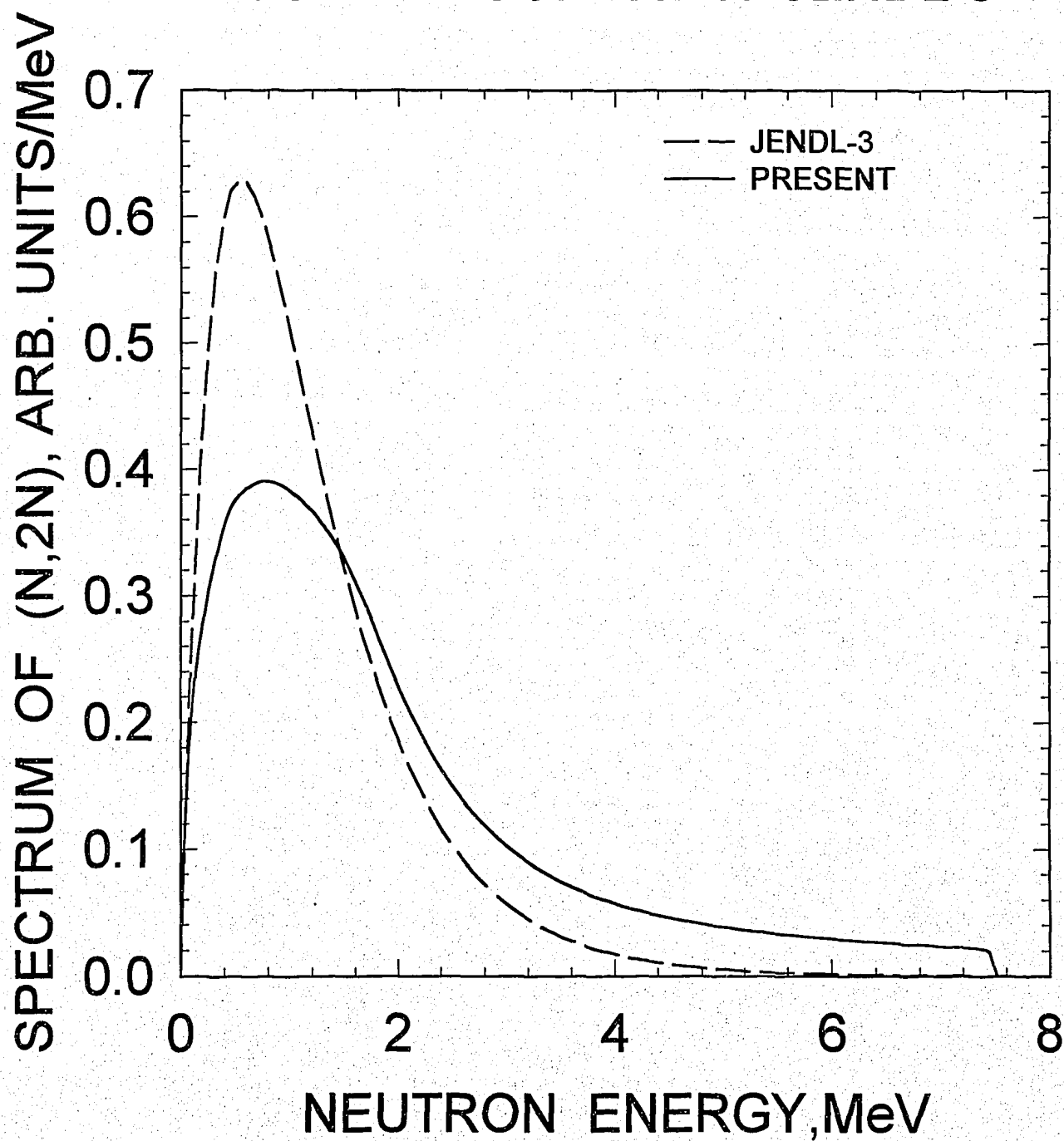
FIG.5.6

^{246}Cm   E$_n$=14 MeV
COMPARISON WITH JENDL-3
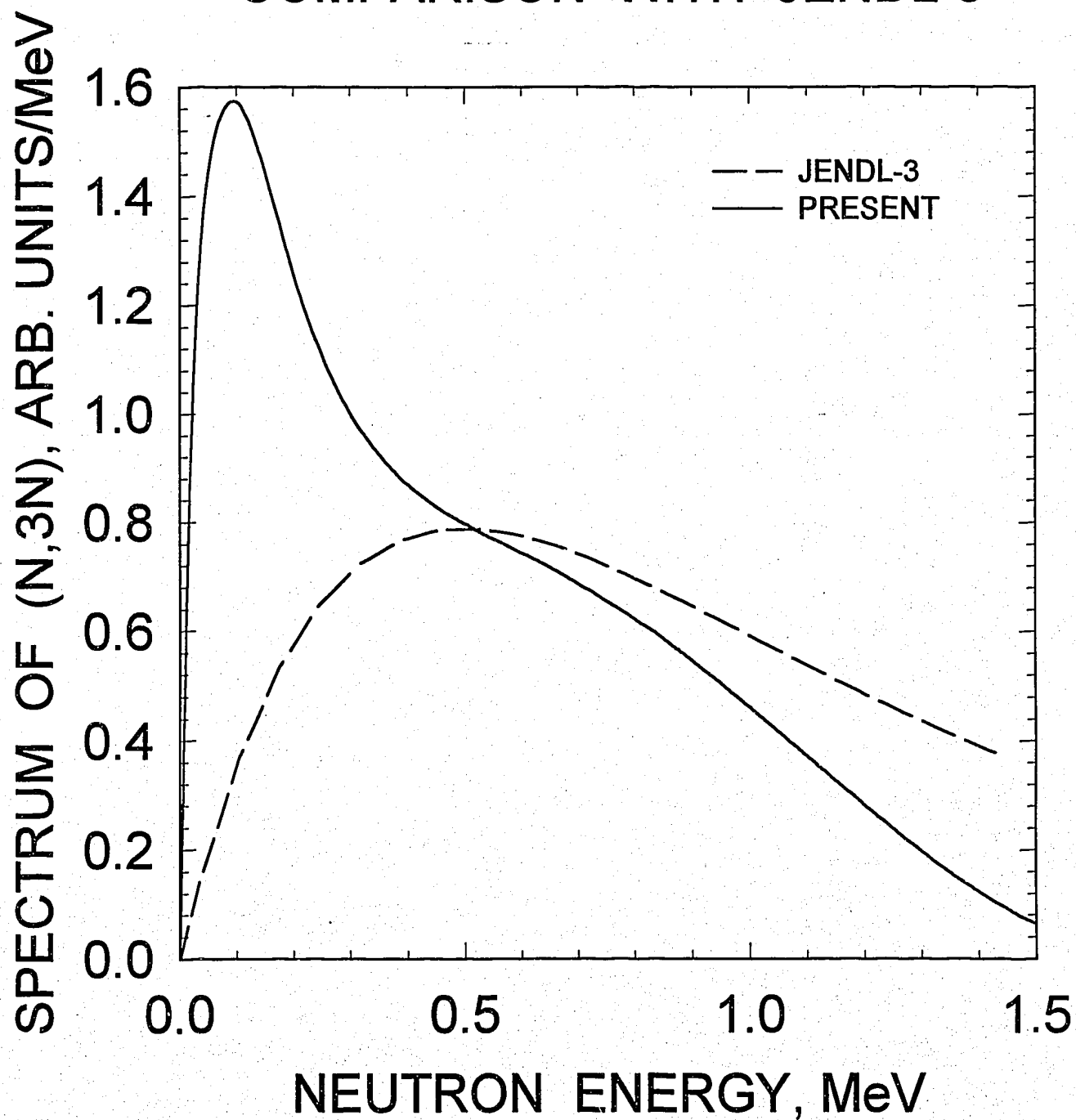
FIG.5.7

^{246}Cm THERMAL FISSION PROMPT NEUTRON SPECTRA RATIO TO JENDL-3 ($T_{MAXW.}$ = 1.48)
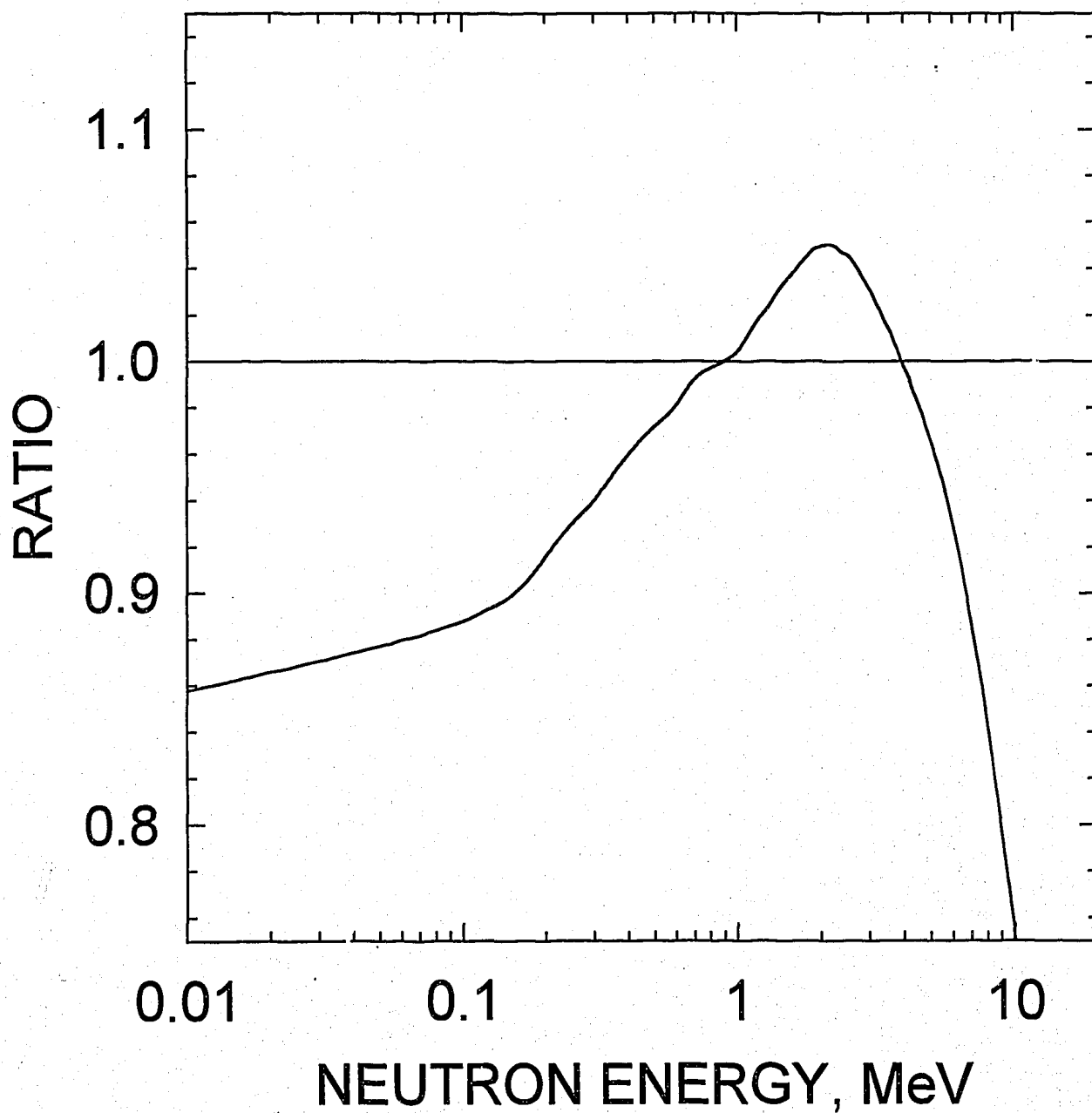
FIG.5.8

^{246}Cm PROMPT FISSION NEUTRON SPECTRA RATIO TO ($T_{MAXW.}$ = 1.48)

E_n = 14 MeV
E_n = 8 MeV
E_n = 1 MeV

RATIO

NEUTRON ENERGY, MeV
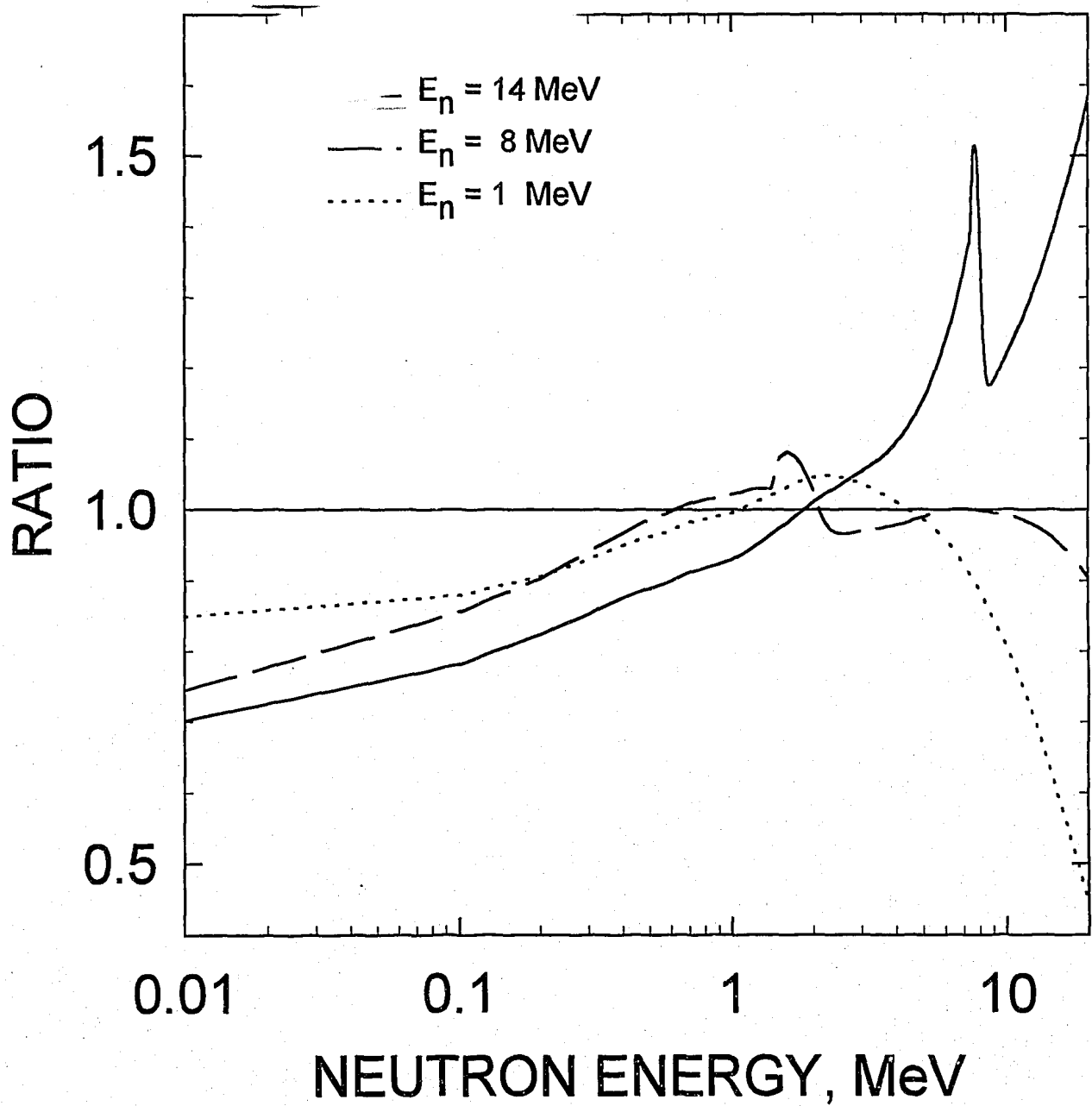
FIG.5.9

^{246}Cm FISSION NEUTRON SPECTRA RATIO TO MADLAND-NIX MODEL CALCULATION
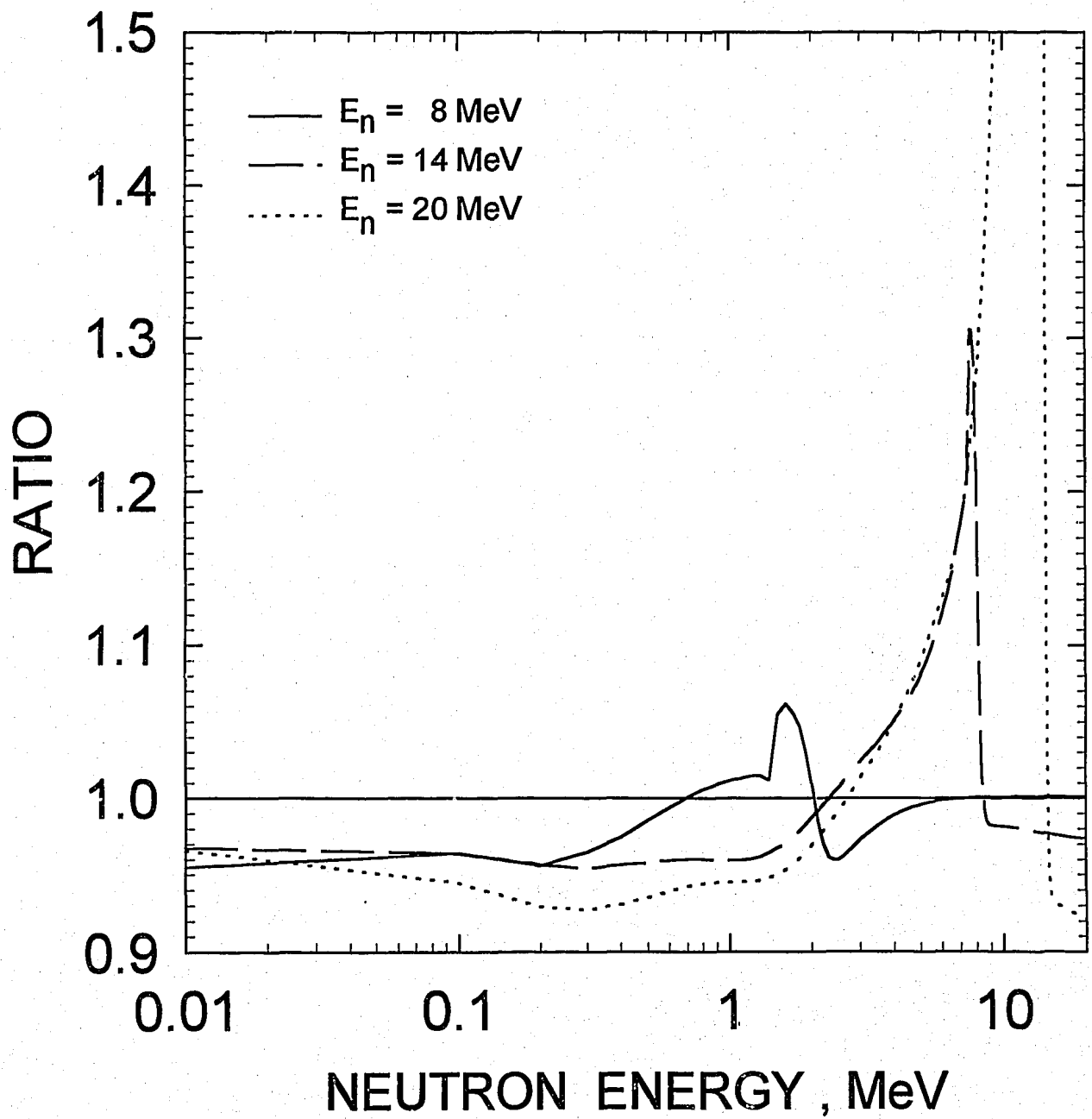
FIG.5.10

²⁴⁶Cm
FISSION NEUTRON SPECTRA
FOR E_n = 8 MeV
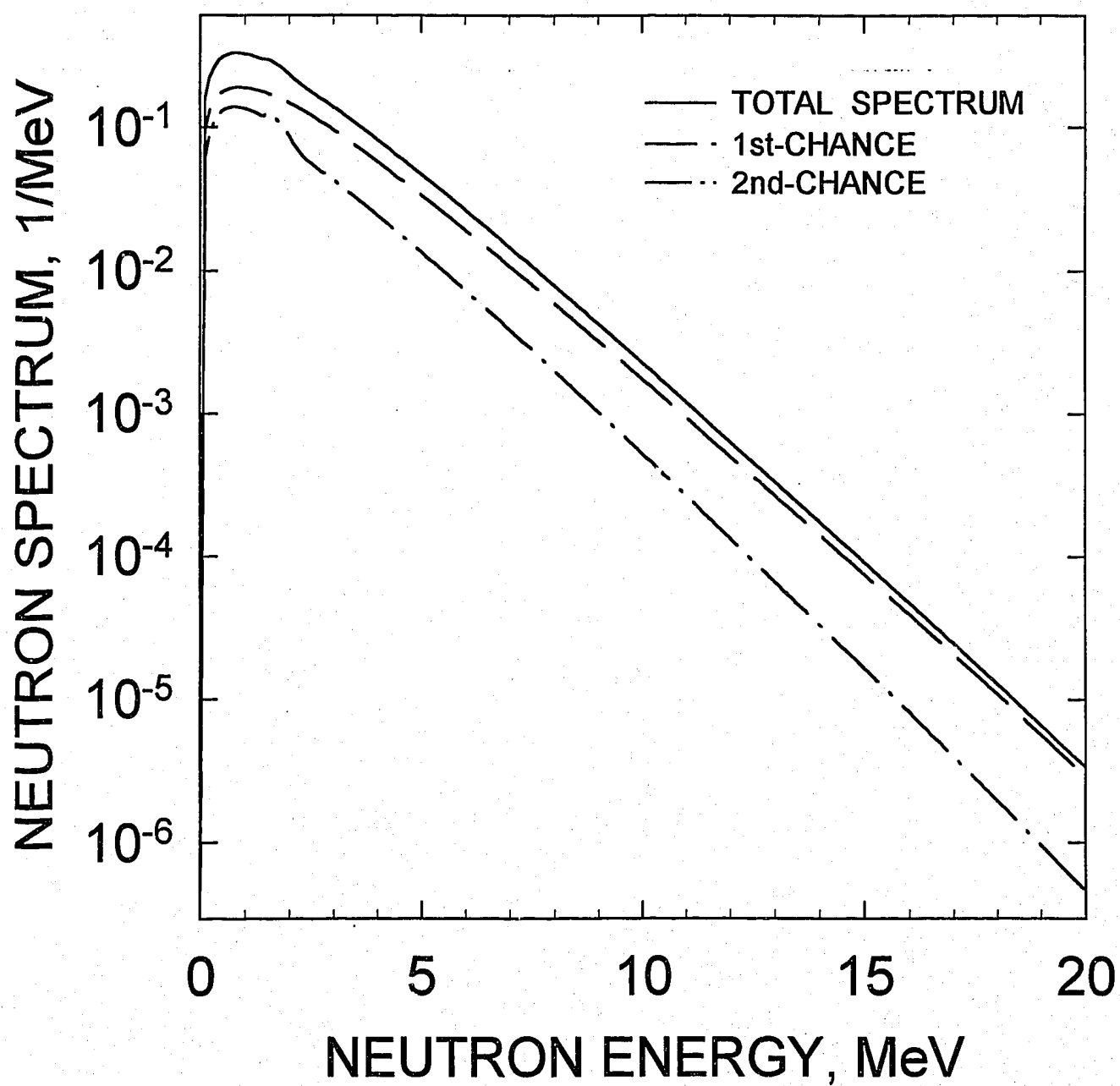
FIG.5.11

^{246}Cm
FISSION NEUTRON SPECTRA
FOR E_n = 14 MeV
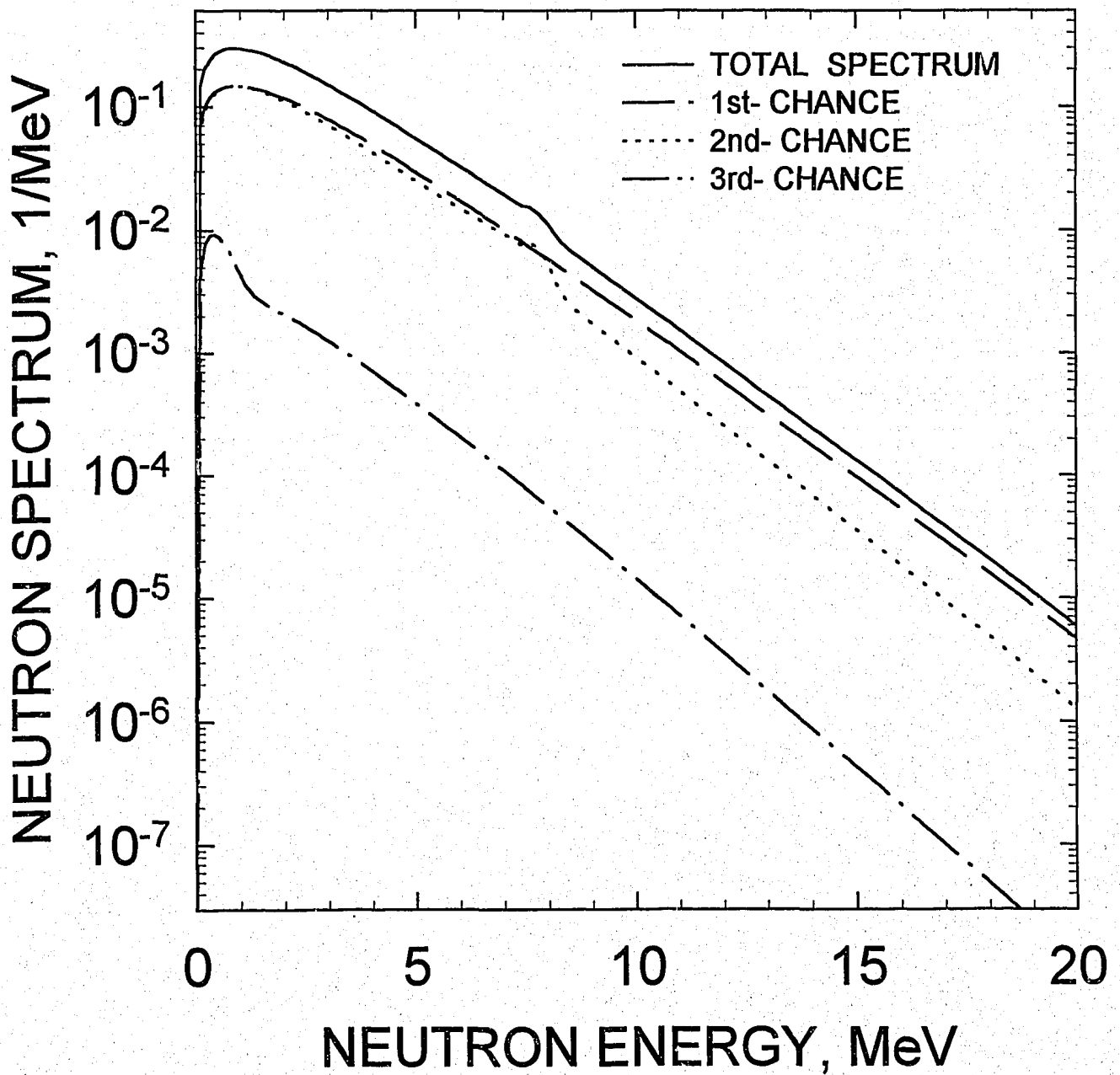
FIG.5.12

^{246}Cm
FISSION NEUTRON SPECTRA
FOR E_n = 20 MeV
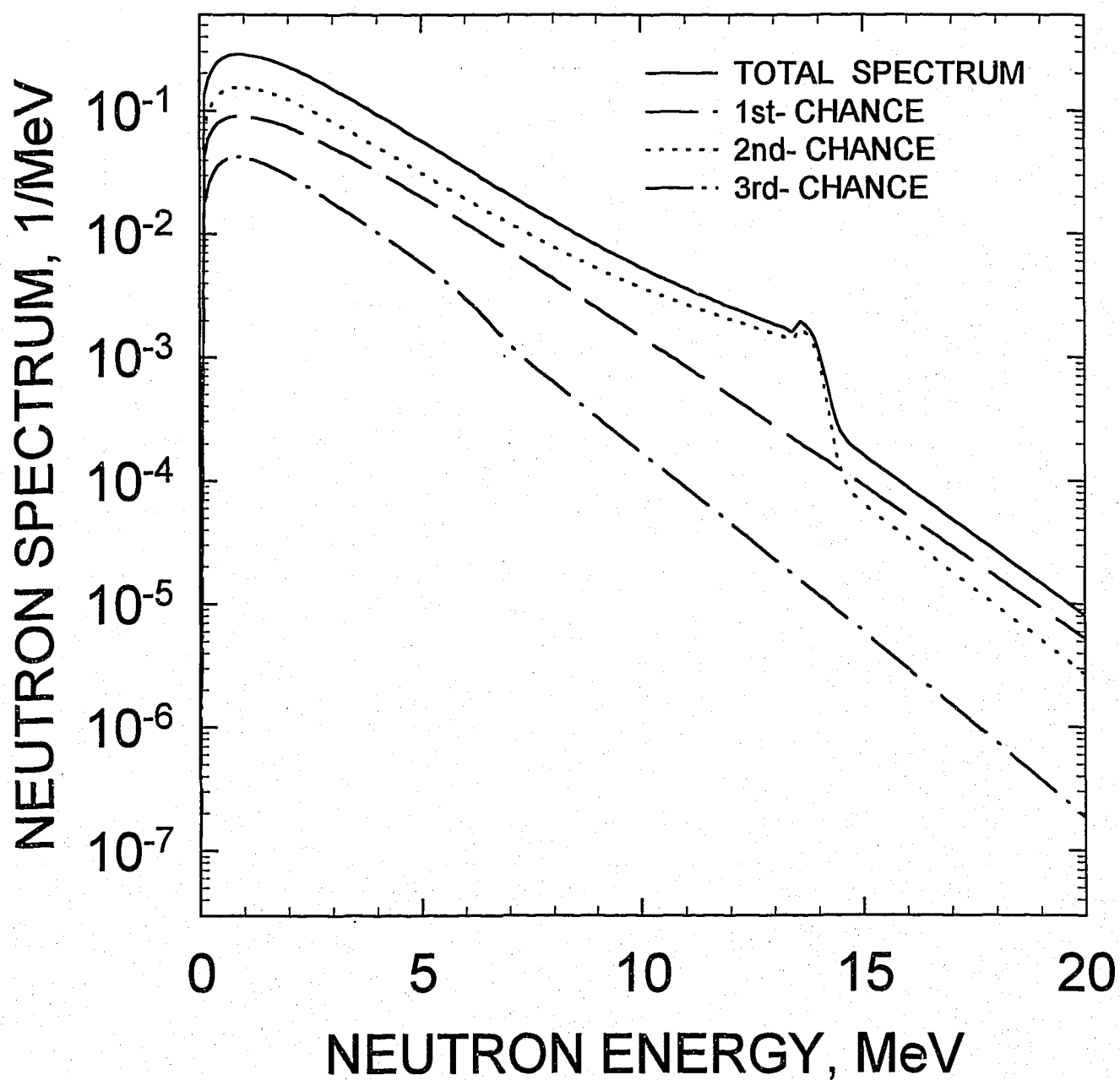
FIG.5.13

Cm MEAN-WEIGHTED EXPERIMENTAL PROMPT FISSION MULTIPLICITY
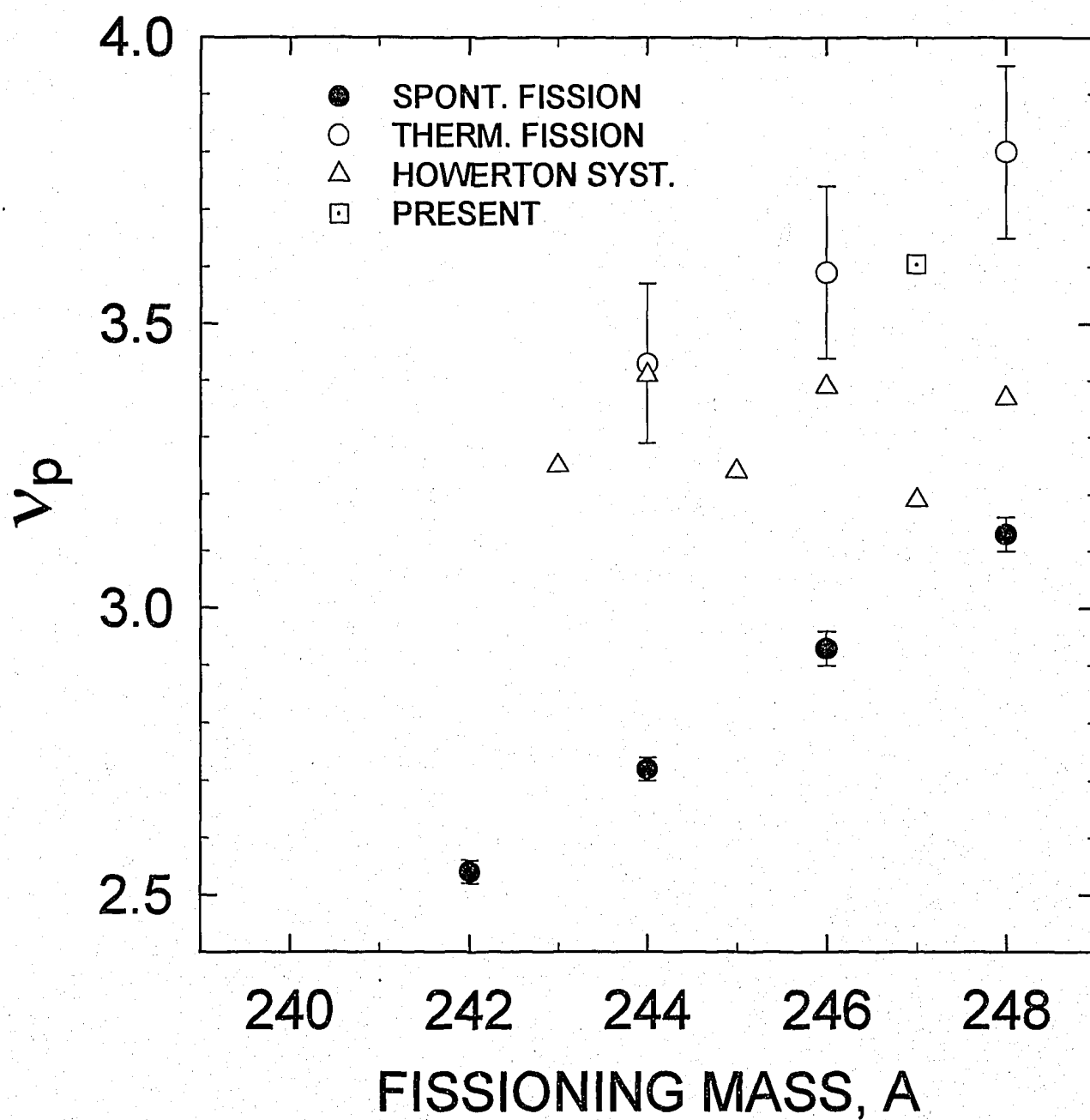
FIG.6.1

Cm EXPERIMENTAL TOTAL FISSION FRAGMENT KINETIC ENERGY
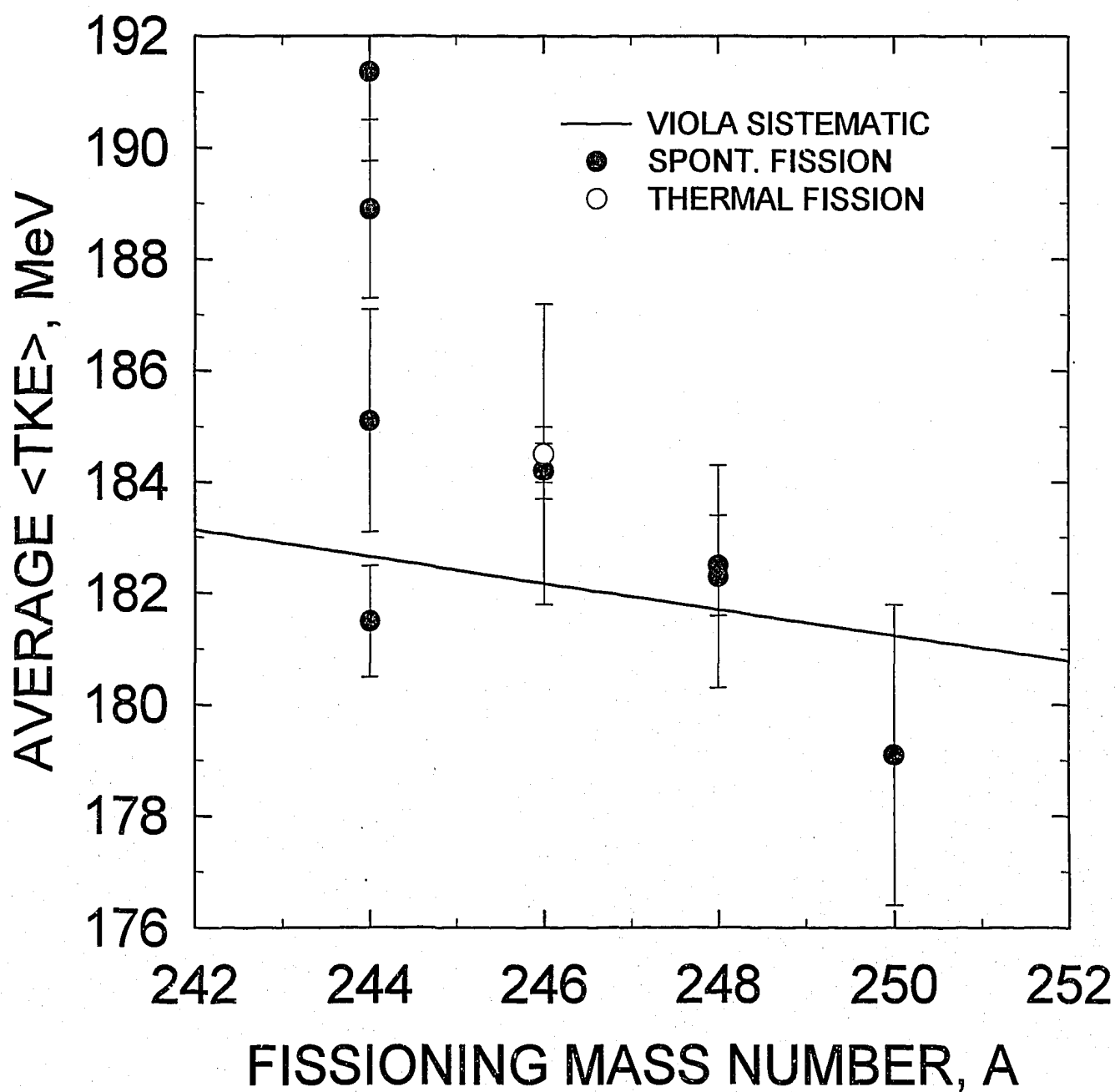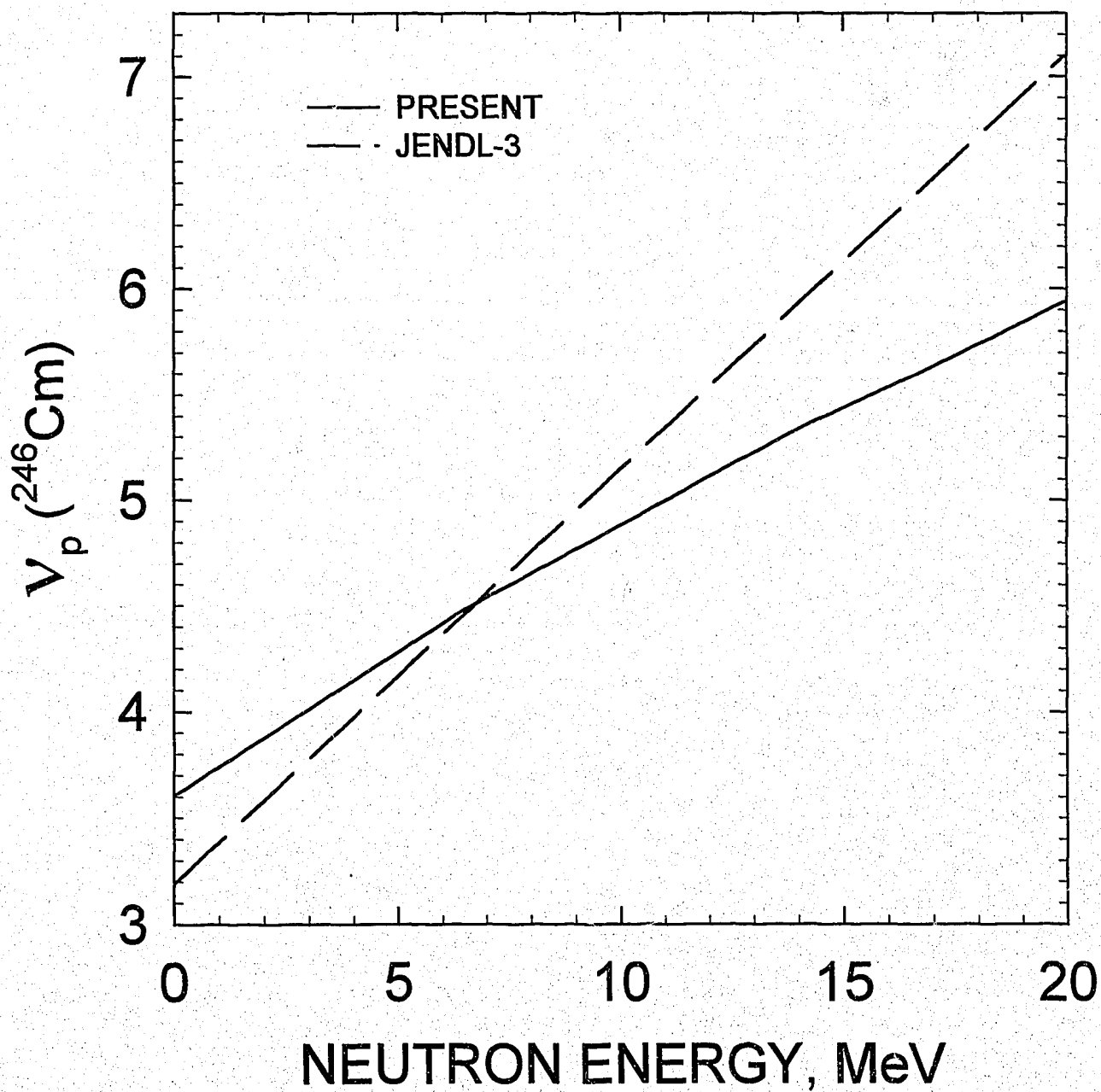
FIG.6.2

^{246}Cm PROMPT NEUTRON MULTIPLICITY

FIG.6.3

```
MS. MAGRIN AVEDIKIAN
INIS ROOM: A2418
INTERNATIONAL ATOMIC ENERGY
    AGENCY
P.O. BOX 100
A-1400 VIENNA
AUSTRIA
```